AD NUMBER
AD863766
LIMITATION CHANGES
TO: **Approved for public release; distribution is unlimited.**
FROM: **Distribution authorized to U.S. Gov't. agencies and their contractors; Administrative/Operational Use; JAN 1970. Other requests shall be referred to Air Force Flight Dynamics Lab., Wright-Patterson AFB, OH 45433.**
AUTHORITY
AFFDL ltr 10 Oct 1972

JAN 26 1970
FEB 11 1970
MAR 2 1970

AEDC-TR-69-232

cy2

FORCE TESTS ON A SEPARABLE-POD CREW ESCAPE CAPSULE IN PROXIMITY TO THE PARENT FUSELAGE AT MACH NUMBERS 2 THROUGH 5

Jerry H. Jones and L. M. Jenke

ARO, Inc.

January 1970

VON KÁRMÁN GAS DYNAMICS FACILITY
ARNOLD ENGINEERING DEVELOPMENT CENTER
AIR FORCE SYSTEMS COMMAND
ARNOLD AIR FORCE STATION, TENNESSEE

NOTICES

FORCE TESTS ON A SEPARABLE-POD CREW ESCAPE CAPSULE IN PROXIMITY TO THE PARENT FUSELAGE AT MACH NUMBERS 2 THROUGH 5

Jerry H. Jones and L. M. Jenke
ARO, Inc.

FOREWORD

The work reported herein was done at the request of the Air Force Flight Dynamics Laboratory (AFFDL), Air Force Systems Command (AFSC), under Program Element 64706F.

The results of tests presented were obtained by ARO, Inc. (a subsidiary of Sverdrup & Parcel and Associates, Inc.), contract operator of the Arnold Engineering Development Center (AEDC), AFSC, Arnold Air Force Station, Tennessee, under Contract F40600-69-C-0001. The tests were conducted from July 7 to 31, 1969, under ARO Project No. VA0942. The manuscript was submitted for publication on September 24, 1969.

This technical report has been reviewed and is approved.

Eugene C. Fletcher
Lt Colonel, USAF
AF Representative, VKF
Directorate of Test

Roy R. Croy, Jr.
Colonel, USAF
Director of Test

ABSTRACT

Static-force tests were conducted on a separable-pod crew escape capsule in close proximity to the forward section of the airplane fuselage. The capsule escape rocket exhaust plume was simulated with high pressure air heated to a total temperature of approximately 100°F. Data were obtained at Mach numbers from 2 through 5 at capsule angles of attack from -15 to 25 deg and angles of sideslip from 0 to 15 deg for various positions of the capsule relative to the fuselage section. All testing was conducted at a fuselage angle of attack and angle of sideslip of zero. Reynolds number, based on the pod model length of 8.978 in., ranged from 1.9×10^6 to 5.2×10^6. Results are presented showing the effects of the fuselage section on the aerodynamic characteristics of the capsule, with and without simulation of the escape rocket exhaust plume. These results indicate that the primary interference effects for the jet-off data are caused by severe flow interactions occurring when the capsule, with its strong bow shock, moves across the fuselage cavity. For the jet-on data the primary interference effects are caused by the jet exhausting into the fuselage cavity, which acts as a flow deflector turning the jet flow back onto the capsule.

CONTENTS

APPENDIXES

I. ILLUSTRATIONS

NOMENCLATURE

A	Reference area (capsule frontal area), 14.520 in.^{2}
C_D	Drag coefficient, drag/$q_\infty A$
C_L	Lift coefficient, lift/$q_\infty A$
C_ℓ	Rolling-moment coefficient, rolling moment/$q_\infty A\ell$
C_m	Pitching-moment coefficient, pitching moment/$q_\infty A\ell$
C_n	Yawing-moment coefficient, yawing moment/$q_\infty A\ell$
C_Y	Side-force coefficient, side force/$q_\infty A$
ℓ	Reference length (capsule length), 8.978 in.
M_∞	Free-stream Mach number
p_c	Jet chamber pressure, psia
p_o	Tunnel stilling chamber pressure, psia
p_∞	Free-stream static pressure, psia
q_∞	Free-stream dynamic pressure, psia
Re_∞	Free-stream unit Reynolds number, in.$^{-1}$
T_o	Tunnel stilling chamber temperature, °R
x	Longitudinal separation distance between the capsule and fuselage, in the wind axis, and measured from the capsule moment reference point before separation to the capsule moment reference point after separation, in.
y	Lateral separation distance between the capsule and fuselage, perpendicular to the x-z plane, and measured as noted for x, in.
z	Vertical separation distance between the capsule and fuselage, perpendicular to the wind axis, and measured as noted for x, in.

α_c	Capsule angle of attack, deg
β_c	Capsule angle of sideslip, deg

Note: Force and moment coefficients are in the stability axis system.

SECTION I
INTRODUCTION

These tests represent Phase III of a wind tunnel test program requested by the Flight Recovery Group (FDFR), AFFDL, to provide data for investigating crew escape systems for high-speed flight vehicles. In Phases I and II (Refs. 1, 2, and 3), the static stability and drag characteristics of the F-104 aircraft separable-nose crew escape capsule were obtained with and without the presence of the forward section of the airplane fuselage.

In the present Phase III tests, static stability and drag data were obtained on a separable-pod capsule supported from a remotely controlled system that positioned the fuselage with respect to the capsule and provided pitch or yaw of the capsule. The fuselage section position relative to the capsule was varied from 22 in. aft to 26 in. forward of the capsule and from 0.2 to 14 in. below the capsule. Laterally, the capsule was aligned with the fuselage and was also positioned 5 in. to the side of the fuselage.

Static-force data were obtained at Mach numbers from 2 through 5 at capsule angles of attack from -15 to 25 deg and capsule angles of sideslip from 0 to 15 deg. The fuselage angle of attack and angle of sideslip were zero. Reynolds number, based on the pod model length of 8.978 in., ranged from 1.9×10^6 to 5.2×10^6. The escape rocket jet plume was simulated with air heated to approximately 100°F.

SECTION II
APPARATUS

2.1 WIND TUNNEL

The 40-in. supersonic tunnel (Gas Dynamic Wind Tunnel, Supersonic (A)) is a continuous, closed-circuit, variable density wind tunnel with an automatically driven, flexible-plate-type nozzle and a 40- by 40-in. test section. The tunnel can be operated at Mach numbers from 1.5 to 6 at maximum stagnation pressures from 29 to 200 psia, respectively, and stagnation temperatures up to 290°F (M_∞ = 6). Minimum operating pressures range from about one-tenth to one-twentieth of the maximum at each Mach number. A more complete description of the tunnel and airflow calibration information may be found in Ref. 4.

2.2 MODELS AND SUPPORT SYSTEM

The separable-pod crew escape capsule model and the fuselage section model (Figs. 1 through 3, Appendix I) were 7-percent-scale models of a hypothetical, two-place, side-by-side, high-speed aircraft. The models were supplied by AFFDL and modified by VKF so that they could be supported on a remotely controlled support system, which is described in Ref. 3.

The escape rocket nozzle was positioned in a cutout on the lower aft portion of the capsule model (Fig. 1c) and was attached to the sting so that the model was isolated from the jet reaction force. Details of the nozzle, which was identical to the nozzle used in the Phase I and II tests, are given in Fig. 1d. The procedures used to calculate the nozzle dimensions and chamber pressures for simulation of the full-scale jet plume shape at various altitudes over the Mach number range are given in Ref. 1.

The fuselage section details are given in Fig. 1b. As shown in this figure, an insert was used in the aft portion of the fuselage to fill a section of the rear wall of the cavity left open by the ejected capsule model. The insert was removed to provide clearance for the capsule sting support when the capsule and fuselage were in close proximity and installed for conditions where the sting cleared the fuselage. The exact conditions for use of the insert are shown in Tables I and II (Appendix II). The three vent holes shown on the fuselage were to allow the jet exhaust gas to escape from the cavity when the capsule was in close proximity to the fuselage.

2.3 INSTRUMENTATION AND PROCEDURES

Capsule force and moment measurements were made with six-component, moment-type, strain-gage balances supplied and calibrated by the von Kármán Gas Dynamics Facility. During the test, it became necessary to replace balance 1 with another balance (balance 2). In order to accomplish this, it was necessary to modify the model and sting assembly. This modification resulted in moving the nozzle thrust axis forward by 0.060 in. Since the jet thrust was not being measured by the balance and the only jet effects that were measured were the plume effects on the flow over the capsule, it was assumed that this small thrust axis shift would not significantly affect the data. This assumption was justified by repeating data previously obtained on balance 1. The conditions tested on balances 1 and 2 are shown in Tables I and II.

Before the test, loadings in a single plane and combined static loadings were applied to the balances which simulated the range of model loadings anticipated for the test. The ranges of uncertainties listed below correspond to the differences between the applied loads and the values calculated with the balance equations used in the final data reduction. The minimum uncertainties given are for loads up to about 10 percent of the maximum applied and are for loadings on the particular component only (no combined loading interaction effects). The maximum uncertainties are for combined loadings.

Balance 1

Balance Component	Design Load	Range of Static Loadings	Range of Uncertainties
Normal force, lb	200	±200	±0.25 to ±0.80
Pitching moment, in.-lb	680	±300	±1.00 to ±2.00
Side force, lb	200	±200	±0.70 to ±1.00
Yawing moment, in.-lb	680	±300	±2.00 to ±3.00
Rolling moment, in.-lb	100	±100	±0.25 to ±0.54
Axial force, lb	100	0 to 100	±0.30 to ±0.40

Balance 2

Balance Component	Design Load	Range of Static Loadings	Range of Uncertainties
Normal force, lb	500	±200	±1.10 to ±2.40
Pitching moment, in.-lb	1850	±400	±2.10 to ±4.00
Side force, lb	250	±200	±0.80 to ±1.30
Yawing moment, in.-lb	925	±400	±1.90 to ±4.00
Rolling moment, in.-lb	100	±100	±0.15 to ±0.50
Axial force, lb	300	±100	±0.50 to ±0.70

The jet chamber pressure was measured with a 1000-psid transducer and is considered accurate to within 1 percent of capacity.

The base pressures were measured with transducers calibrated for full-scale ranges of 15, 5, and 1 psid, referenced to a near vacuum, which are considered accurate to within 0.3 percent of full scale.

The model attitude and position were measured with calibrated potentiometers, recorded on digital voltmeters, and the accuracies of each are listed on the following page.

Drive System	Range	Uncertainty
α_c, β_c, deg	-15 to 25	±0.05
x, in.	-24 to 40	±0.10
y, in.	-2 to 10	±0.05
z, in.	0 to 14	±0.08

Each data group was obtained by setting α_c or β_c, y, and z and varying x. In order to obtain data more rapidly, x was varied continuously as the data were being taken; consequently, the x values obtained were not in even increments. A curve fit program was later used to calculate all test parameters for any desired value of x. Given the values of x, y, and z, this program would pick the six data points closest to the given x, fit a fifth-degree equation to the data, and retabulate the results for varying α_c or β_c. Plotted data in this form will be supplied to AFFDL to aid in their analysis of the results. For the purpose of a timely documentation of the test results, however, the data presented herein are in the original form as a function of x.

SECTION III
RESULTS AND DISCUSSION

A summary of the test conditions is presented in Table III, and Tables I and II present a summary of the model attitudes tested. Because of excessive model vibrations encountered with the jet on and the capsule in close proximity to the fuselage section, no data were taken, jet on, for z < 3 in. Only general comments on the results are given herein; the final analysis in relation to the concept of this capsule as a practical system will be done by AFFDL.

The effects of the presence of the fuselage section on the lift, drag, and pitching-moment characteristics of the escape capsule, jet off, are shown in Figs. 4 through 11 for Mach numbers 2, 3, 4, and 5. For these and all other data presented, the number of data points obtained was generally considered sufficient to illustrate data trends without fairing curves through the individual data points. Of primary interest here are the pitching-moment data. For the condition of zero lateral separation (y = 0) and a close-in vertical separation distance of z = 3 in., the trends of the pitching-moment curves are similar for all Mach numbers. Specifically, peaks are apparent in the data, particularly at about $x \approx +2$ and -2 in. with a dip at $x \approx 0$. These data variations are attributed to the severe flow interactions occurring when the capsule, with its strong detached shock, moves across the fuselage cavity. The shock

systems involved in these interactions and the resulting large regions of separated flow over the fuselage section are shown in the schlieren photographs of the two models at various attitudes and for each Mach number given in Figs. 5, 7, 9, and 11. These photographs and the data figures show, as one would expect, that the interference effects between the two bodies decrease as the capsule is moved away from the fuselage (z and y increased). It may also be noted that for the close proximity conditions (z = 3 and 4 in.) at Mach numbers of 3 and above, variations in the lift and drag data were obtained similar to those of the pitching-moment data. These data excursions were similar regardless of the capsule pitch attitude. Pitching the capsule to angle of attack seemed to change only the level of the coefficients.

Capsule side-force, yawing-moment, and rolling-moment characteristics, jet off, for Mach numbers 2, 3, 4, and 5 are presented in Figs. 12 through 15 for the models in the sideslip attitude. For no lateral separation (y = 0), these data show only small variations for $\beta_c = 0$ at all Mach numbers and vertical separation distances (z). This would be expected since the fuselage interference flow field about the capsule should be symmetrical in the sideslip plane. As the capsule sideslip angle was increased from zero and thus moved the capsule out of the plane of symmetry, noticeable interference effects were obtained. The most significant variations in these data were obtained in the yawing moment. With the capsule displaced laterally to y = -5 in., the fuselage interference flow field was nonsymmetrical even for $\beta_c = 0$. These data (Figs. 12e, 13e, 14e, and 15d) show that the interference effects at $\beta_c = 0$ were of the same order of magnitude of those for $\beta_c > 0$.

Similar results, as shown previously for the capsule in pitch and sideslip, are presented in Figs. 16 through 27 with flow simulation of the escape rocket exhaust plume. For the condition of the capsule free from fuselage interference (maximum negative x), the jet-on pitch data as compared to jet off show an increase in lift, a decrease in pitching moment, and little change in drag (for example, Figs. 10e and 22e). The sideslip data for this condition show only small variations in side force, yawing moment, and rolling moment (compare Figs. 15c and 27b). The pitch data variations noted above can be attributed to a jet-induced increased pressure on the lower rear surface of the capsule which would not appreciably affect drag (because of the base drag correction) or sideslip data.

The trends of the interference effects for these data were very similar to those for jet off except for an increase in magnitude. The variations around $x \approx 0$ become very large when the capsule is in close proximity to the fuselage and also increase with increasing Mach number

(for example, Figs. 4a and 16a for Mach number 2 and Figs. 10a and 22a for Mach number 5). These jet-on effects around $x = 0$ are probably the result of the jet exhausting into the fuselage cavity, which acts as a flow deflector turning the jet flow back onto the capsule. The jet exhaust produced violent flow separation on the fuselage, as can be seen in the schlieren photographs presented.

A limited amount of jet-off data was obtained at $x = 0$, $y = 0$, and $\alpha_c = 0$ with the capsule less than 3 in. vertically (z) from the fuselage. These data are included in Fig. 28, which presents capsule lift, pitching moment, and drag data, jet off and jet on, as a function of vertical separation distance, z. The increase in lift, pitching moment, and drag as z increases from 0.2 in., jet off, is a direct result of the capsule front face becoming more exposed to the flow. For the conditions where fuselage interference exists ($z \lesssim 6$ in.), the jet-on data, as compared to jet off, show an increase in lift and pitching moment and only small variations in drag. Although no jet-on data were obtained for $z < 3$ in., Fig. 28 gives an indication of the large effects that may be present.

SECTION IV
CONCLUDING REMARKS

From the subject tests in Tunnel A of VKF, the following conclusions can be stated:

1. The primary interference effects for the jet-off condition were obtained in the pitch plane with the capsule in close proximity to the fuselage and were attributed to severe flow interactions occurring when the capsule, with its strong detached shock, moved across the fuselage cavity.
2. For the condition of interference-free data, the jet-on pitch data as compared to jet off showed an increase in lift, a decrease in pitching moment, and little change in drag. These variations were attributed to a jet-induced increased pressure on the lower rear surface of the capsule.
3. The interference effects for jet on were similar to those for jet off except for an increase in magnitude, particularly around $x \approx 0$ with the capsule in close proximity to the fuselage. This was probably the result of the jet exhausting into the fuselage cavity, which acted as a flow deflector turning the jet flow back onto the capsule.

4. For the condition where fuselage interference exists at $x = 0$, $y = 0$, $\alpha_c = 0$, the jet-on data as compared to jet off showed an increase in lift and pitching moment and only small variations in drag.

REFERENCES

1. Jenke, L. M., Jones, J. H., and Myers, A. W. "Force Tests on a Separable-Nose Crew Escape Capsule with Cold Flow Rocket Jet Simulation at Mach Numbers 1.5 through 6." AEDC-TR-66-74 (AD481301), April 1966.

2. Jones, J. H. "Force Tests on a Separable-Nose Crew Escape Capsule in Proximity to the Parent Fuselage at Mach Numbers 1.5 through 4.5." AEDC-TR-66-140 (AD487406), August 1966.

3. Jones, J. H. and Pfaff, L. J. "Force Tests on a Separable-Nose Crew Escape Capsule in Proximity to the Parent Fuselage with Cold Flow Rocket Plume Simulation at Mach Numbers 2 through 5." AEDC-TR-68-278 (AD848311), February 1969.

4. Test Facilities Handbook (Eighth Edition). "Von Kármán Gas Dynamics Facility, Vol. 4." Arnold Engineering Development Center, December 1969.

APPENDIXES

I. ILLUSTRATIONS

II. TABLES

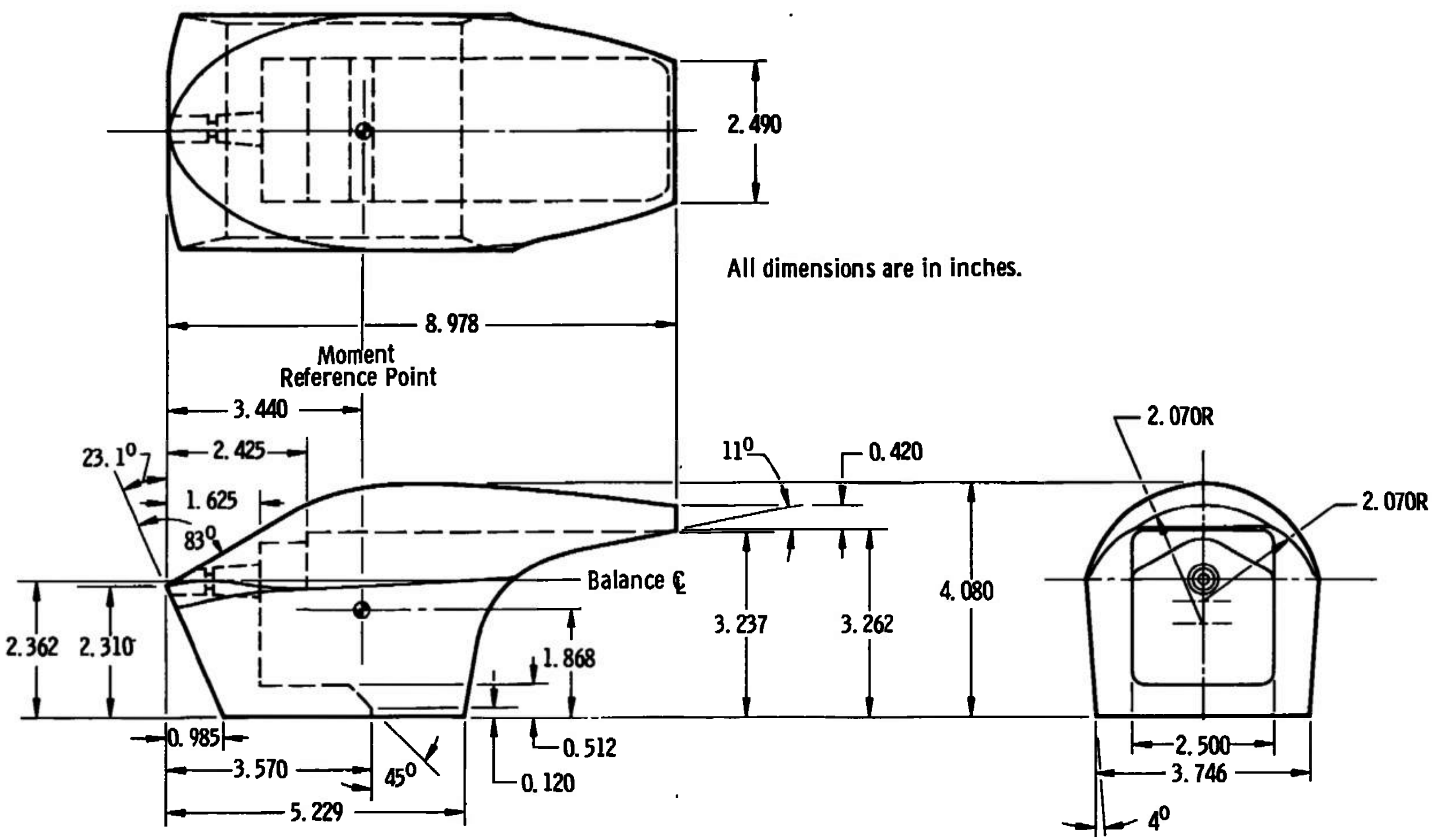

a. Capsule Details
Fig. 1 Model Details

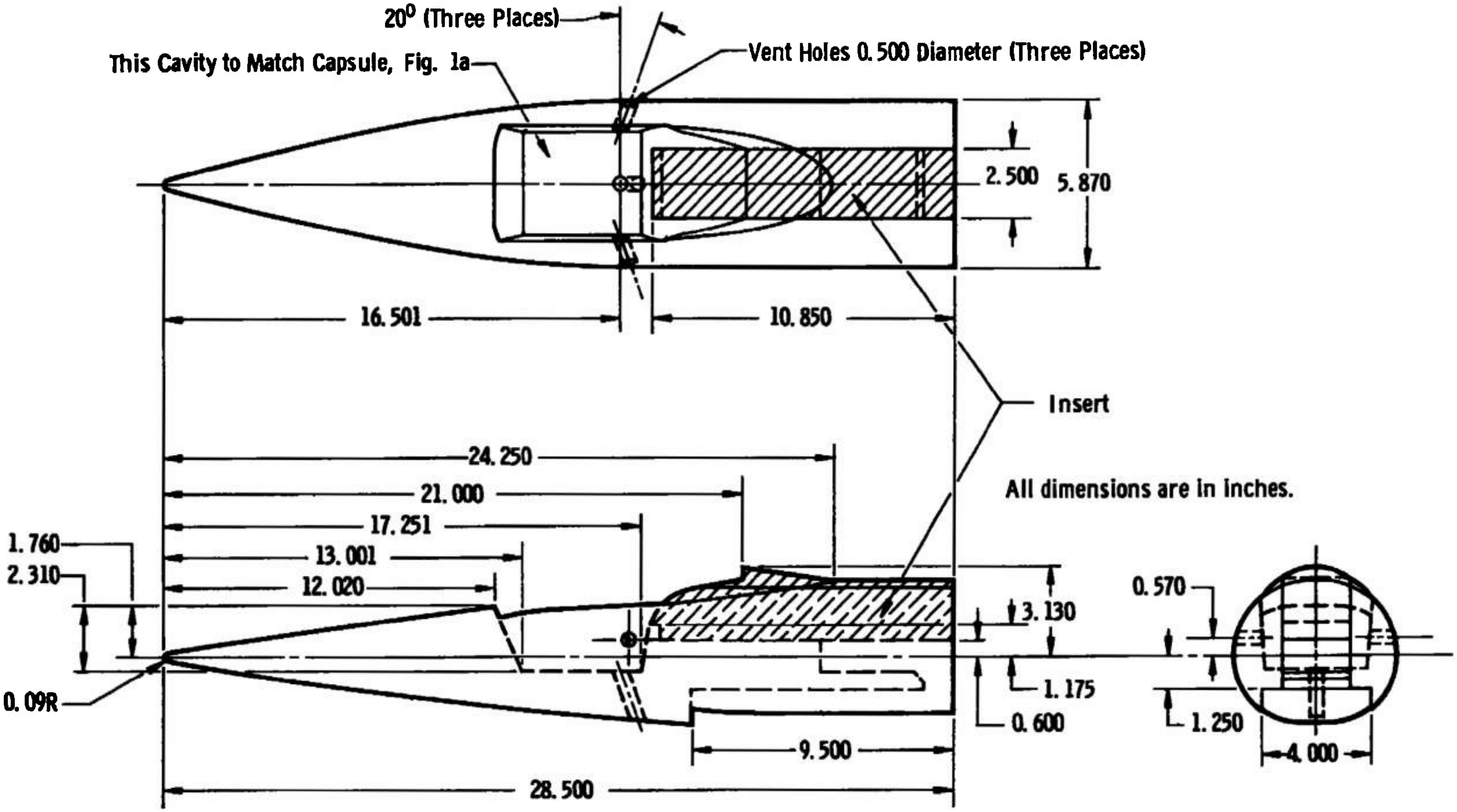

b. Fuselage Details
Fig. 1 Continued

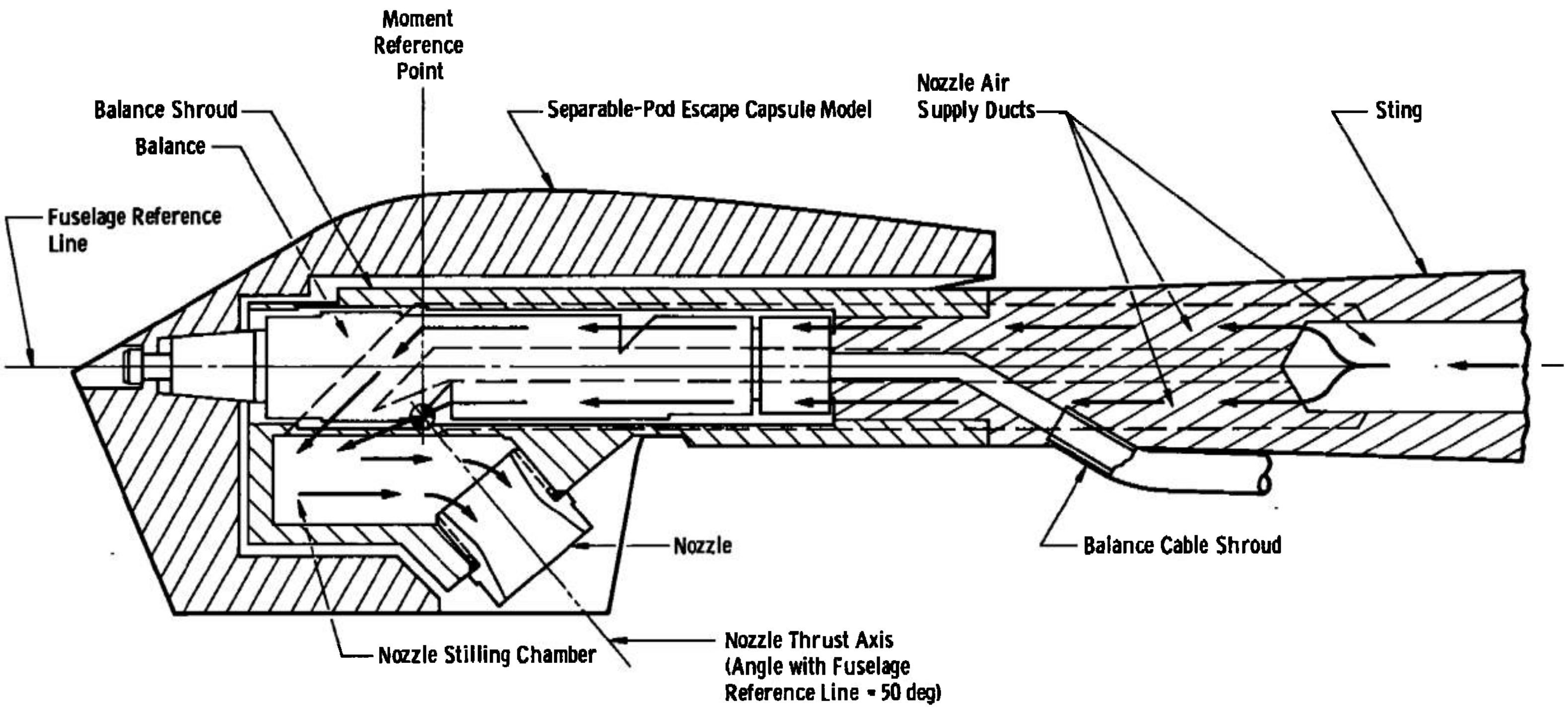

c. Capsule Installation Sketch
Fig. 1 Continued

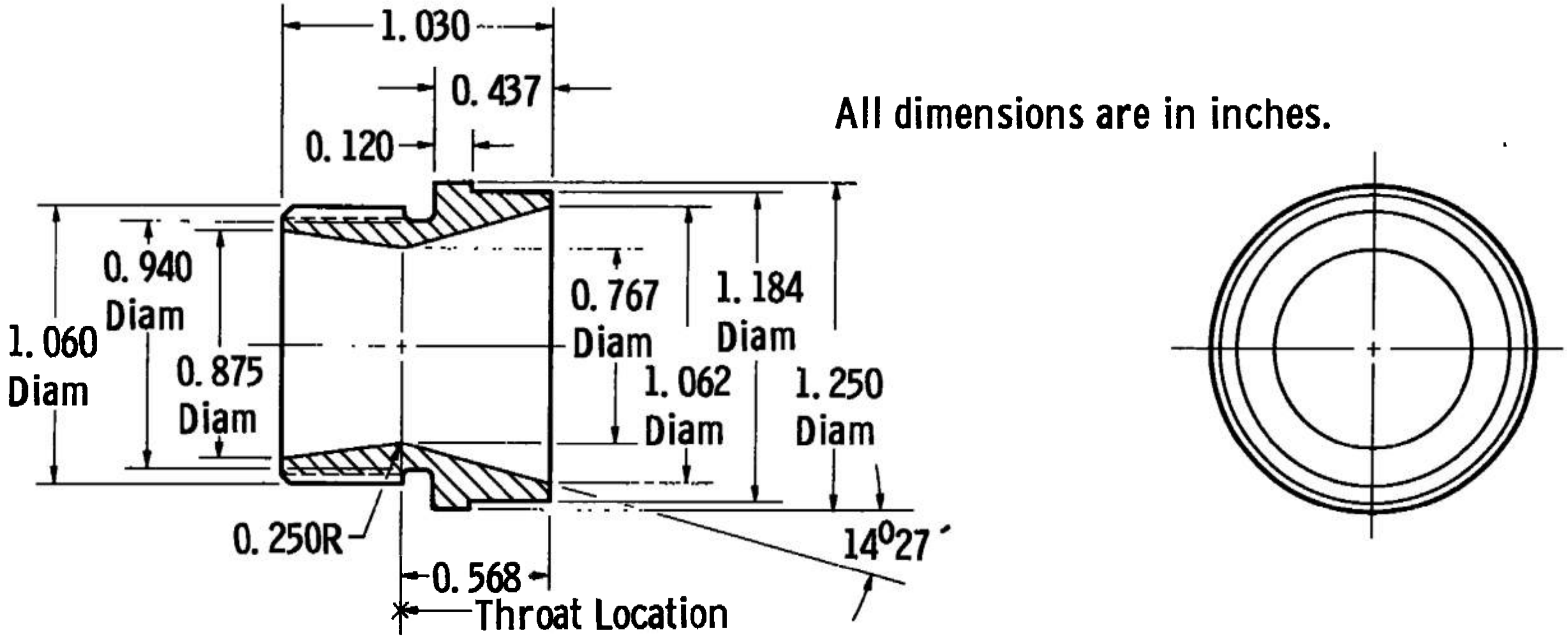

d. Nozzle Details
Fig. 1 Concluded

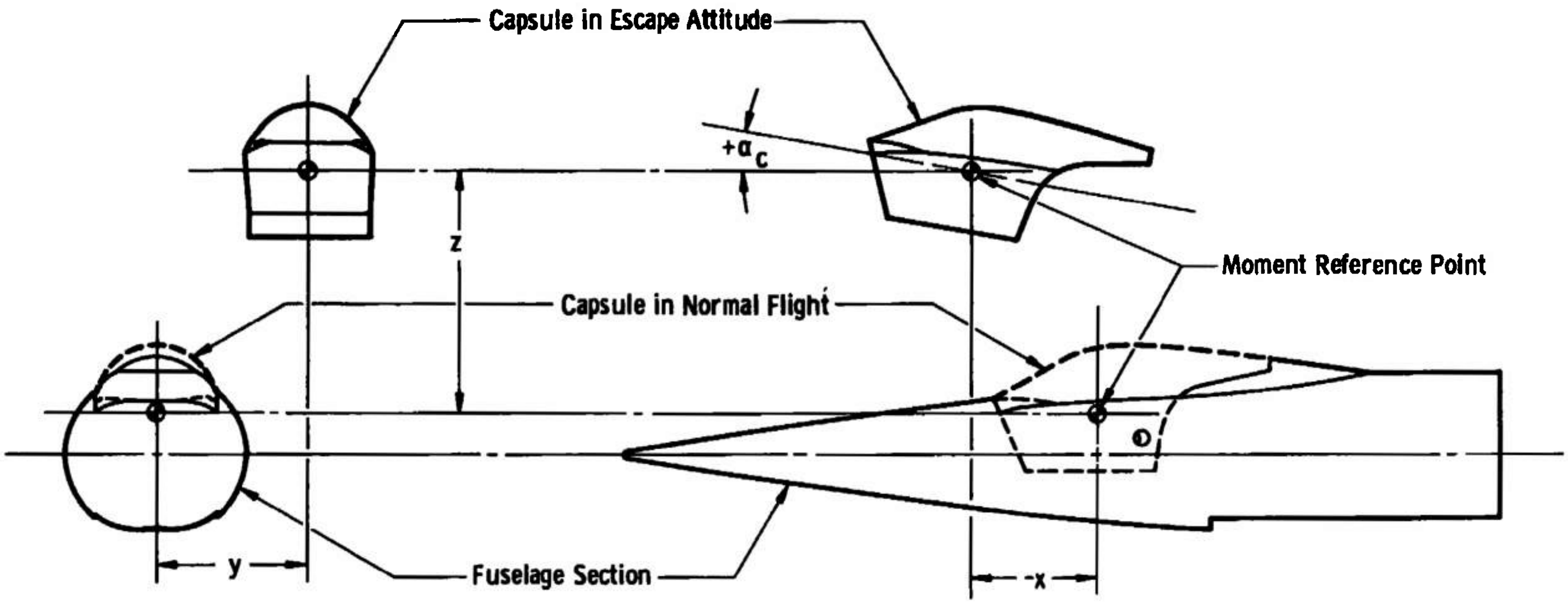

a. Pitch Plane

Fig. 2 Capsule and Fuselage Proximity Details

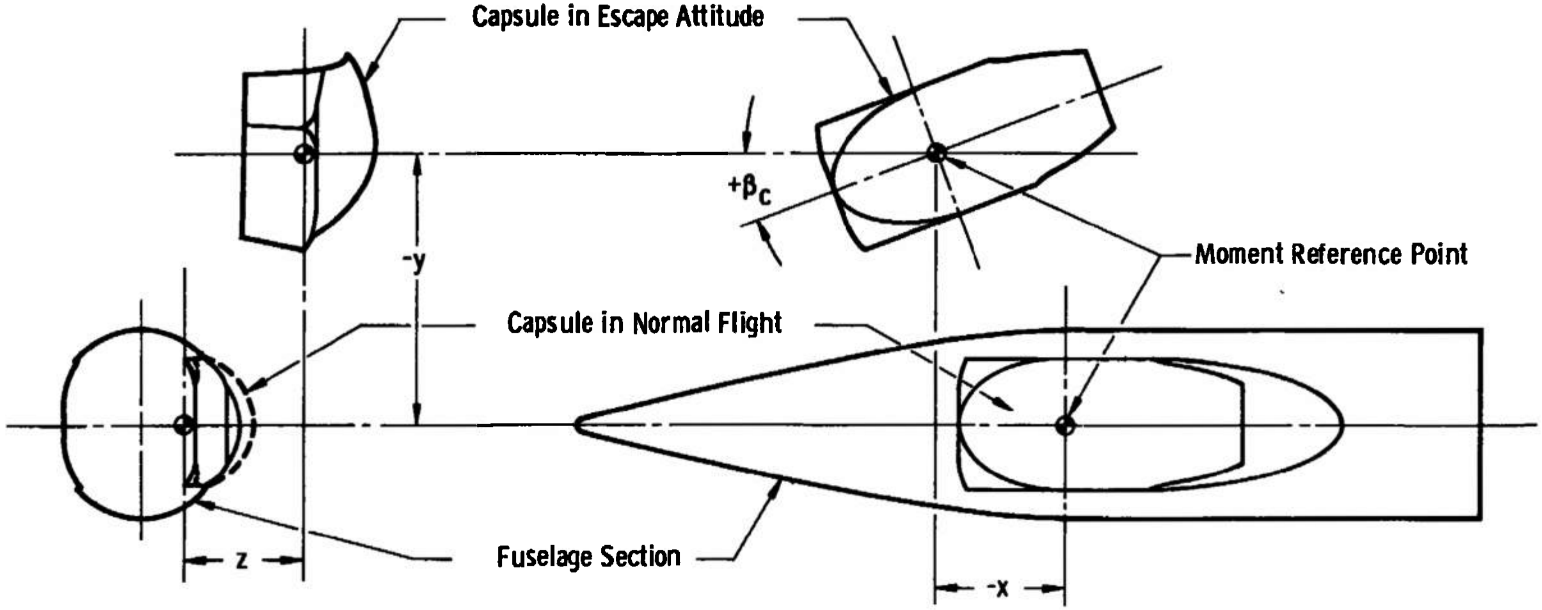

b. Yaw Plane
Fig. 2 Concluded

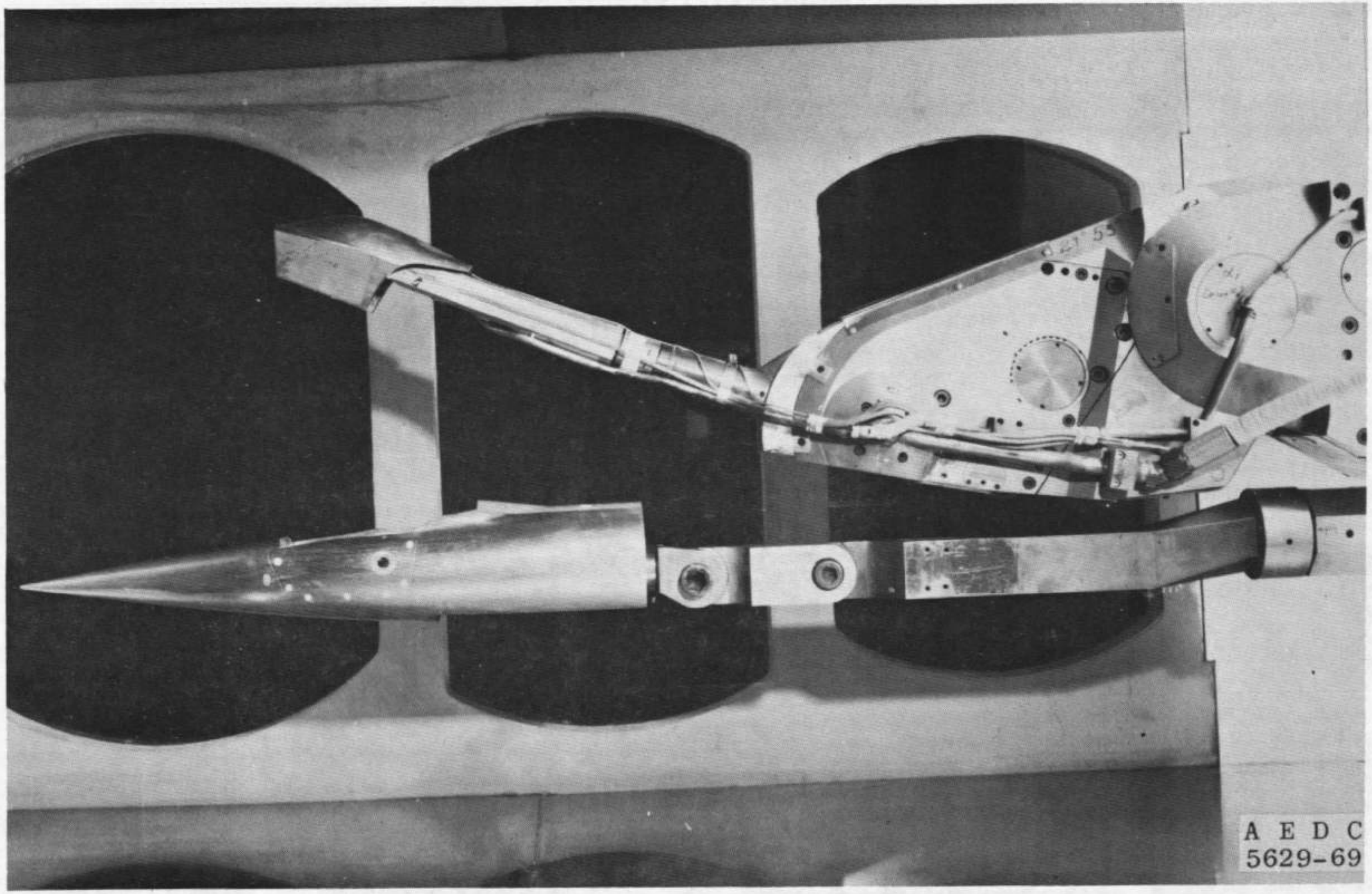

a. Capsule Pitch Installation
Fig. 3 Installation Photographs

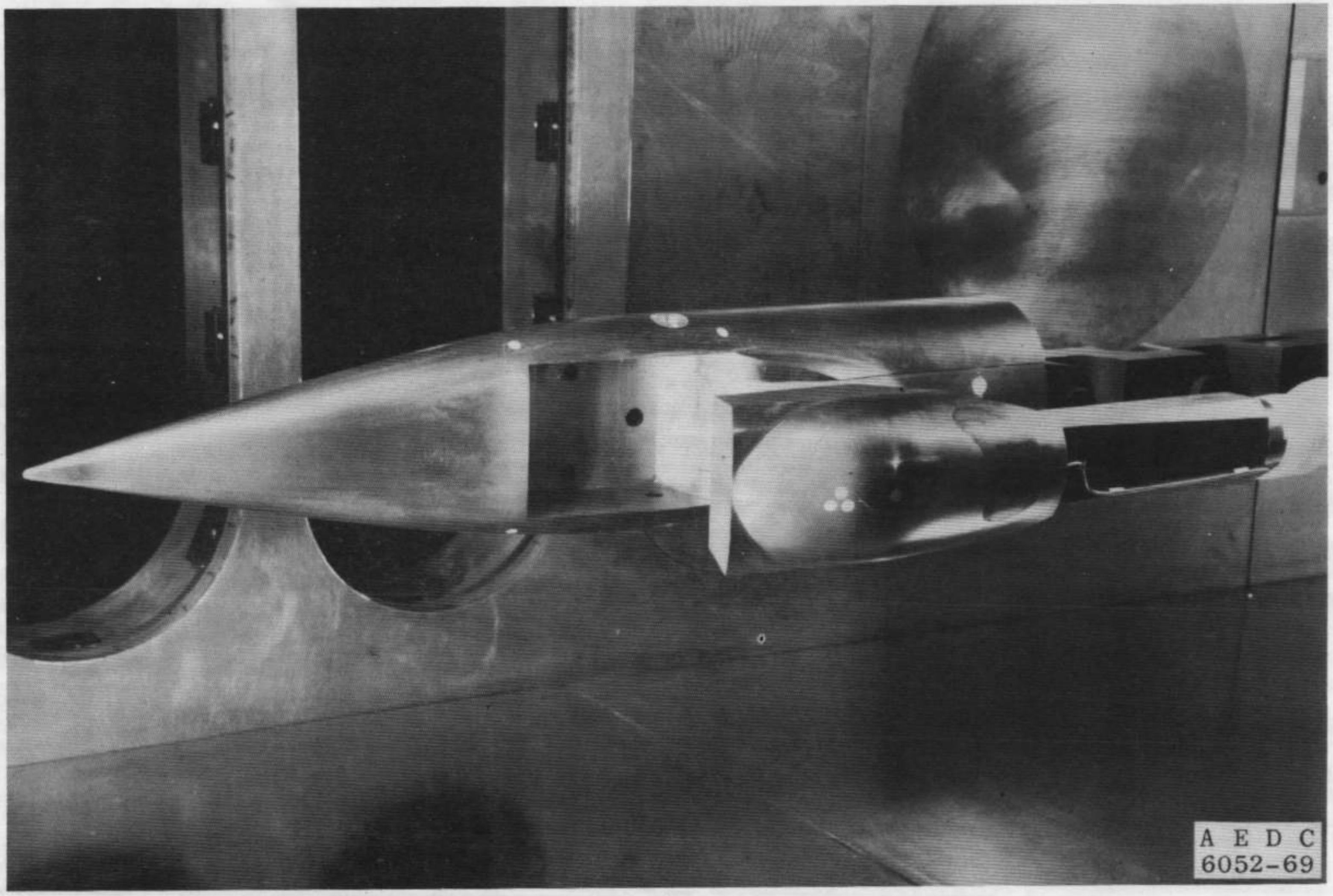

b. Capsule Sideslip Installation
Fig. 3 Concluded

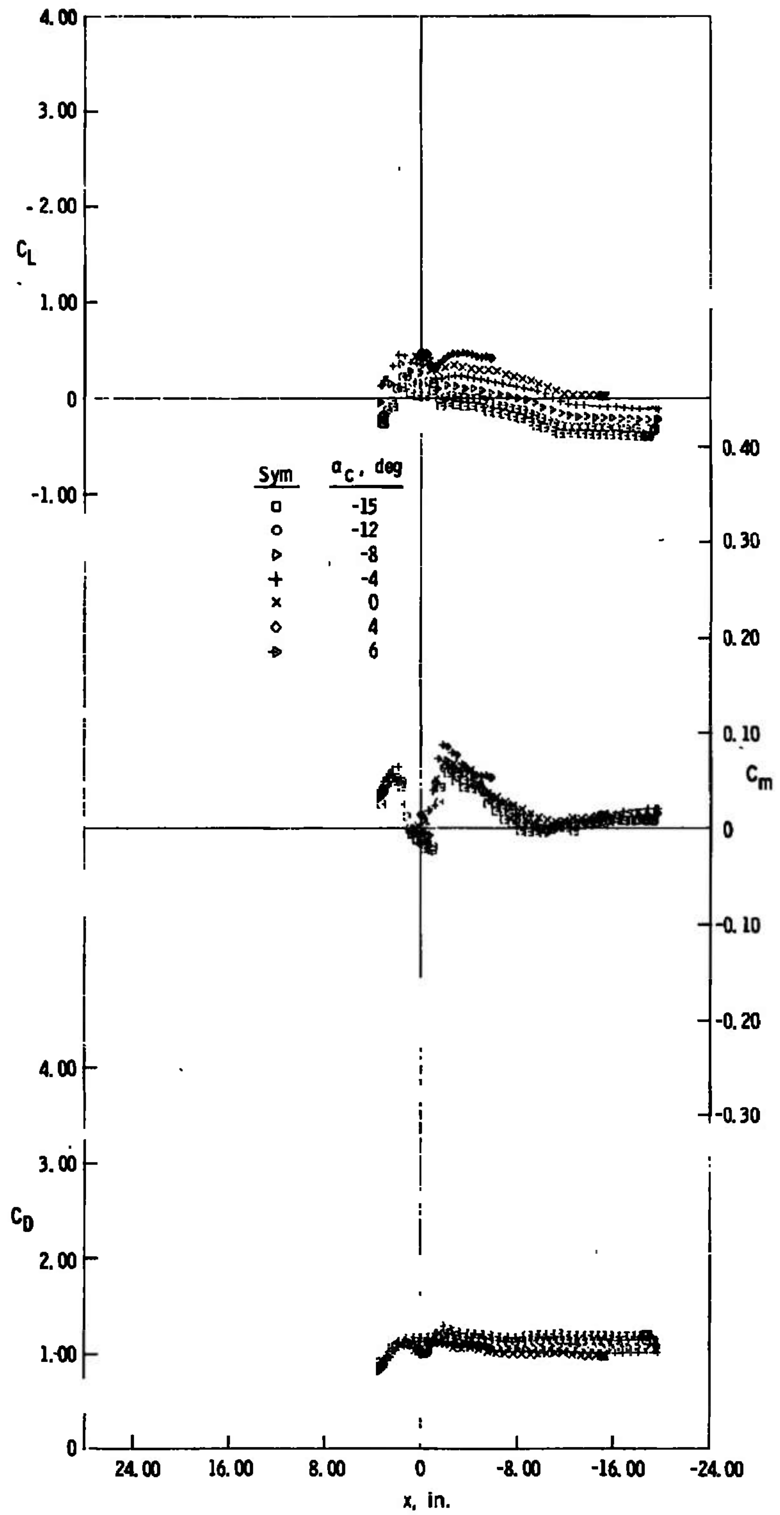

a. z = 3 in., y = 0

Fig. 4 Lift, Pitching-Moment, and Drag Characteristics of the Capsule, Jet Off, M_∞ = 2

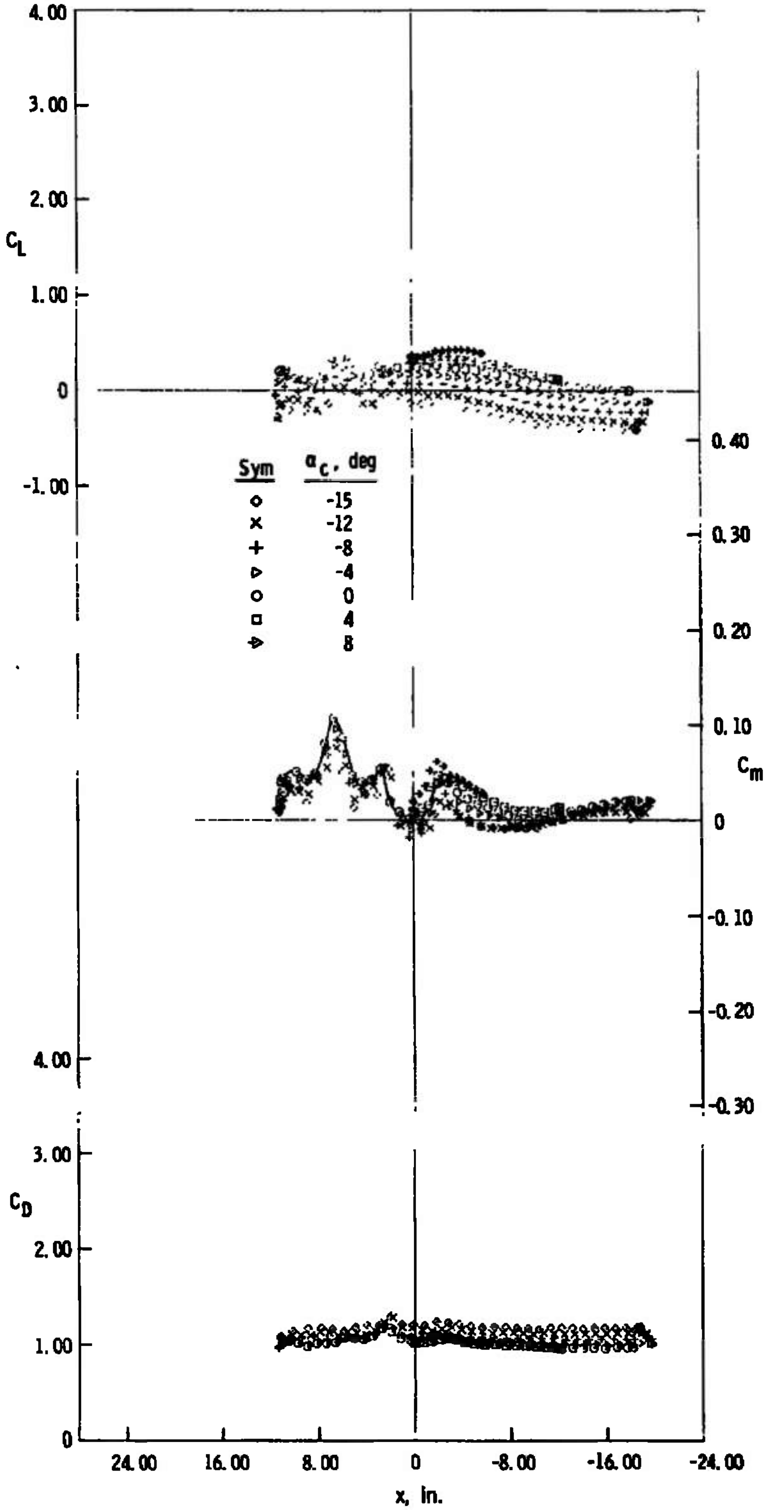

b. z = 4 in., y = 0

Fig. 4 Continued

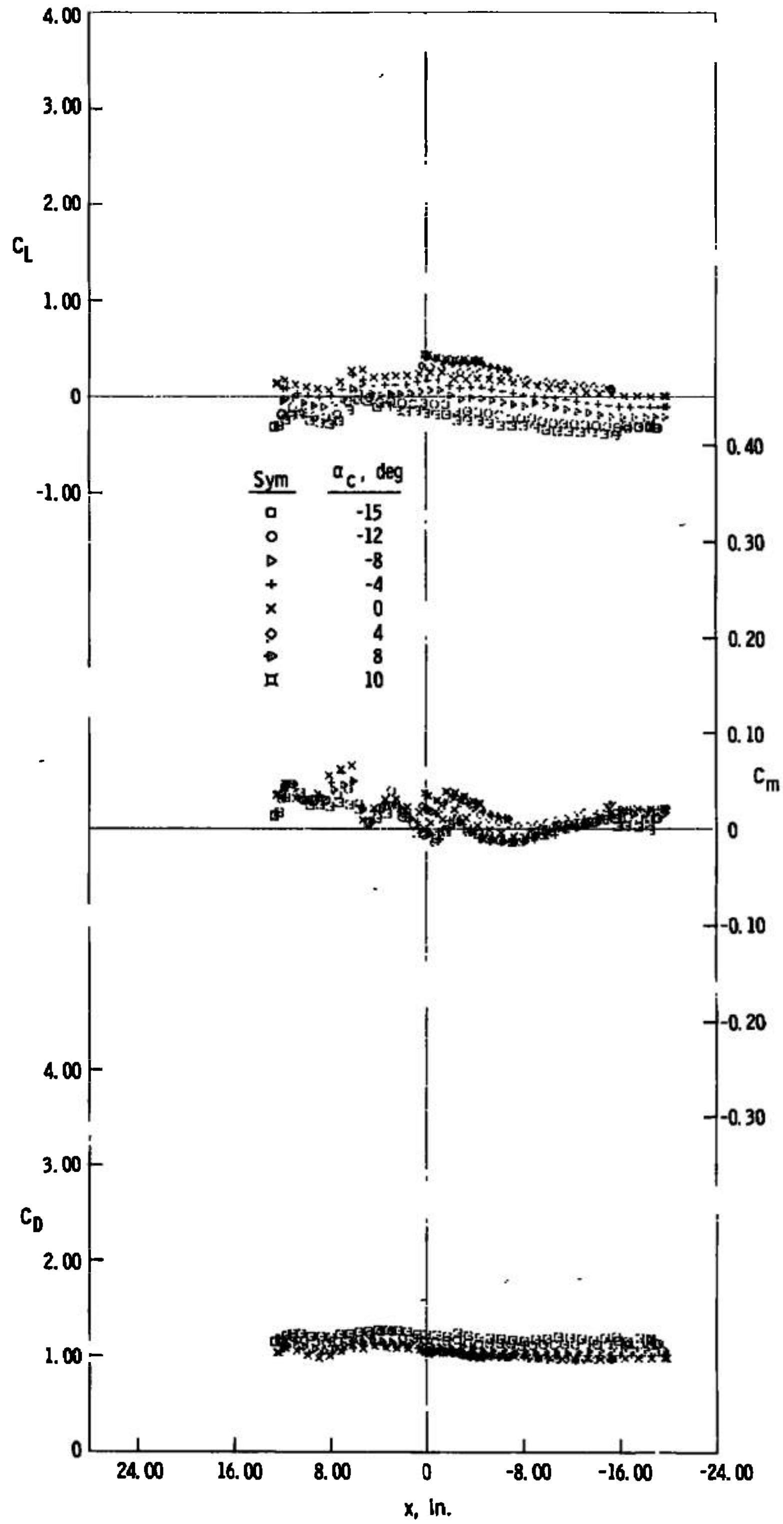

c. z = 5 in., y = 0
Fig. 4 Continued

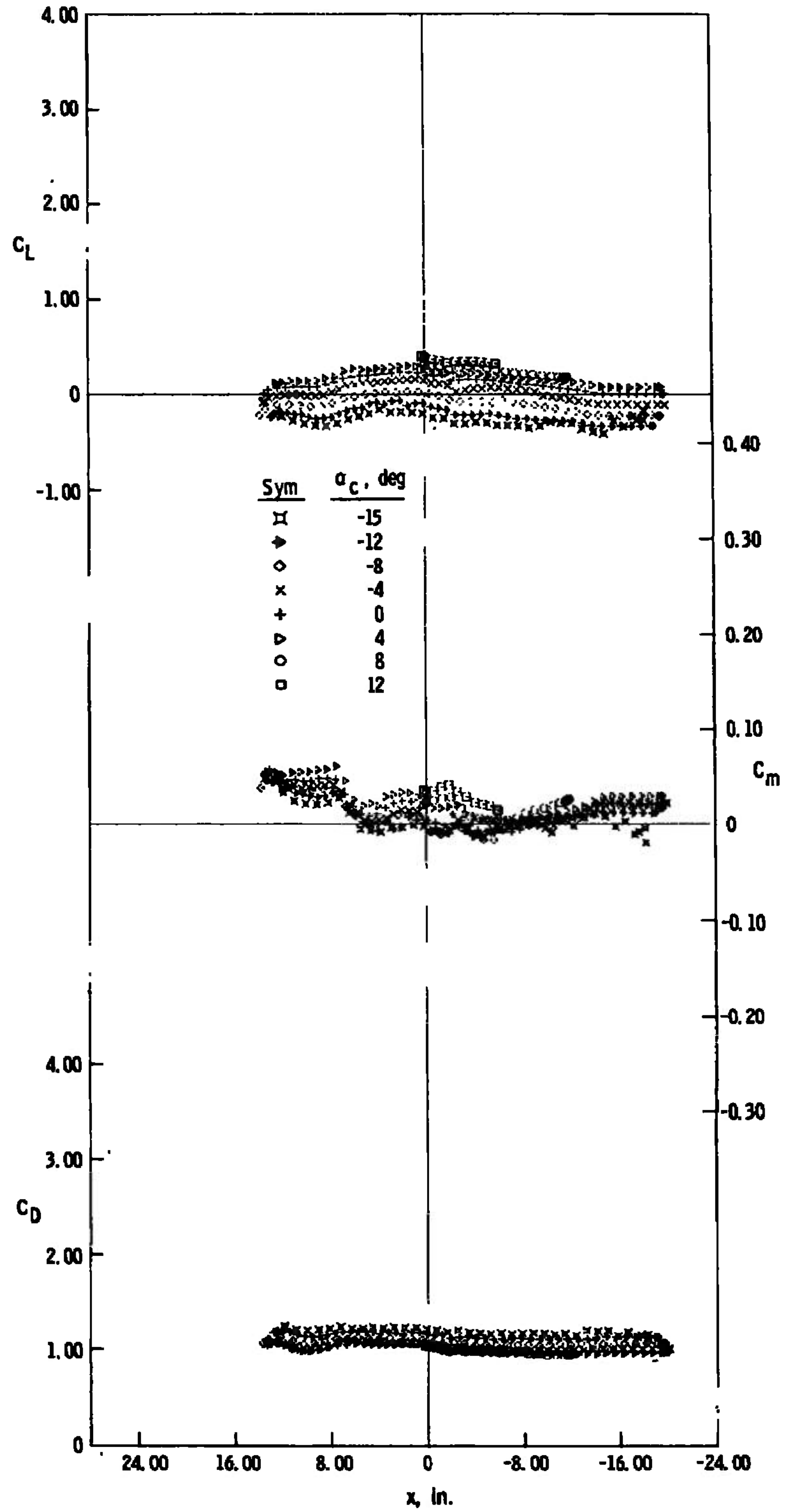

d. z = 6 in., y = 0
Fig. 4 Continued

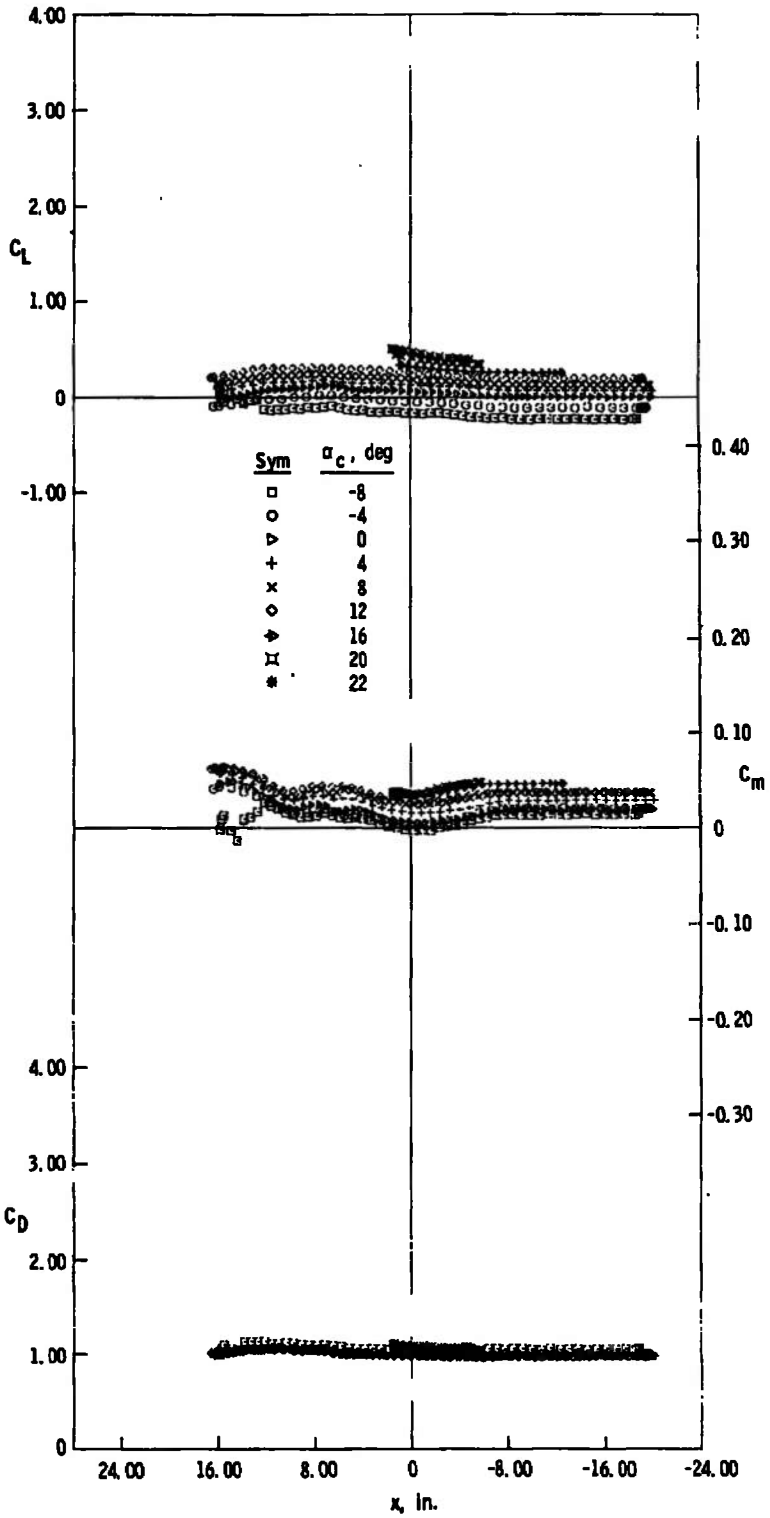

e. z = 10 in., y = 0

Fig. 4 Continued

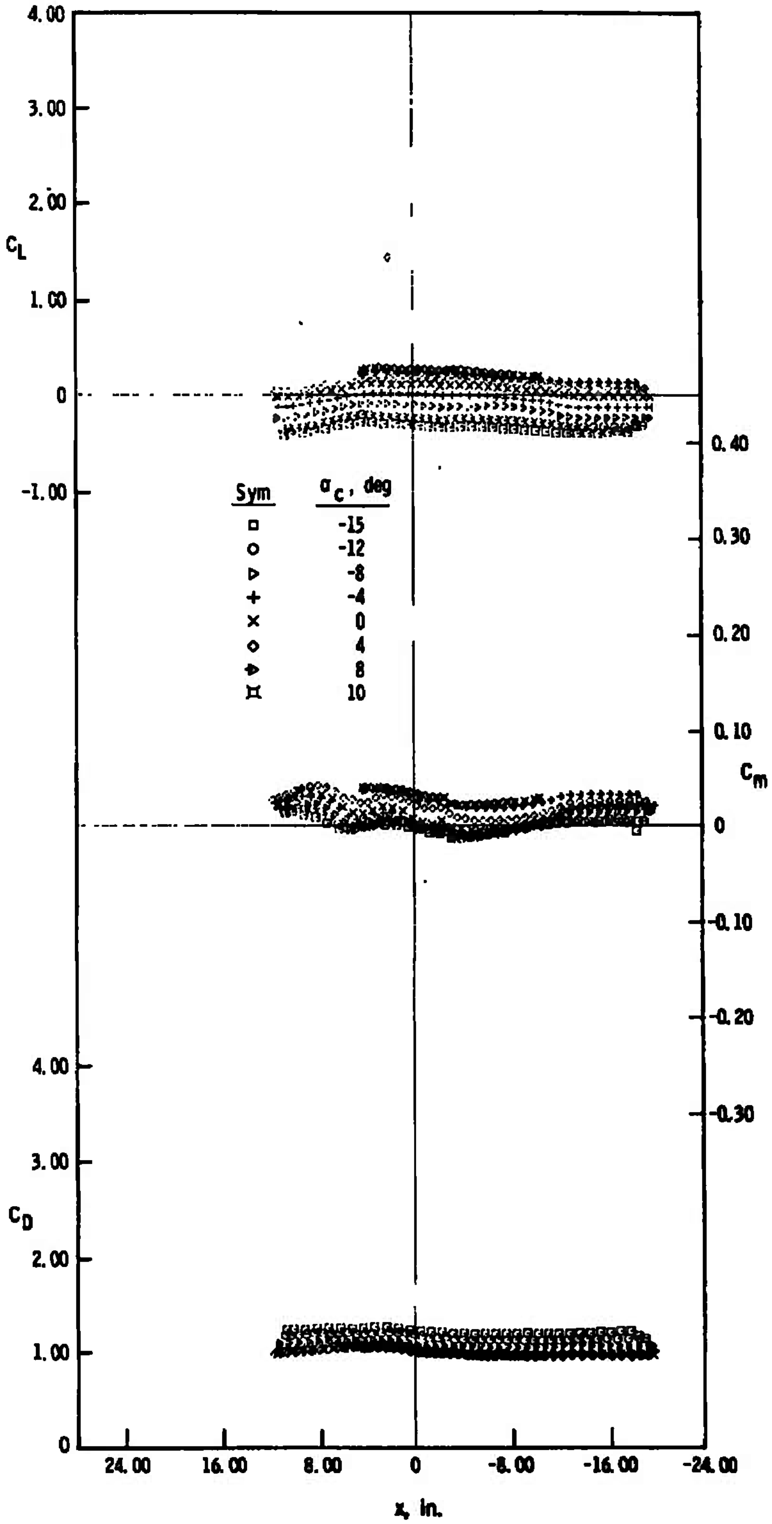

f. z = 5 in., y = 5 in.
Fig. 4 Concluded

a. α_c = –4 deg
y = 0
z = 3 in.
x = 2.1 in.

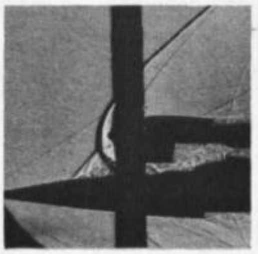

b. α_c = 0
y = 0
z = 3 in.
x = –1.0 in.

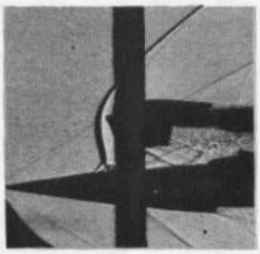

c. α_c = 0
y = 0
z = 4 in.
x = –2.2 in.

d. α_c = –15 deg
y = 0
z = 4 in.
x = 2.2 in.

e. α_c = 0
y = 0
z = 5 in.
x = 11.5 in.

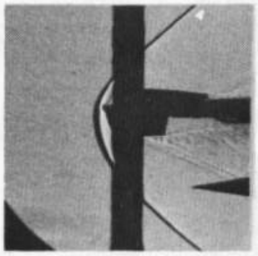

f. α_c = 0
y = 0
z = 5 in.
x = –19.5 in.

g. α_c = –8 deg
y = 0
z = 6 in.
x = 6.5 in.

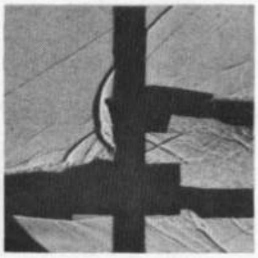

h. α_c = 4 deg
y = 0
z = 6 in.
x = 9.9 in.

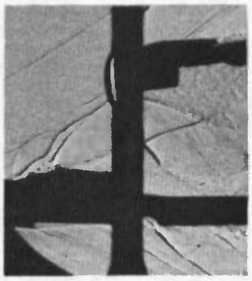

i. α_c = –8 deg
y = 0
z = 10 in.
x = 14.1 in.

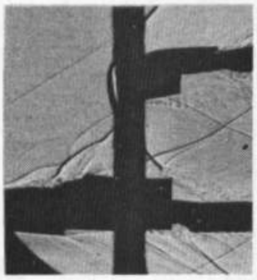

j. α_c = –8 deg
y = 0
z = 10 in.
x = 11.6 in.

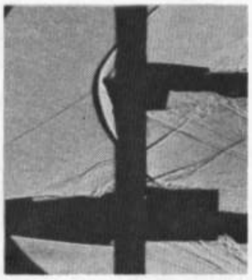

k. α_c = 0
y = 0
z = 10 in.
x = 6.4 in.

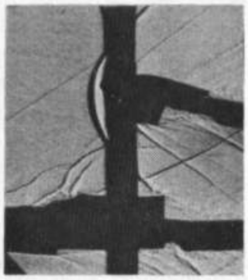

l. α_c = 12 deg
y = 0
z = 10 in.
x = 5.5 in.

Fig. 5 Schlieren Photographs, Jet Off, $M_\infty = 2$

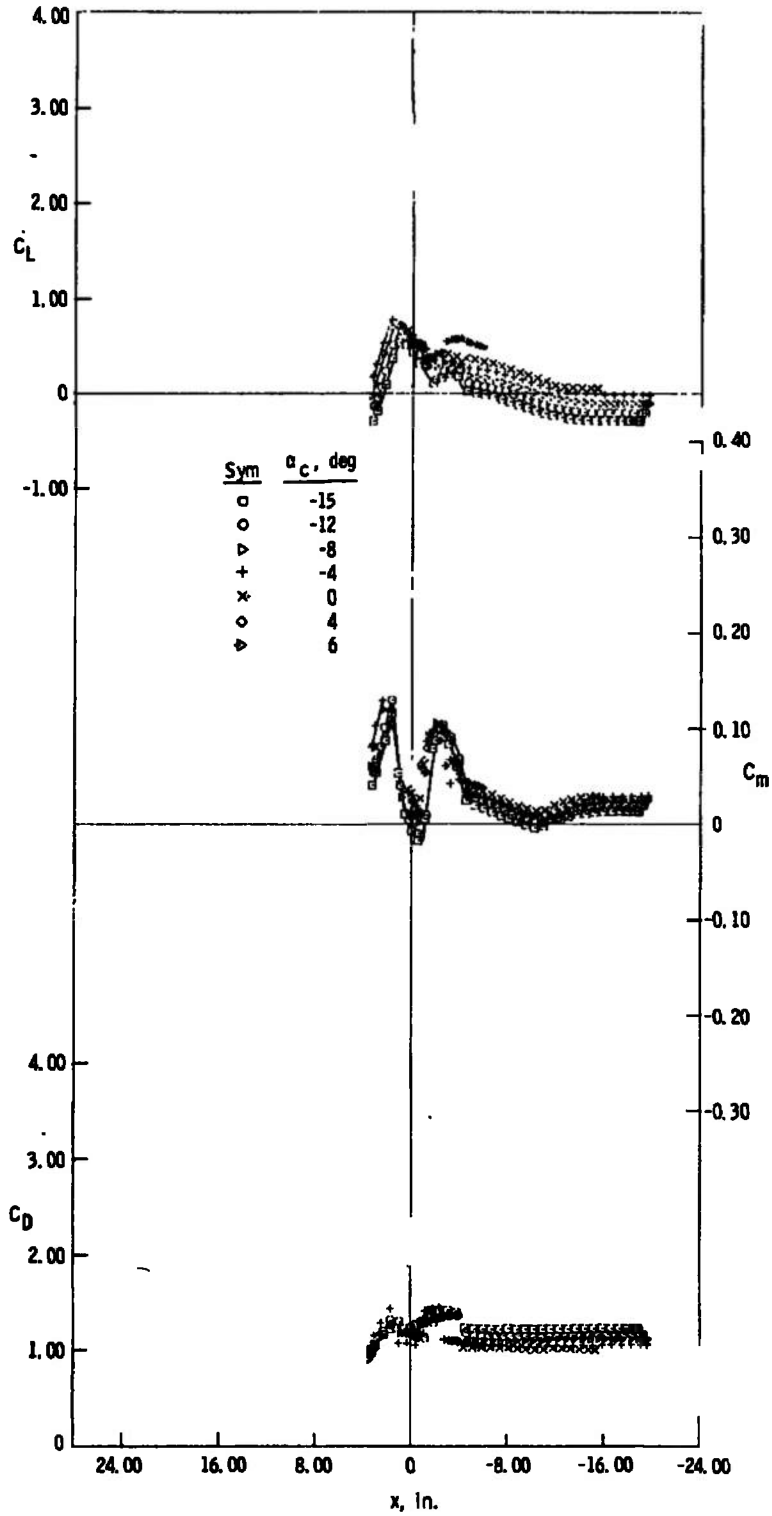

a. z = 3 in., y = 0

Fig. 6 Lift, Pitching-Moment, and Drag Characteristics of the Capsule, Jet Off, $M_\infty = 3$

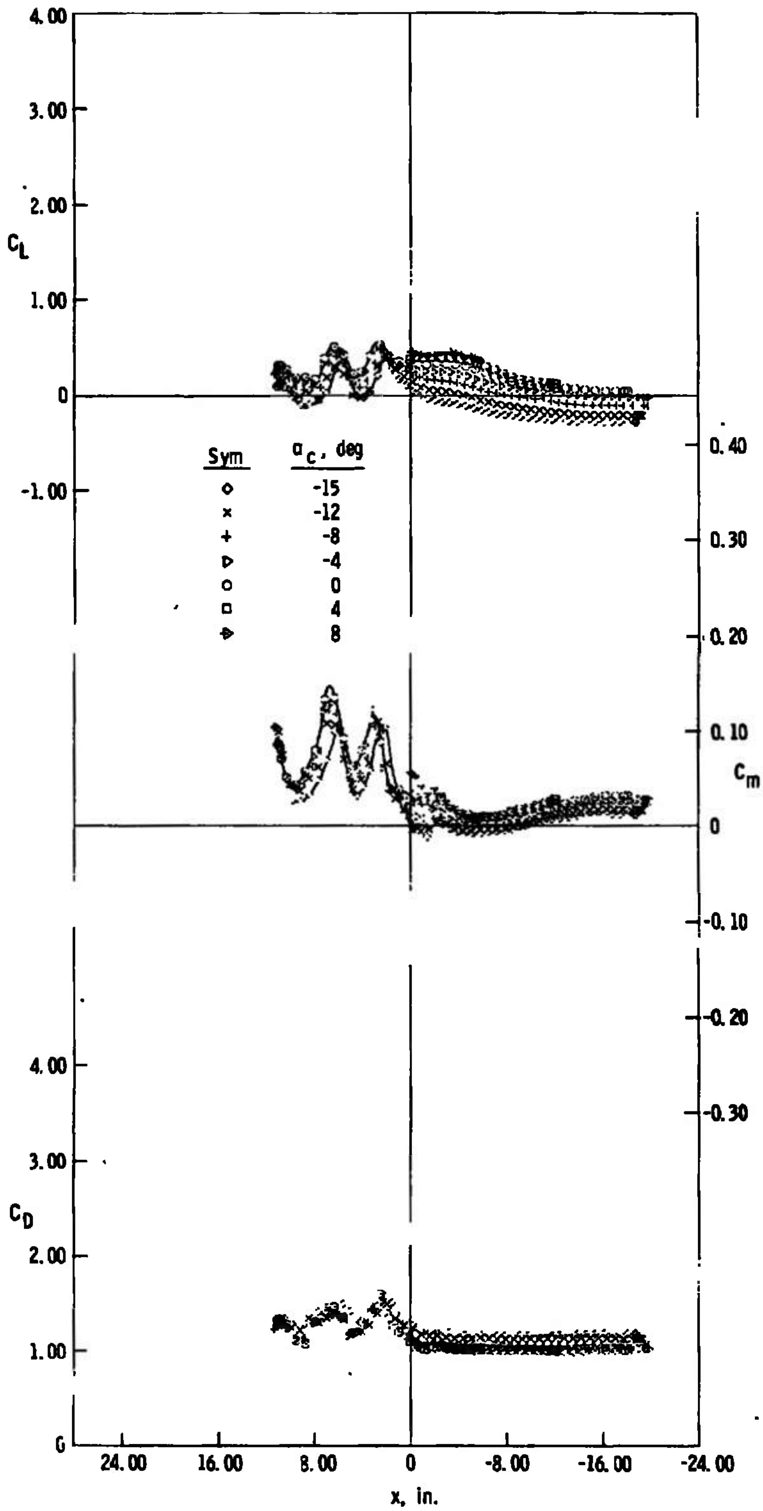

b. z = 4 in., y = 0

Fig. 6 Continued

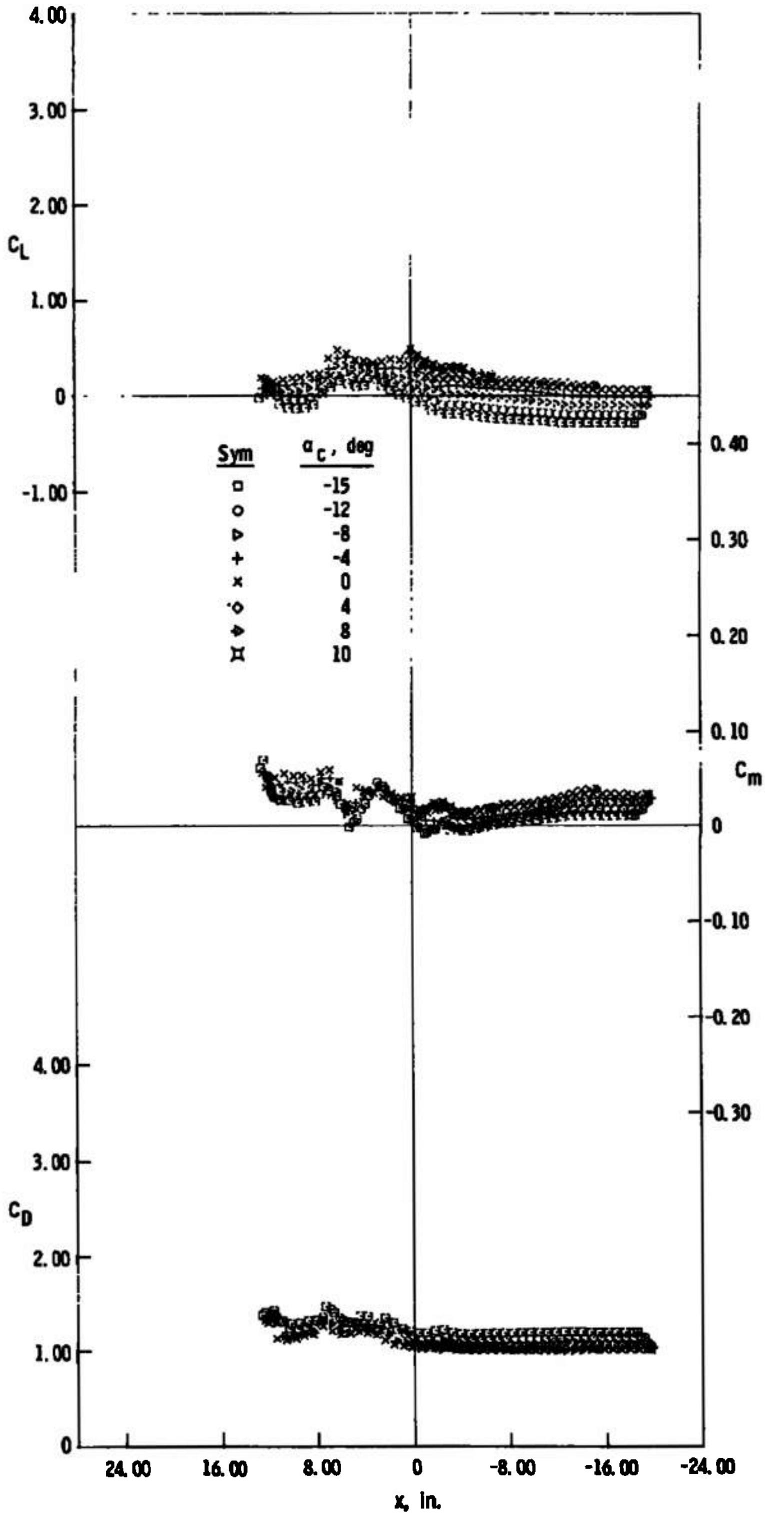

c. z = 5 in., y = 0
Fig. 6 Continued

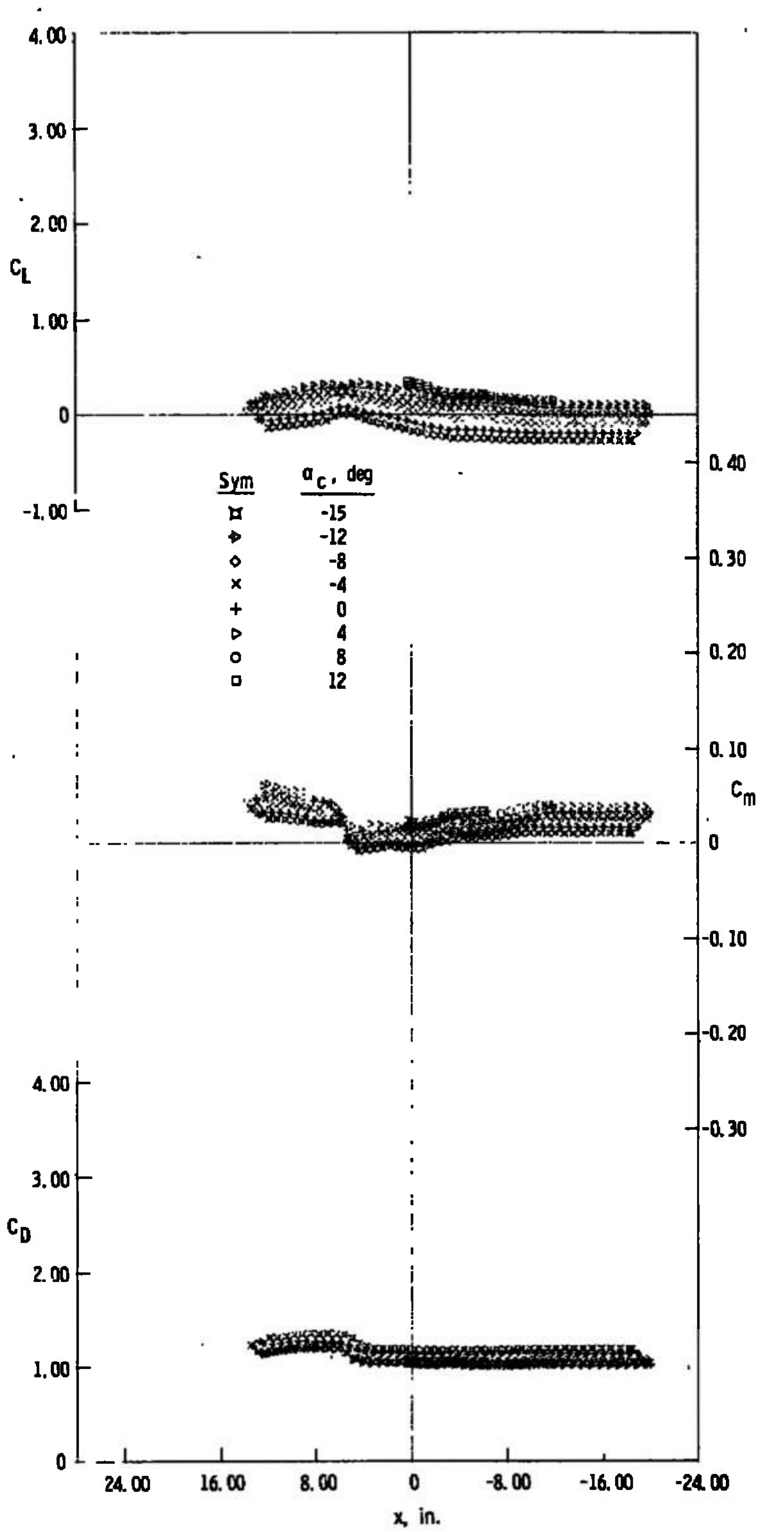

d. $z = 6$ in., $y = 0$
Fig. 6 Continued

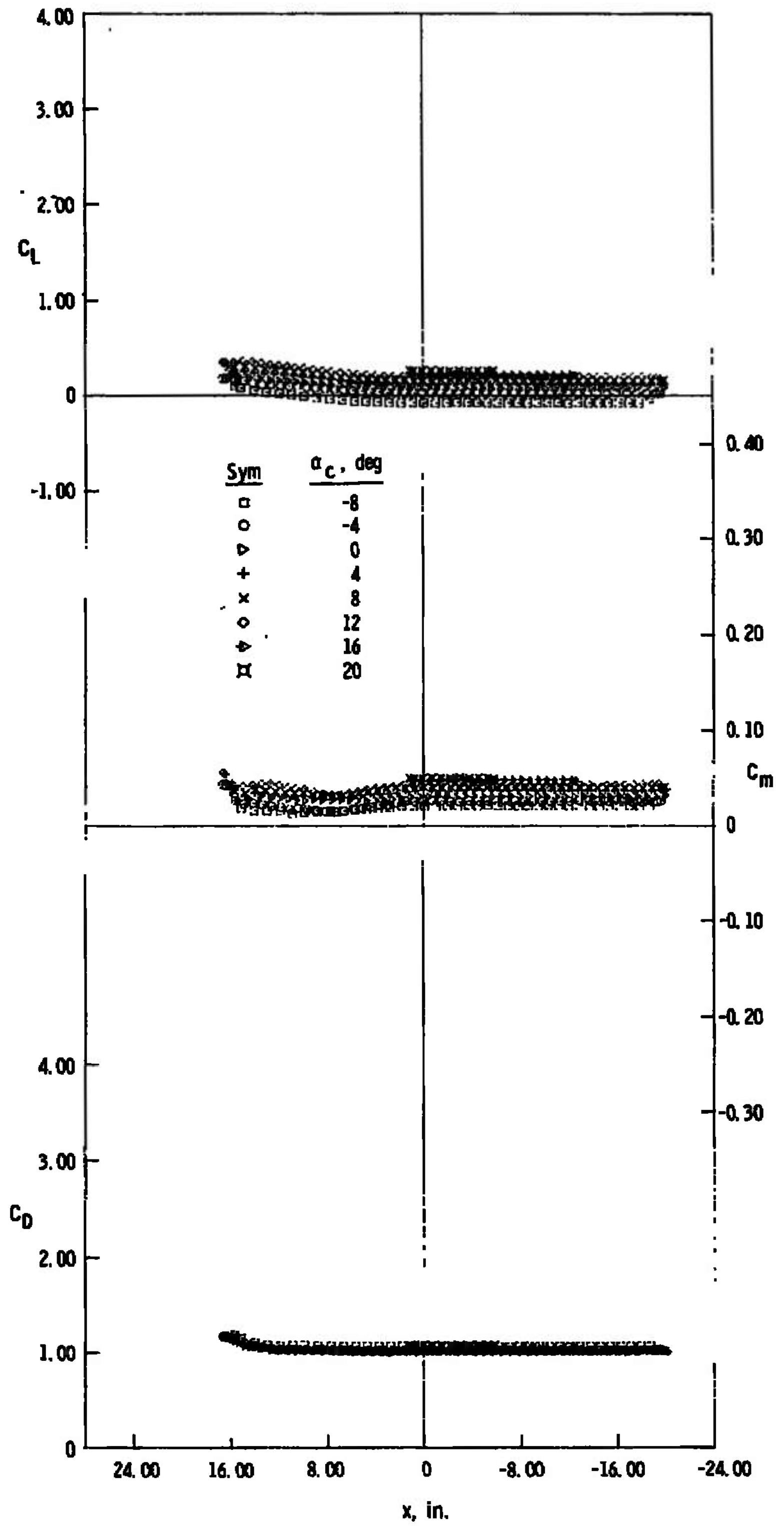

e. z = 10 in., y = 0
Fig. 6 Continued

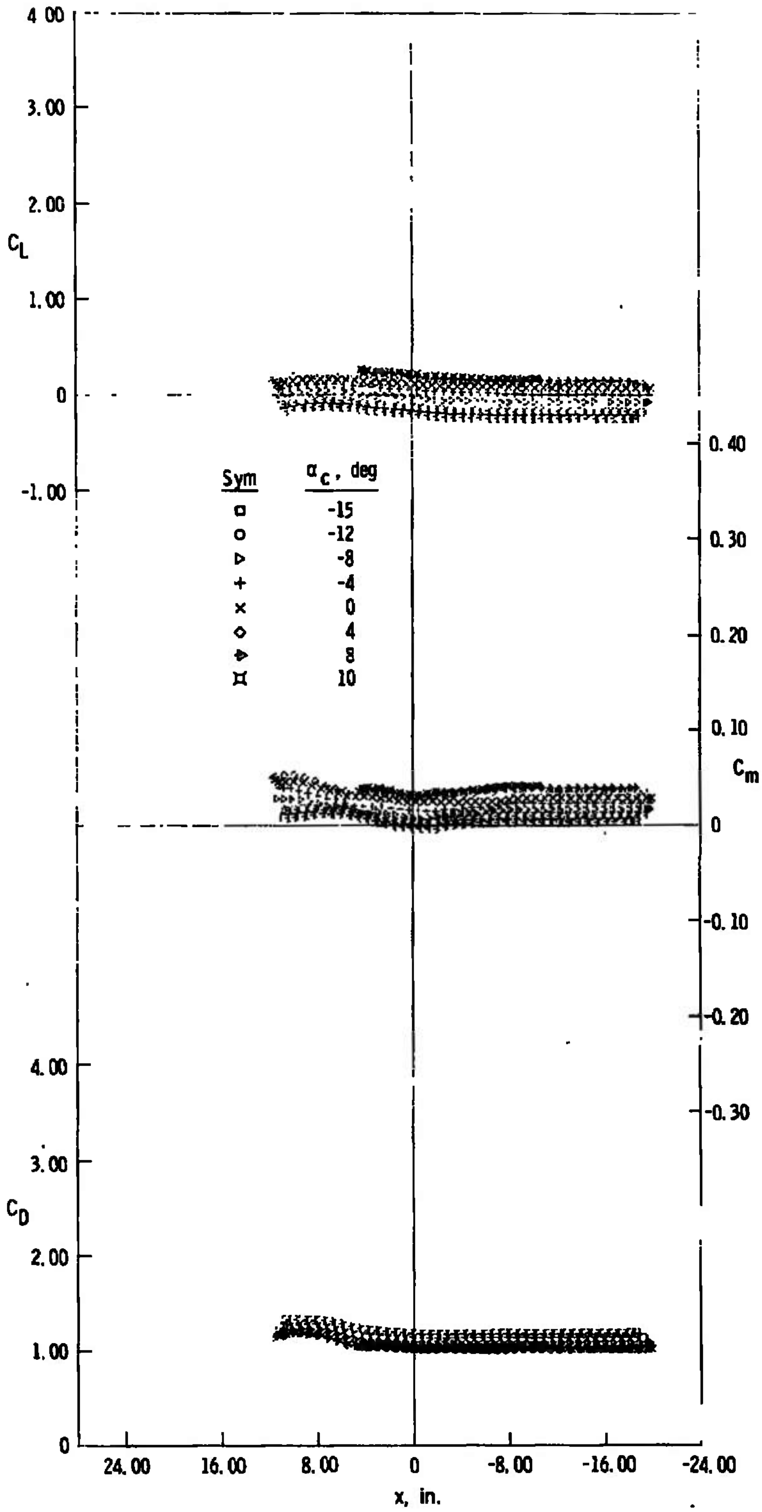

f. z = 5 in., y = 5 in.
Fig. 6 Concluded

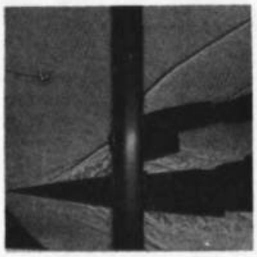

a. $\alpha_c = -15$ deg
$y = 0$
$z = 3$ in.
$x = -2.5$ in.

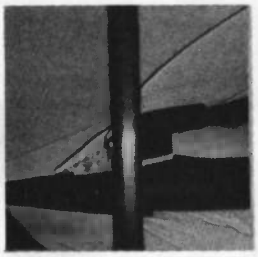

b. $\alpha_c = -12$ deg
$y = 0$
$z = 3$ in.
$x = 3.2$ in.

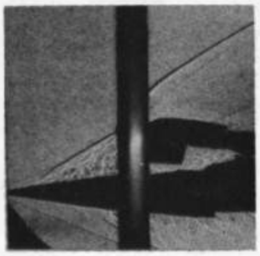

c. $\alpha_c = 4$ deg
$y = 0$
$z = 3$ in.
$x = -0.7$ in.

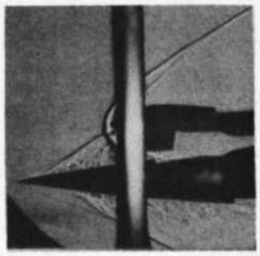

d. $\alpha_c = 0$ deg
$y = 0$
$z = 3$ in.
$x = -3.5$ in.

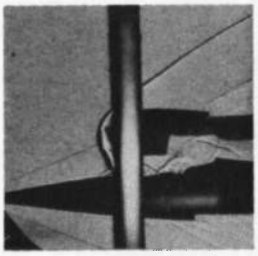

e. $\alpha_c = 0$
$y = 0$
$z = 4$ in.
$x = -0.7$ in.

f. $\alpha_c = 0$
$y = 0$
$z = 4$ in.
$x = 4.5$ in.

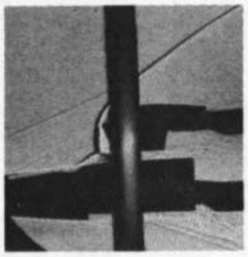

g. $\alpha_c = 0$
$y = 0$
$z = 4$ in.
$x = 8.6$ in.

h. $\alpha_c = 0$
$y = 0$
$z = 4$ in.
$x = 11.8$ in.

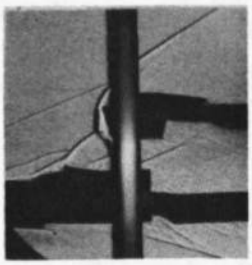

i. $\alpha_c = 4$ deg
$y = 0$
$z = 6$ in.
$x = 12.3$ in.

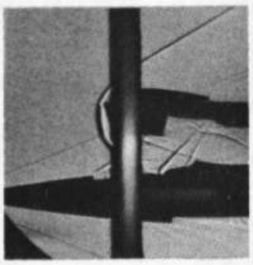

j. $\alpha_c = 4$ deg
$y = 0$
$z = 6$ in.
$x = 1.2$ in.

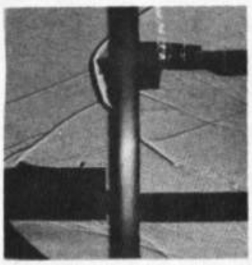

k. $\alpha_c = 0$
$y = 0$
$z = 10$ in.
$x = 15.7$ in.

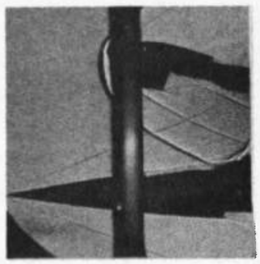

l. $\alpha_c = 12$ deg
$y = 0$
$z = 10$ in.
$x = -2.5$ in.

Fig. 7 Schlieren Photographs, Jet Off, $M_\infty = 3$

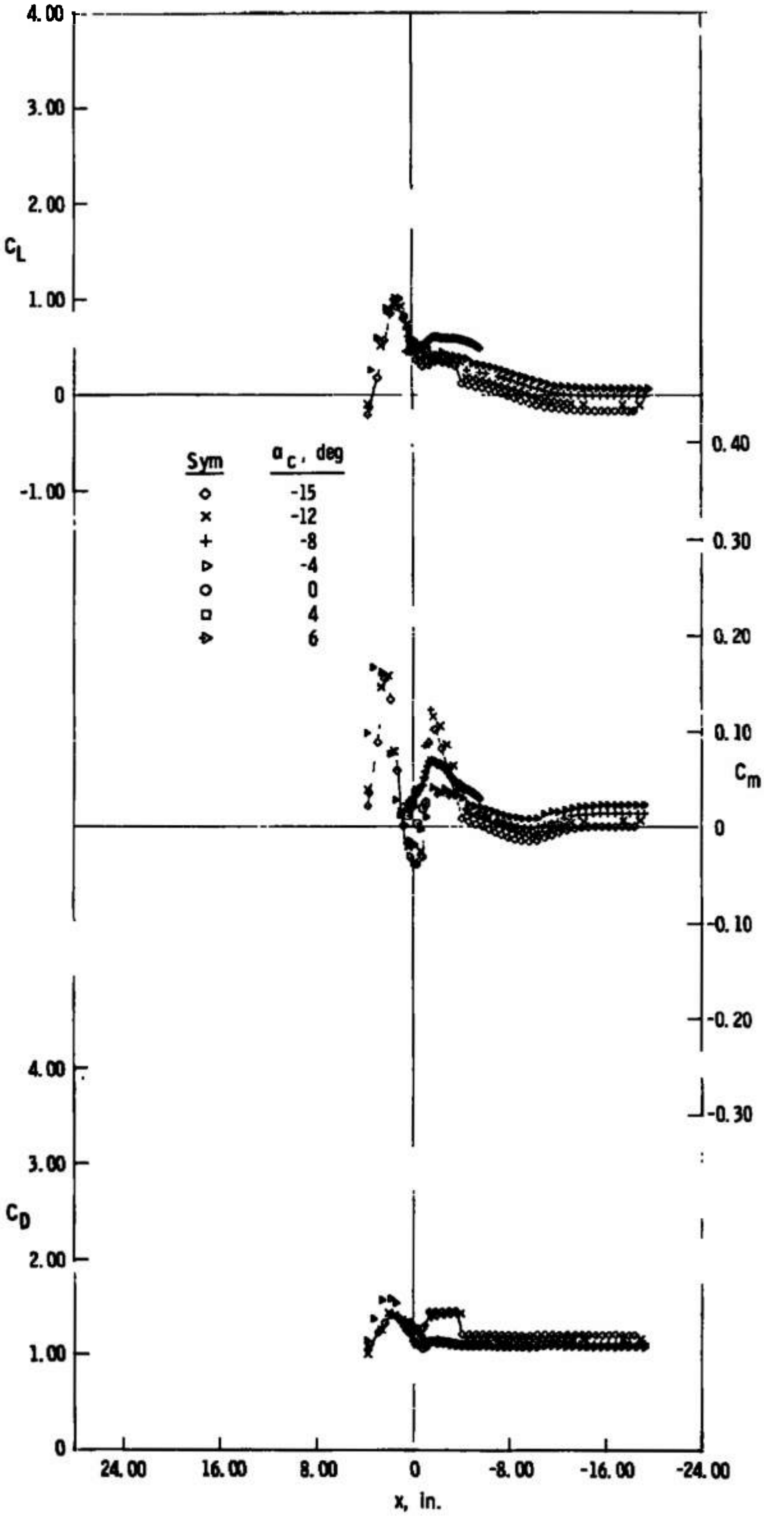

a. $z = 3$ in., $y = 0$

Fig. 8 Lift, Pitching-Moment, and Drag Characteristics of the Capsule, Jet Off, $M_\infty = 4$

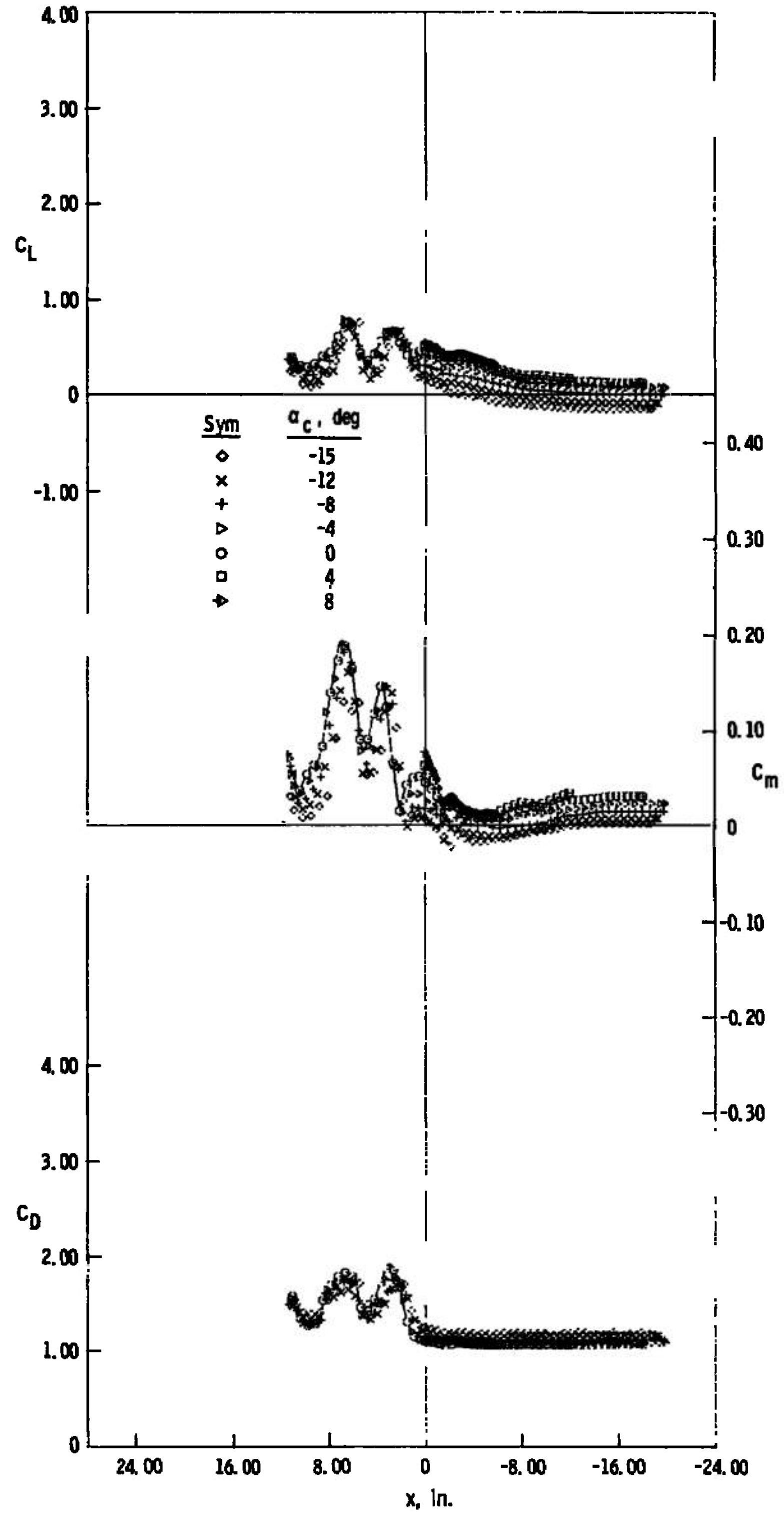

b. z = 4 in., y = 0

Fig. 8 Continued

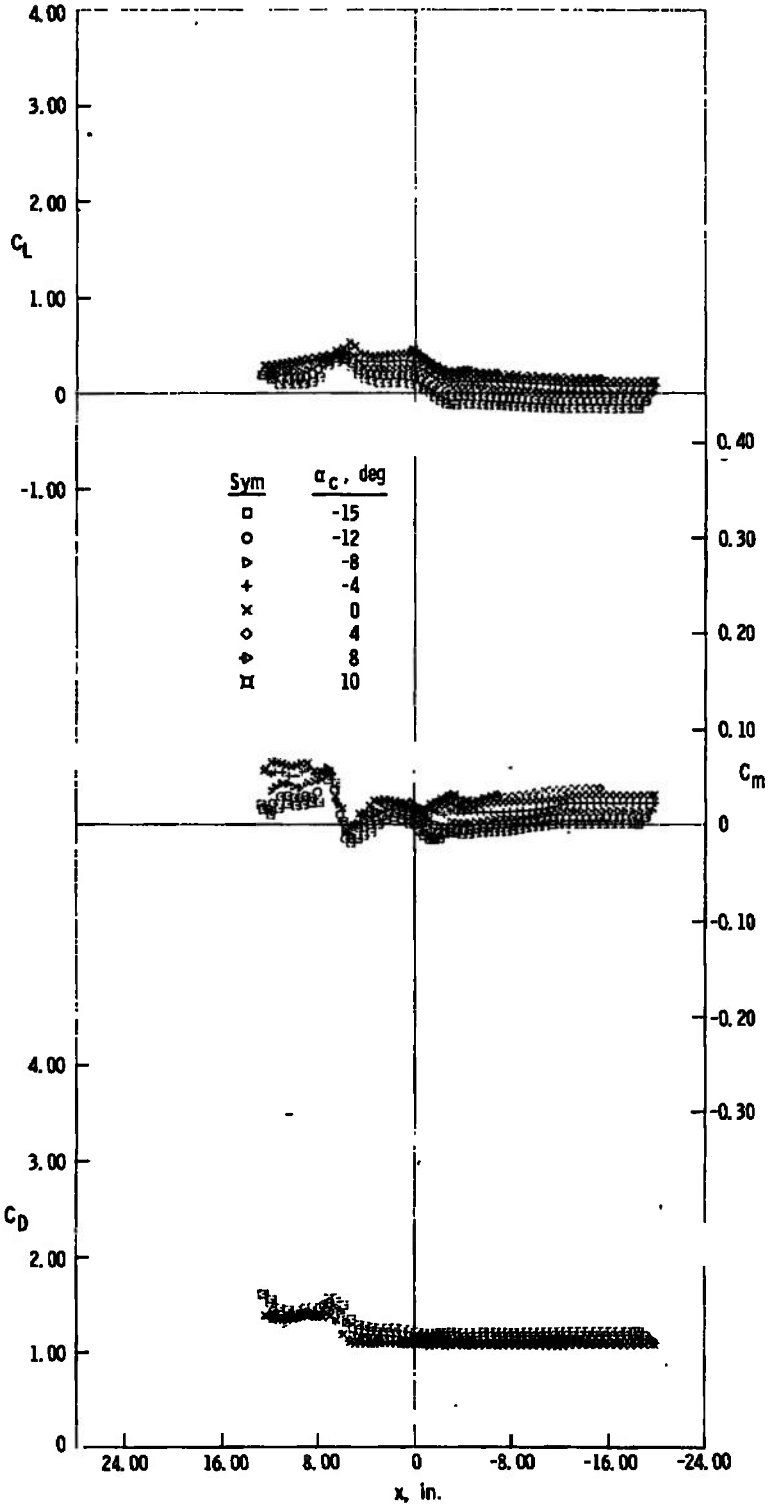

c. z = 5 in., y = 0

Fig. 8 Continued

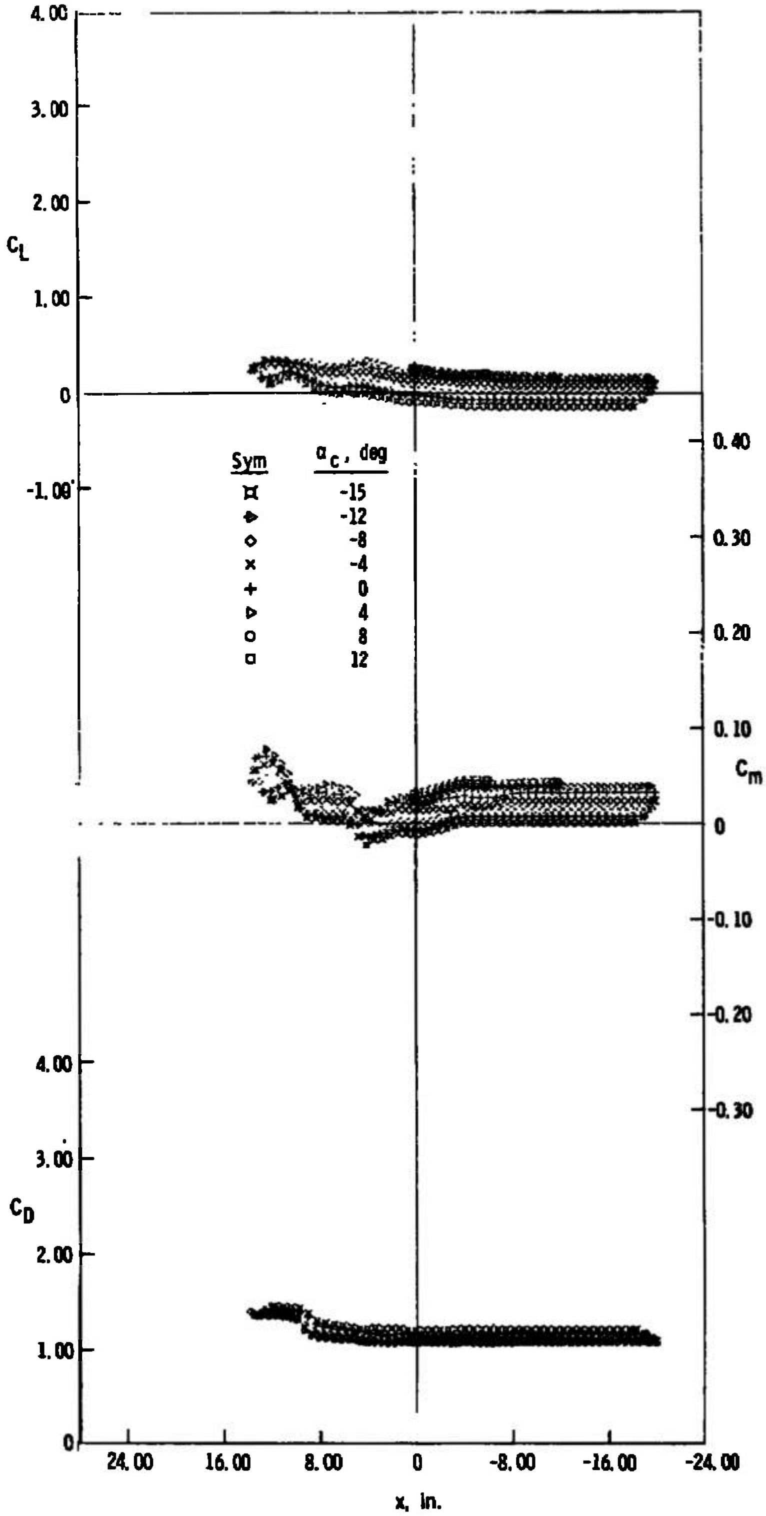

d. $z = 6$ in., $y = 0$
Fig. 8 Continued

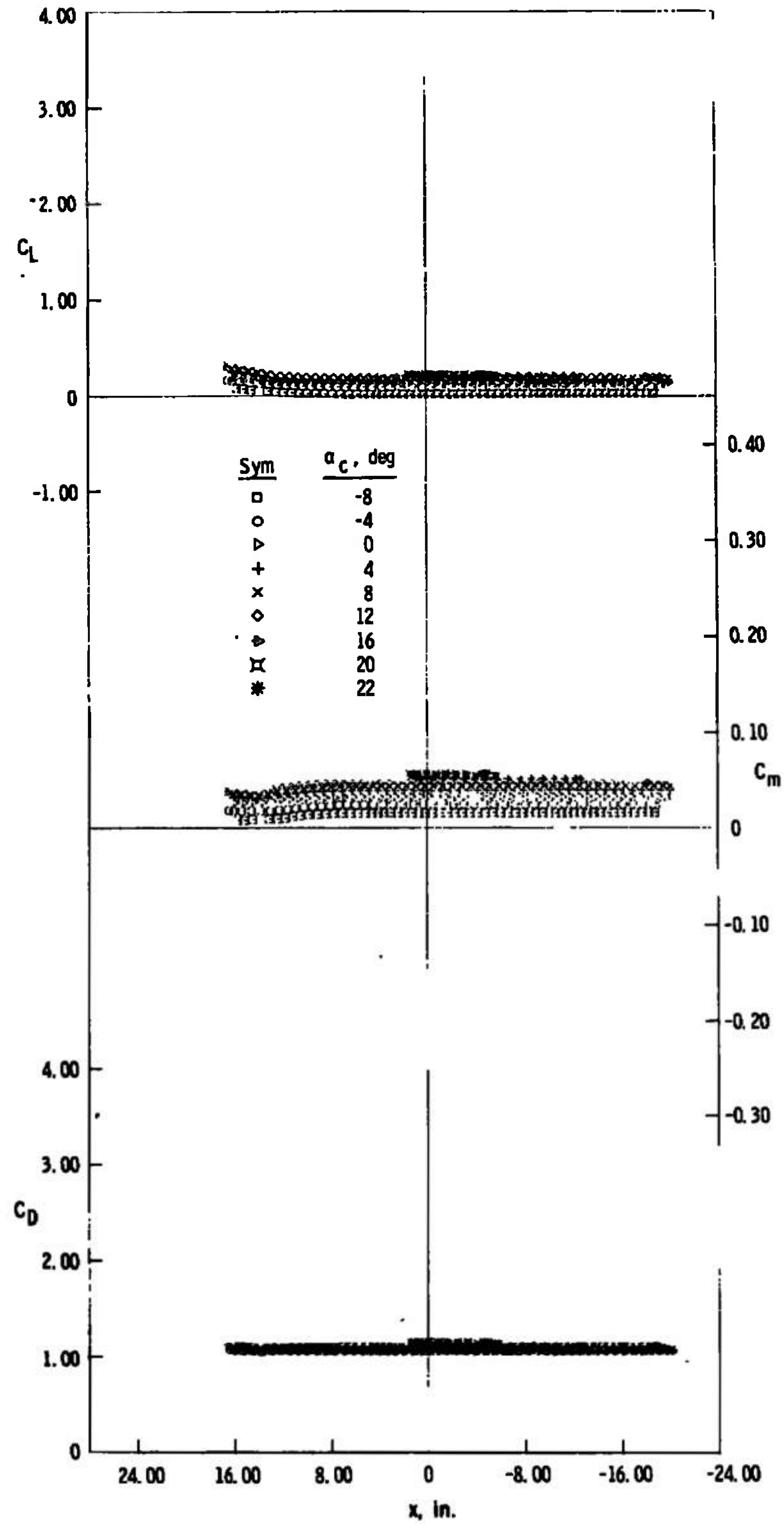

e. z = 10 in., y = 0
Fig. 8 Continued

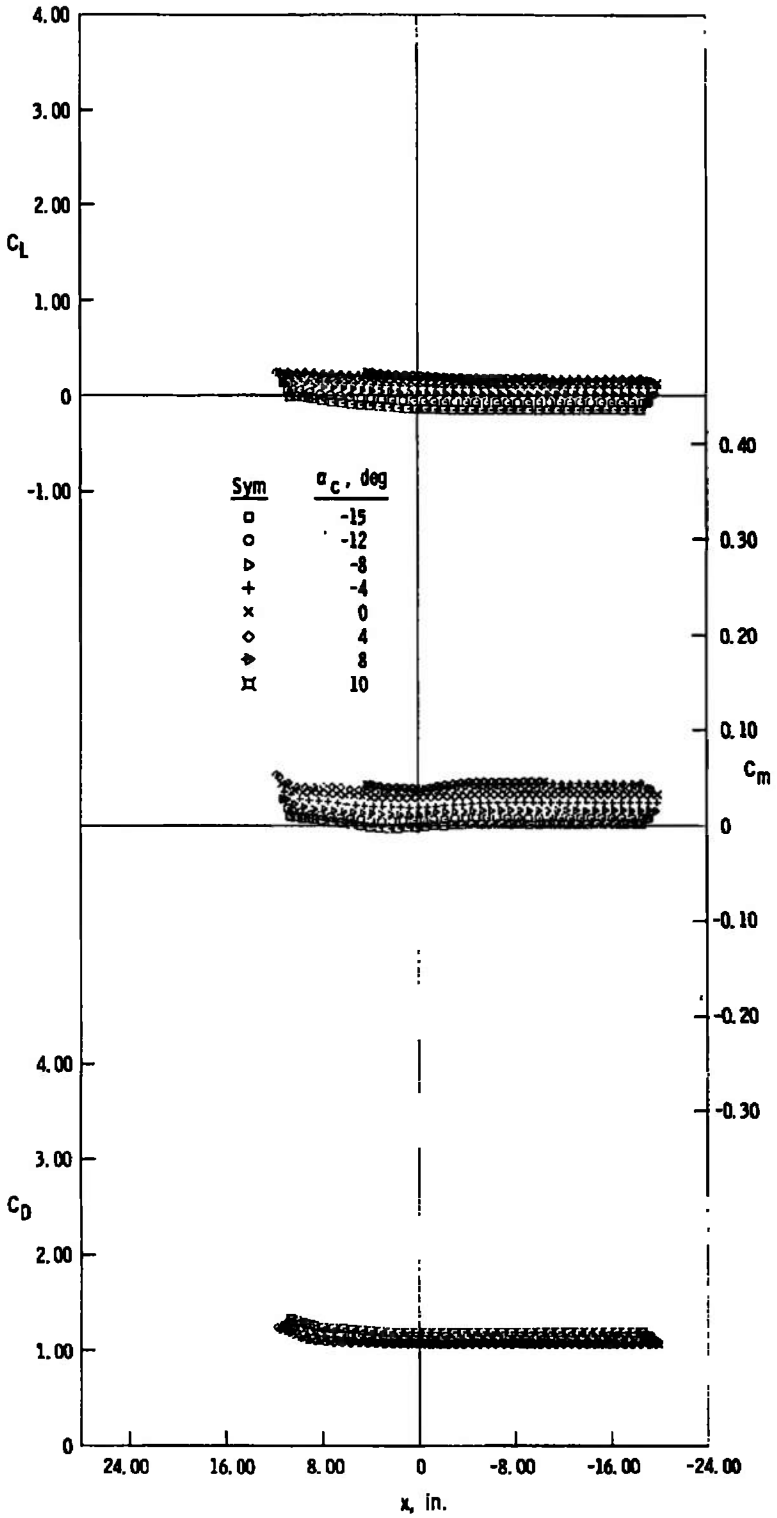

f. z = 5 in., y = 5 in.
Fig. 8 Concluded

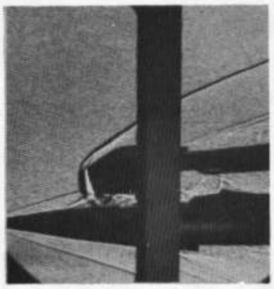
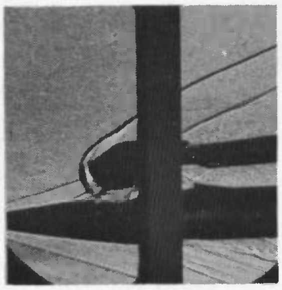
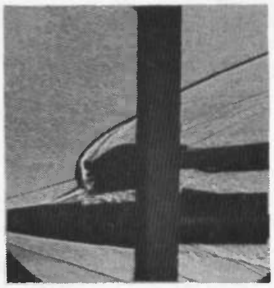
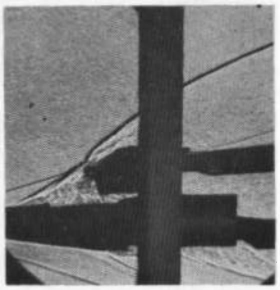

a. α_c = –4 deg
y = 0
z = 3 in.
x = –2.9 in.

b. α_c = –4 deg
y = 0
z = 3 in.
x = –0.5 in.

c. α_c = –4 deg
y = 0
z = 3 in.
x = 0.3 in.

d. α_c = –4 deg
y = 0
z = 3 in.
x = 3.3 in.

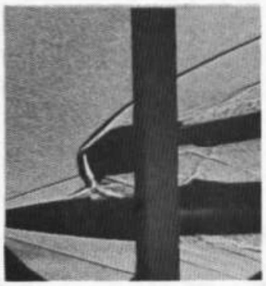
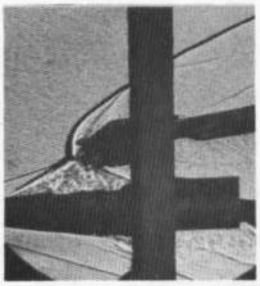
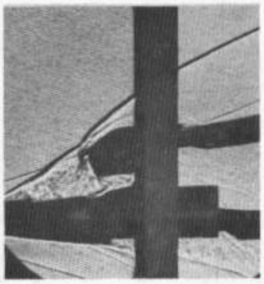
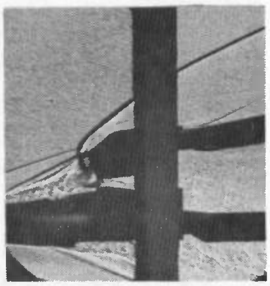

e. α_c = –8 deg
y = 0
z = 4 in.
x = –0.5 in.

f. α_c = –8 deg
y = 0
z = 4 in.
x = 2.5 in.

g. α_c = –8 deg
y = 0
z = 4 in.
x = 4.6 in.

h. α_c = –8 deg
y = 0
z = 4 in.
x = 7.6 in.

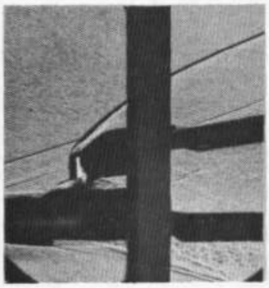
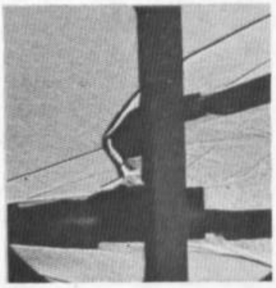
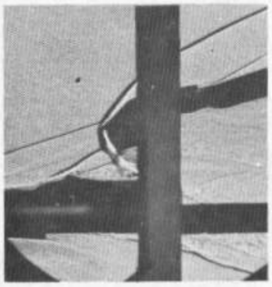
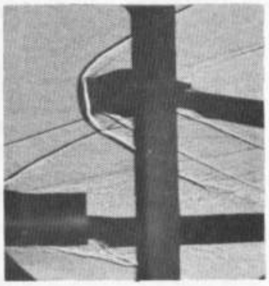

i. α_c = –8 deg
y = 0
z = 4 in.
x = 8.9 in.

j. α_c = –15 deg
y = 0
z = 6 in.
x = 7.7 in.

k. α_c = –15 deg
y = 0
z = 6 in.
x = 11.8 in.

l. α_c = 12 deg
y = 0
z = 10 in.
x = 16.5 in.

Fig. 9 Schlieren Photographs, Jet Off, M_∞ = 4

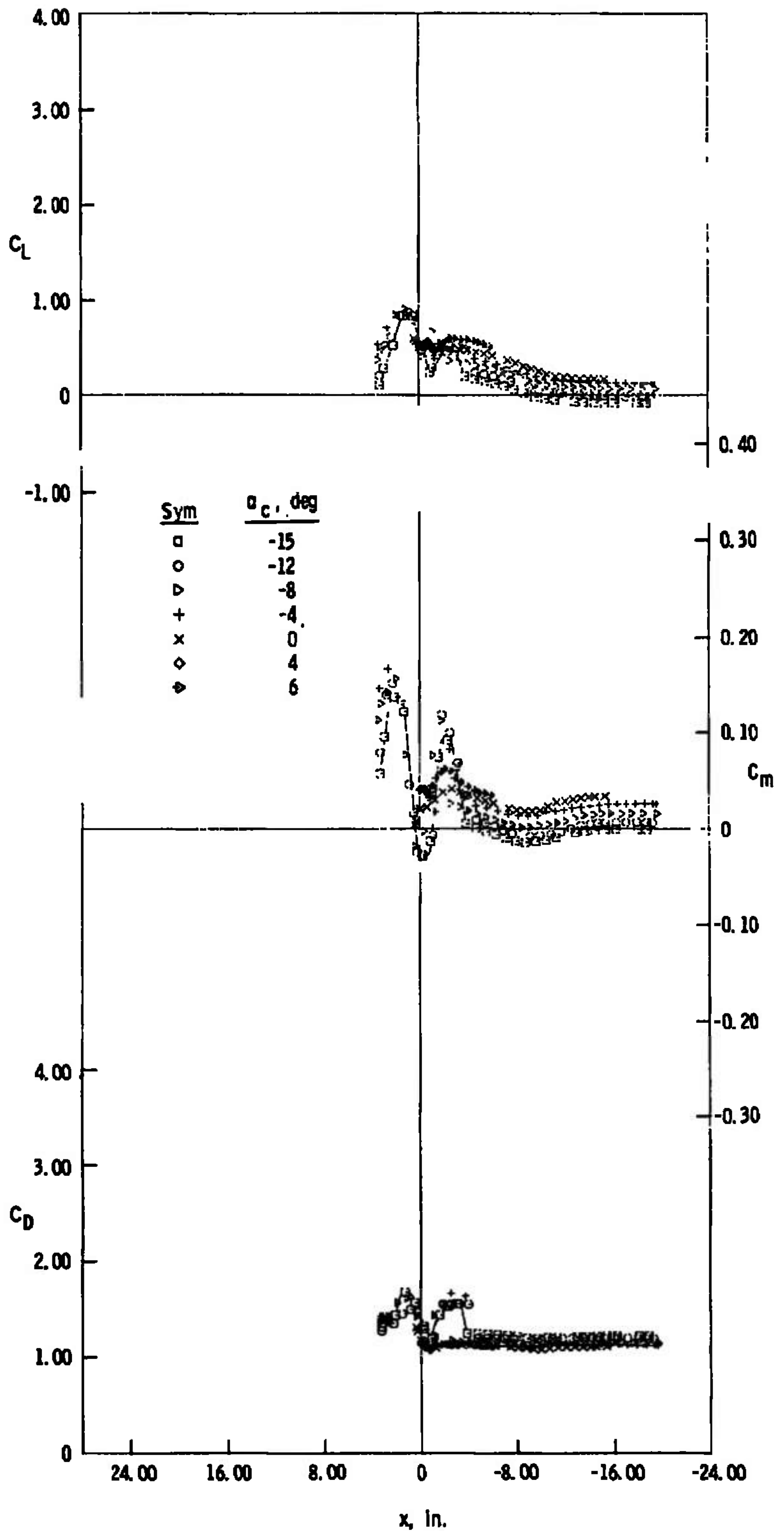

a. z = 3 in., y = 0

Fig. 10 Lift, Pitching-Moment, and Drag Characteristics of the Capsule, Jet Off, $M_\infty = 5$

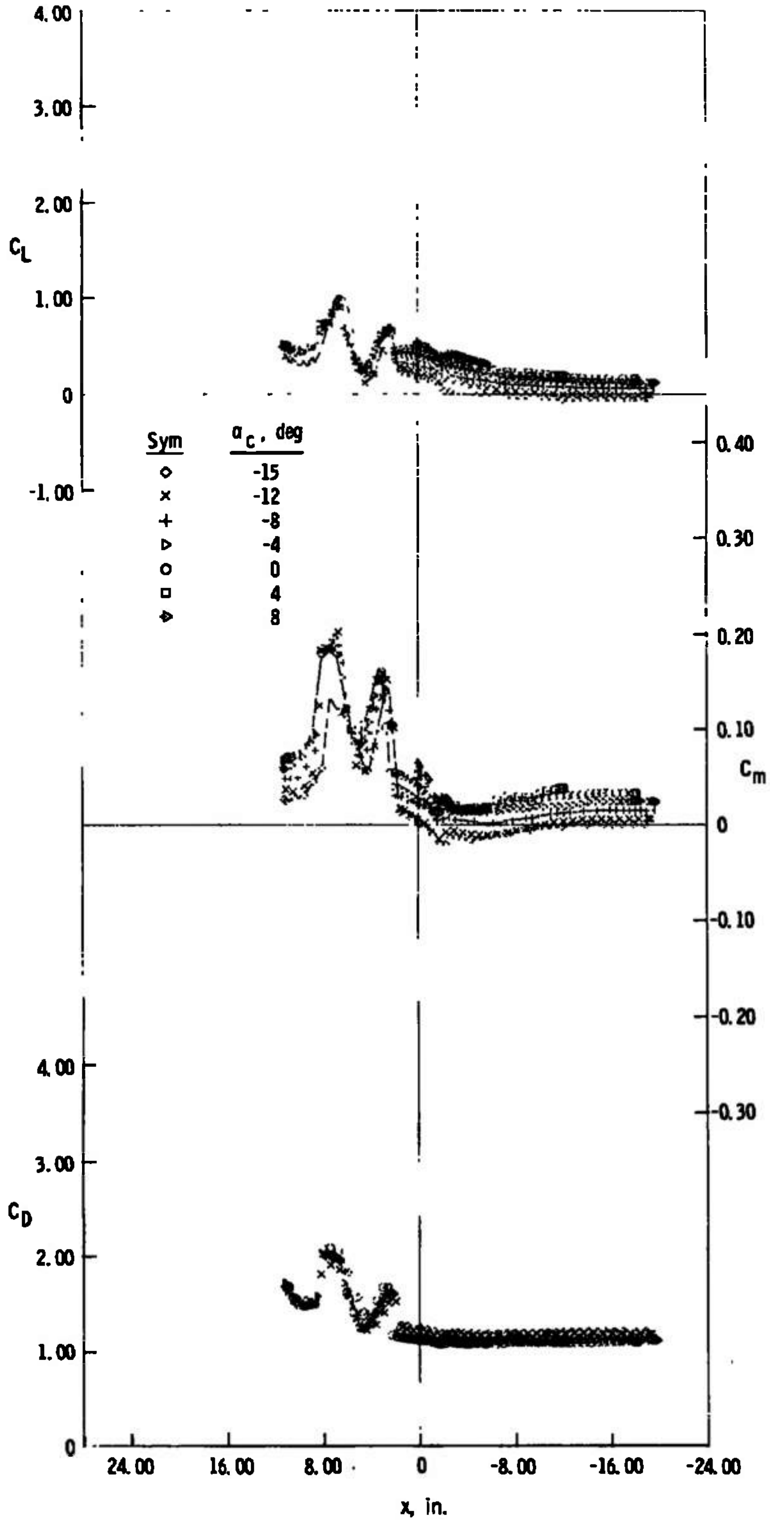

b. z = 4 in., y = 0
Fig. 10 Continued

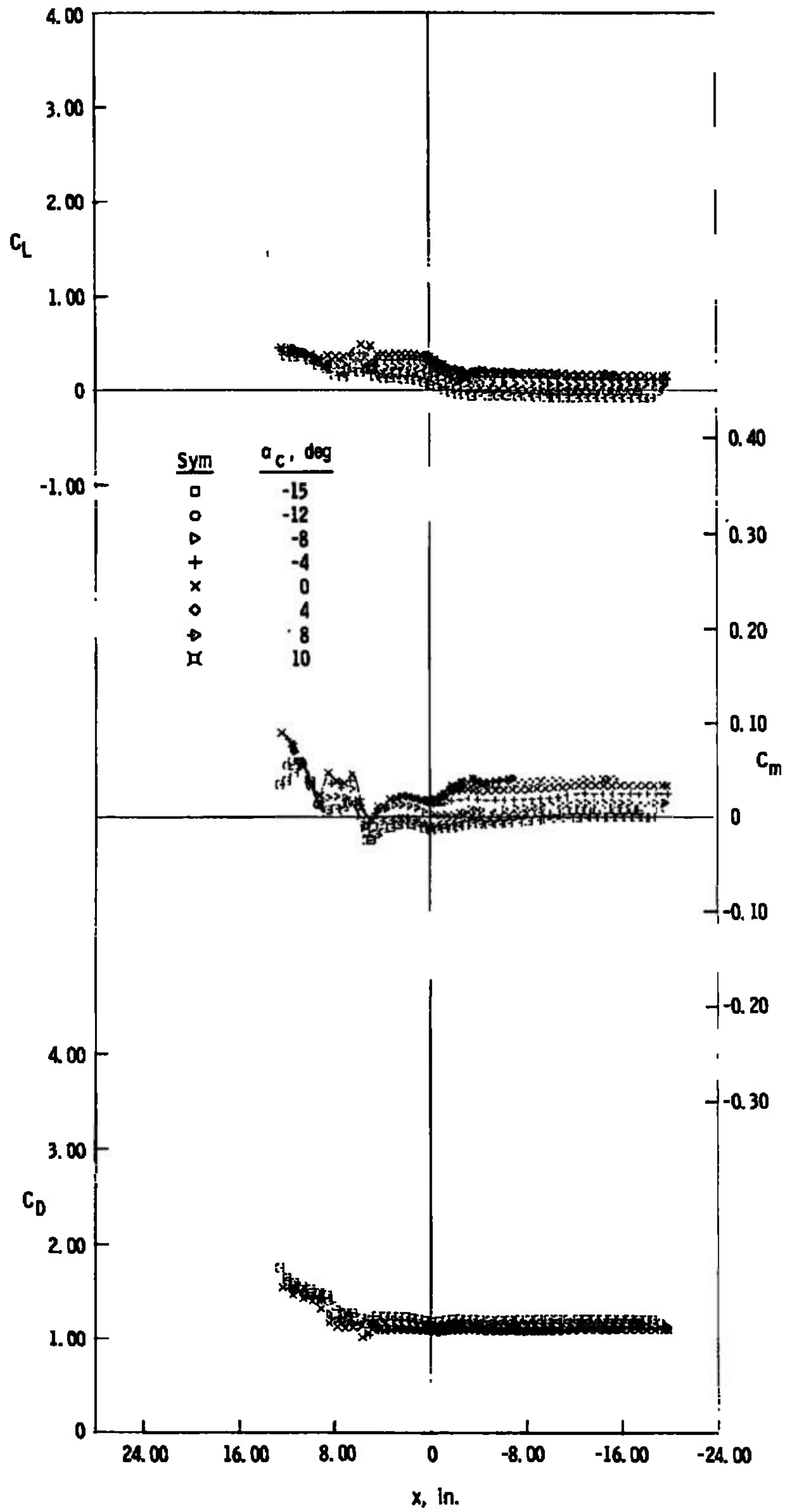

c. z = 5 in., y = 0
Fig. 10 Continued

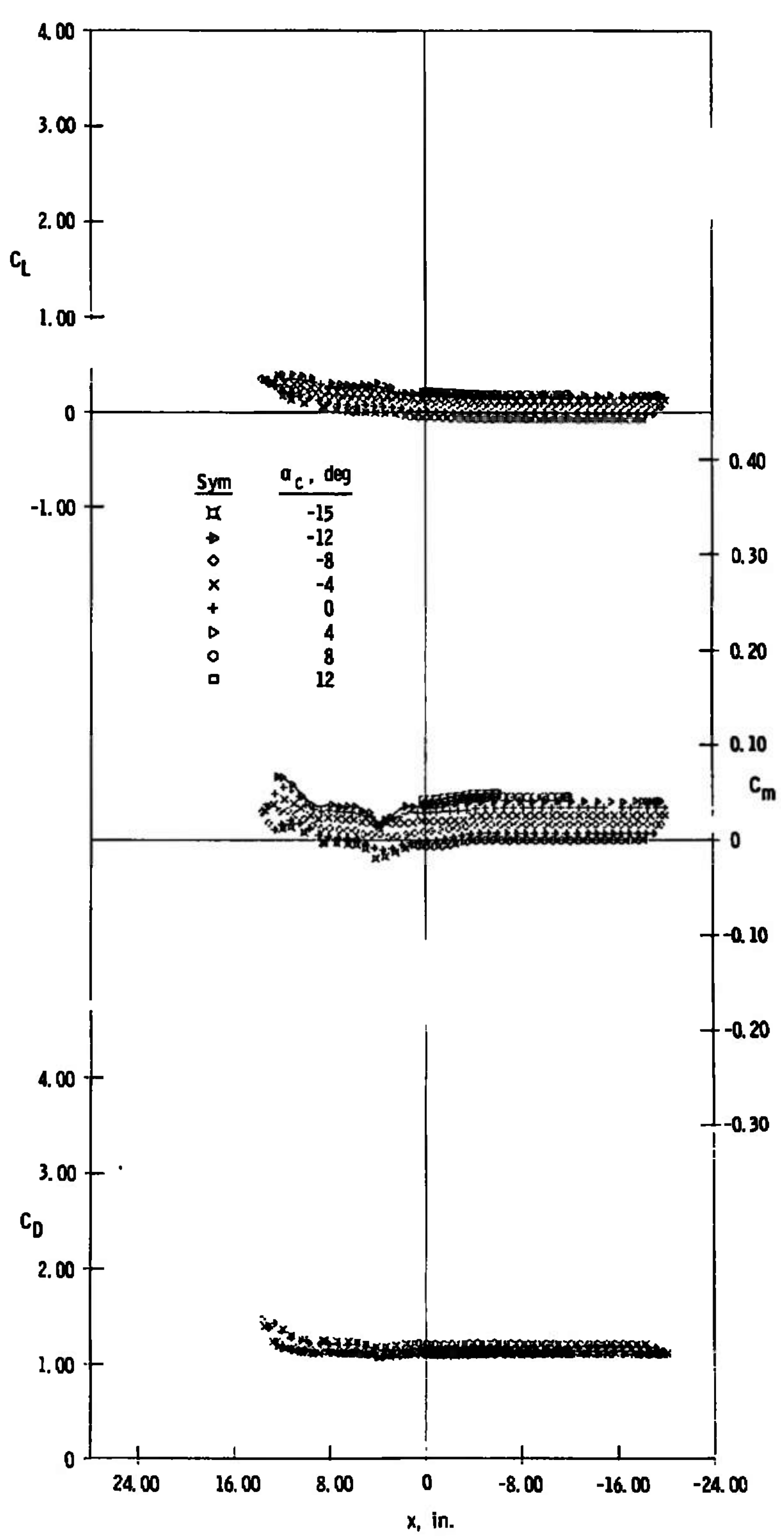

d. z = 6 in., y = 0

Fig. 10 Continued

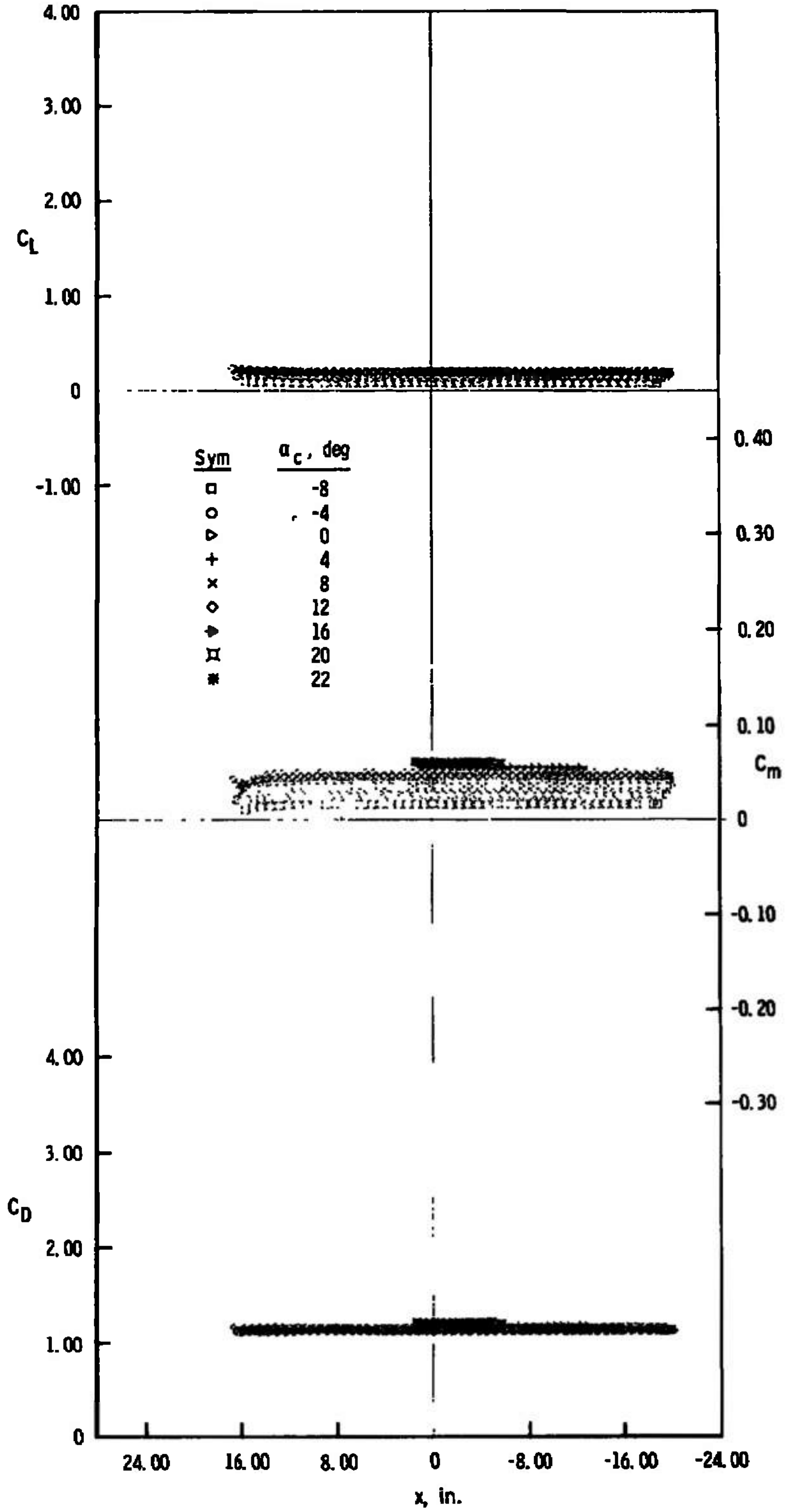

e. z = 10 in., y = 0

Fig. 10 Continued

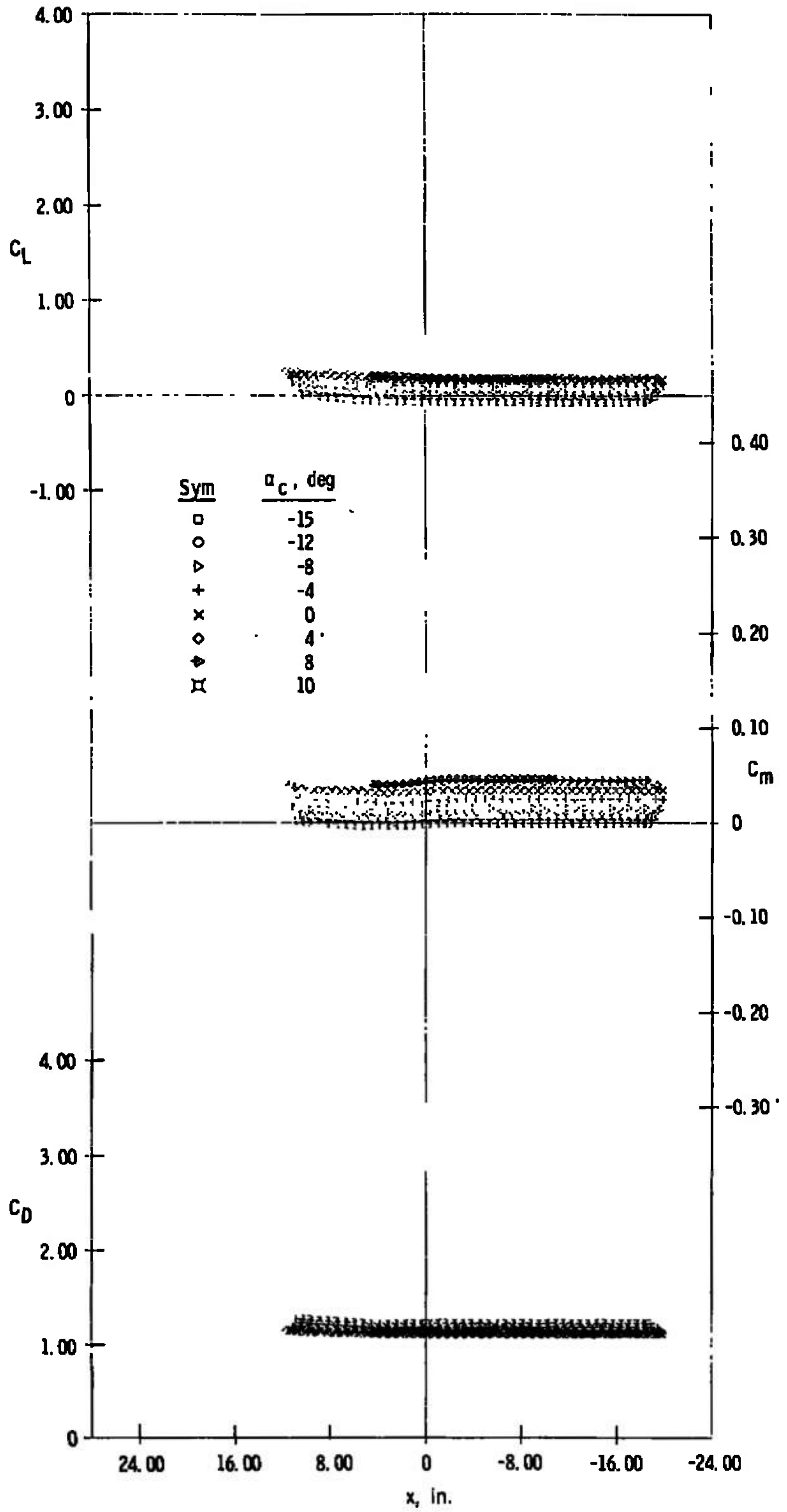

f. z = 5 in., y = 5 in.
Fig. 10 Concluded

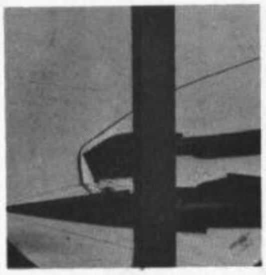

a. α_c = –4 deg
y = 0
z = 3 in.
x = –4.0 in.

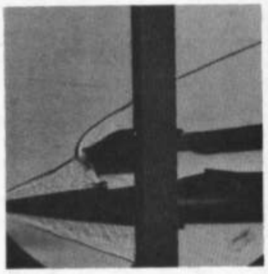

b. α_c = –4 deg
y = 0
z = 3 in.
x = –2.0 in.

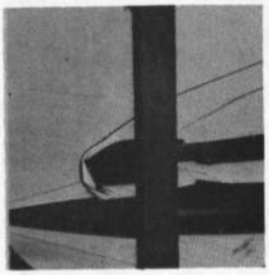

c. α_c = –4 deg
y = 0
z = 3 in.
x = –1.0 in.

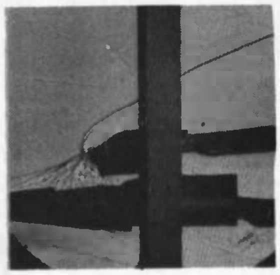

d. α_c = –4 deg
y = 0
z = 3 in.
x = 3.0 in.

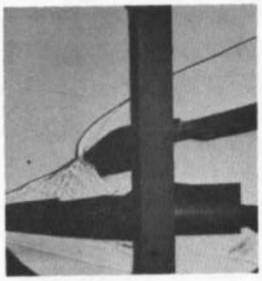

e. α_c = –12 deg
y = 0
z = 4 in.
x = 2.8 in.

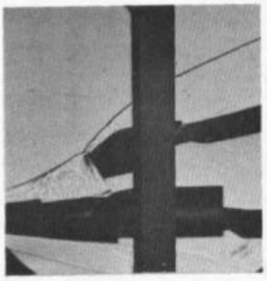

f. α_c = –12 deg
y = 0
z = 4 in.
x = 4.6 in.

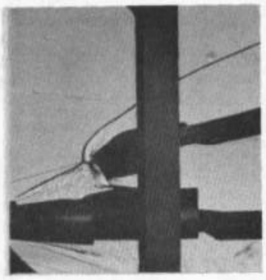

g. α_c = –12 deg
y = 0
z = 4 in.
x = 7.2 in.

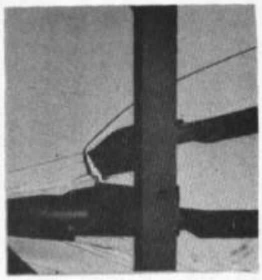

h. α_c = –12 deg
y = 0
z = 4 in.
x = 8.6 in.

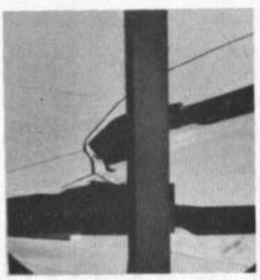

i. α_c = –15 deg
y = 0
z = 5 in.
x = 9.0 in.

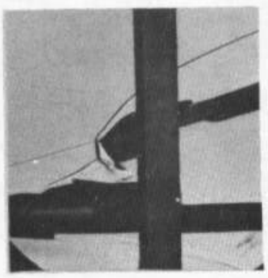

j. α_c = –15 deg
y = 0
z = 5 in.
x = 11.4 in.

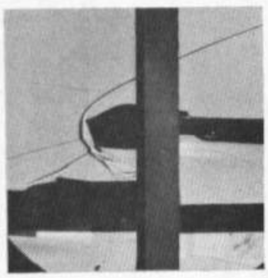

k. α_c = 4 deg
y = 0
z = 6 in.
x = 12.0 in.

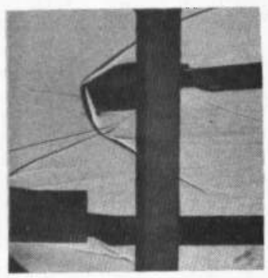

l. α_c = –4 deg
y = 0
z = 10 in.
x = 17.0 in.

Fig. 11 Schlieren Photographs, Jet Off, M_∞ = 5

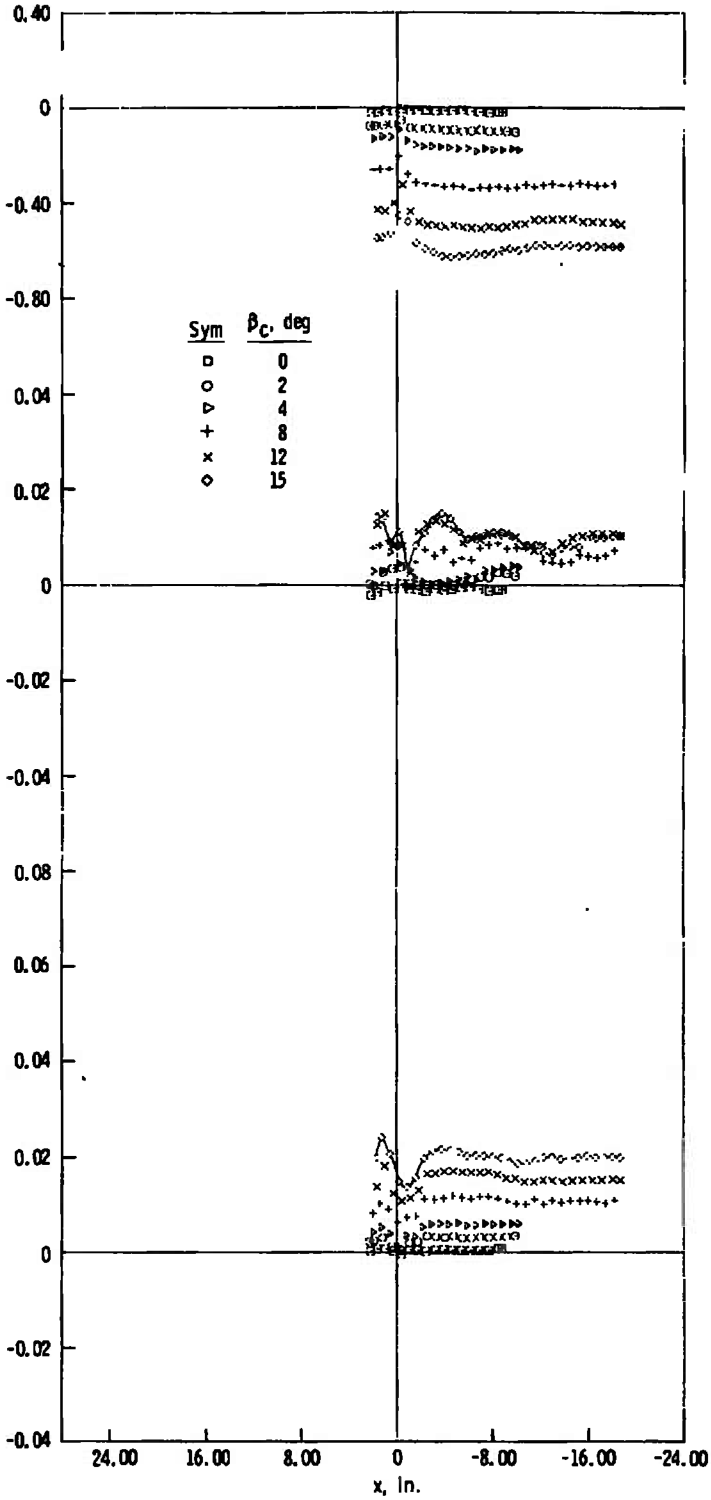

a. z = 3 in., y = 0

Fig. 12 Side-Force, Yawing-Moment, and Rolling-Moment Characteristics of the Capsule, Jet Off, $M_\infty = 2$

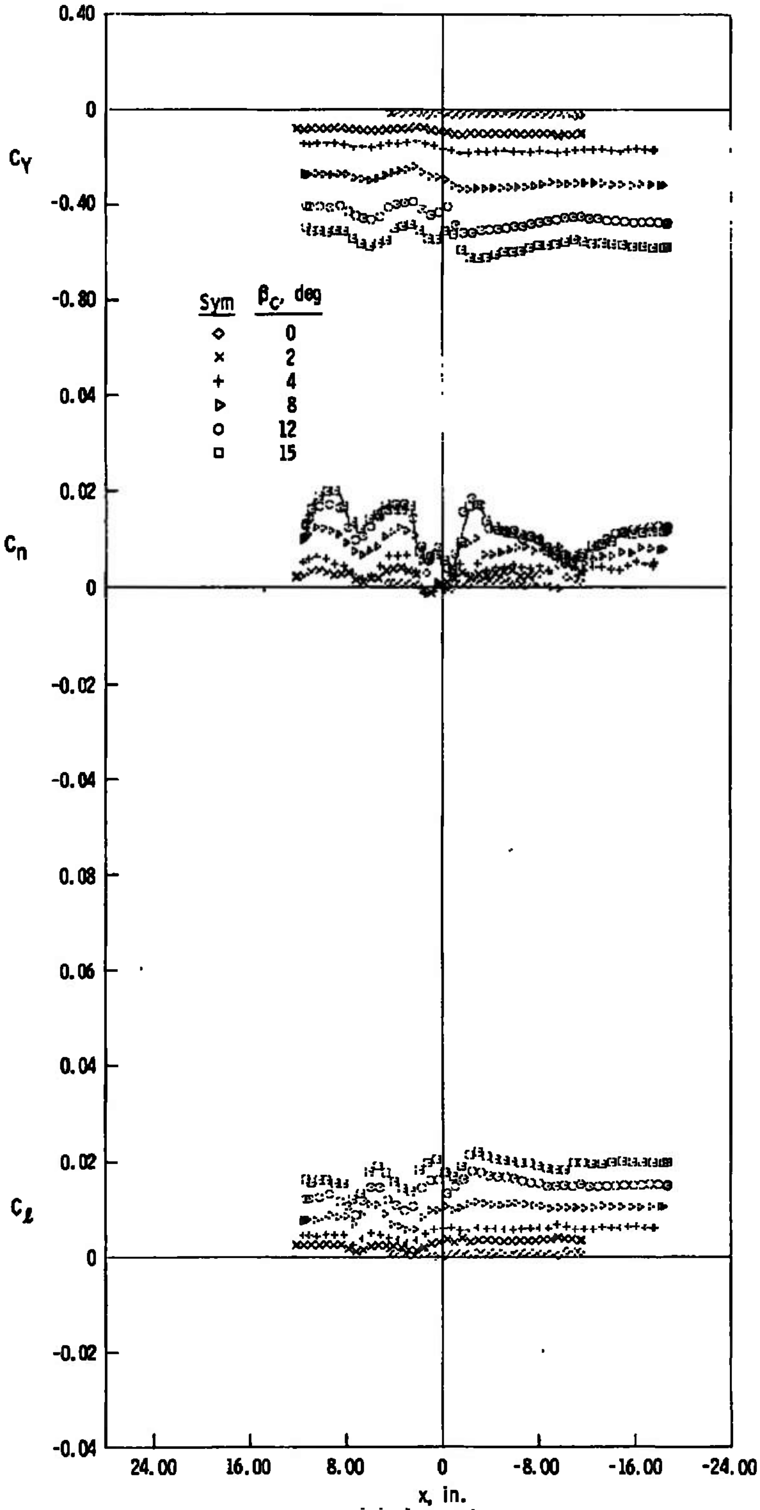

b. z = 4 in., y = 0

Fig. 12 Continued

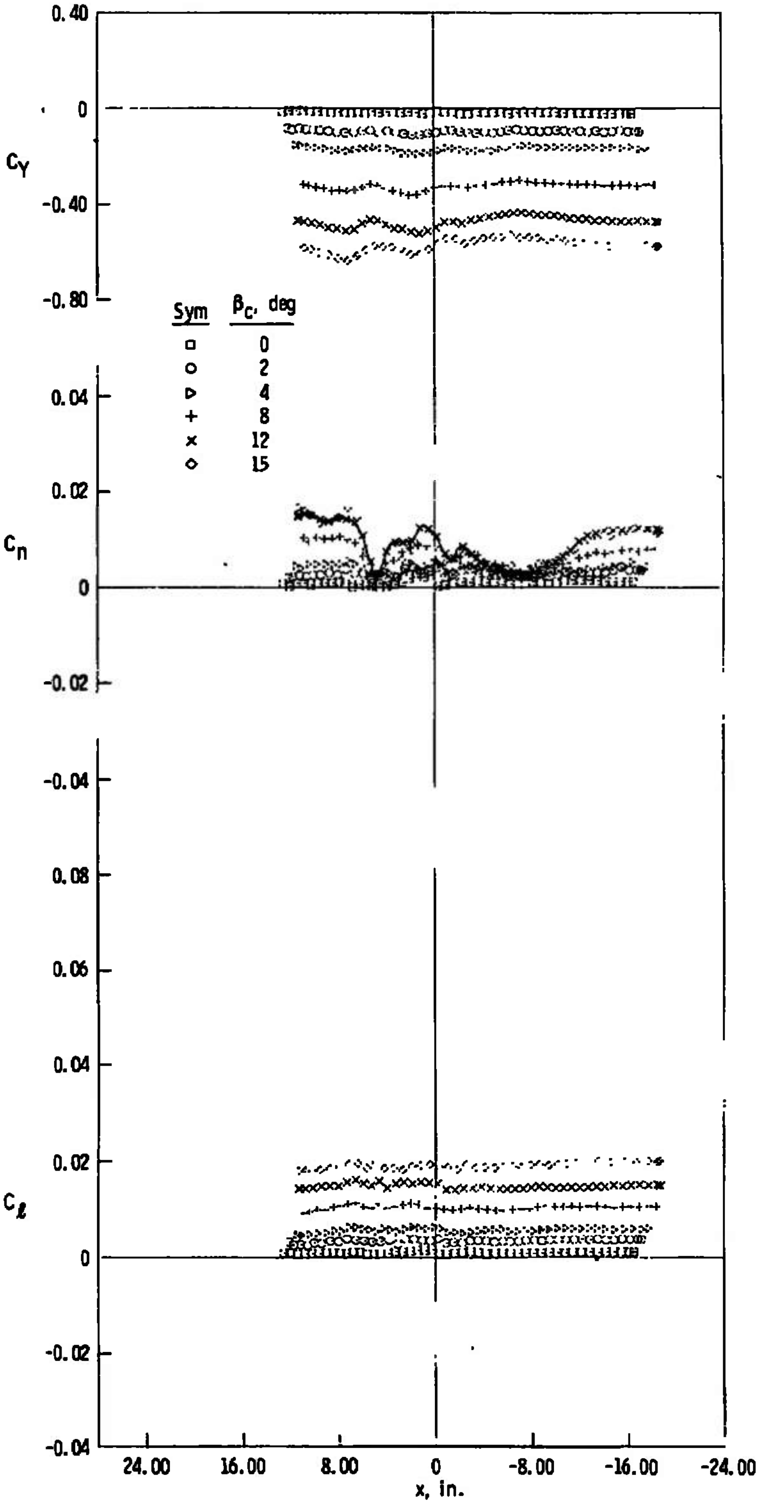

c. z = 6 in., y = 0
Fig. 12 Continued

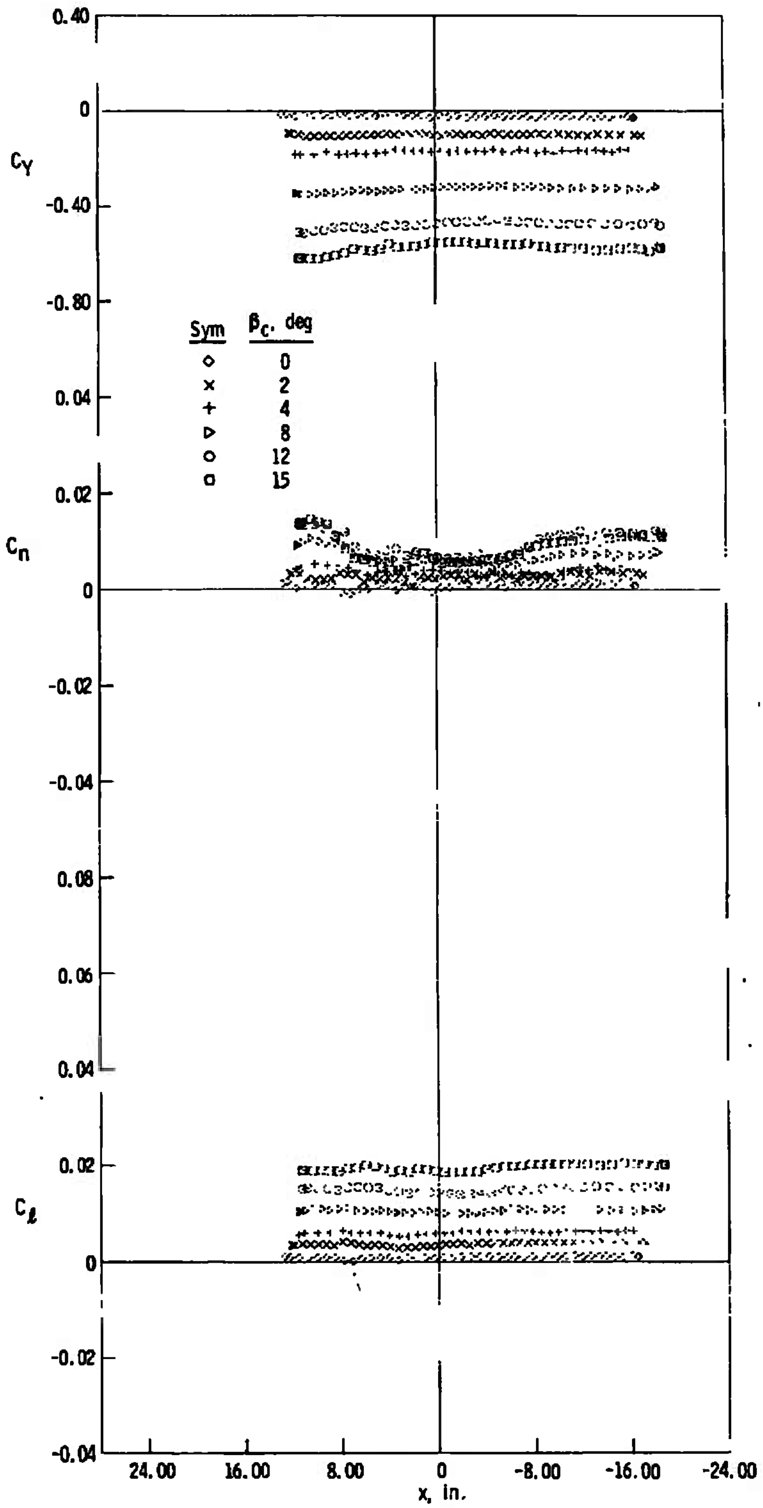

d. z = 8 in., y = 0
Fig. 12 Continued

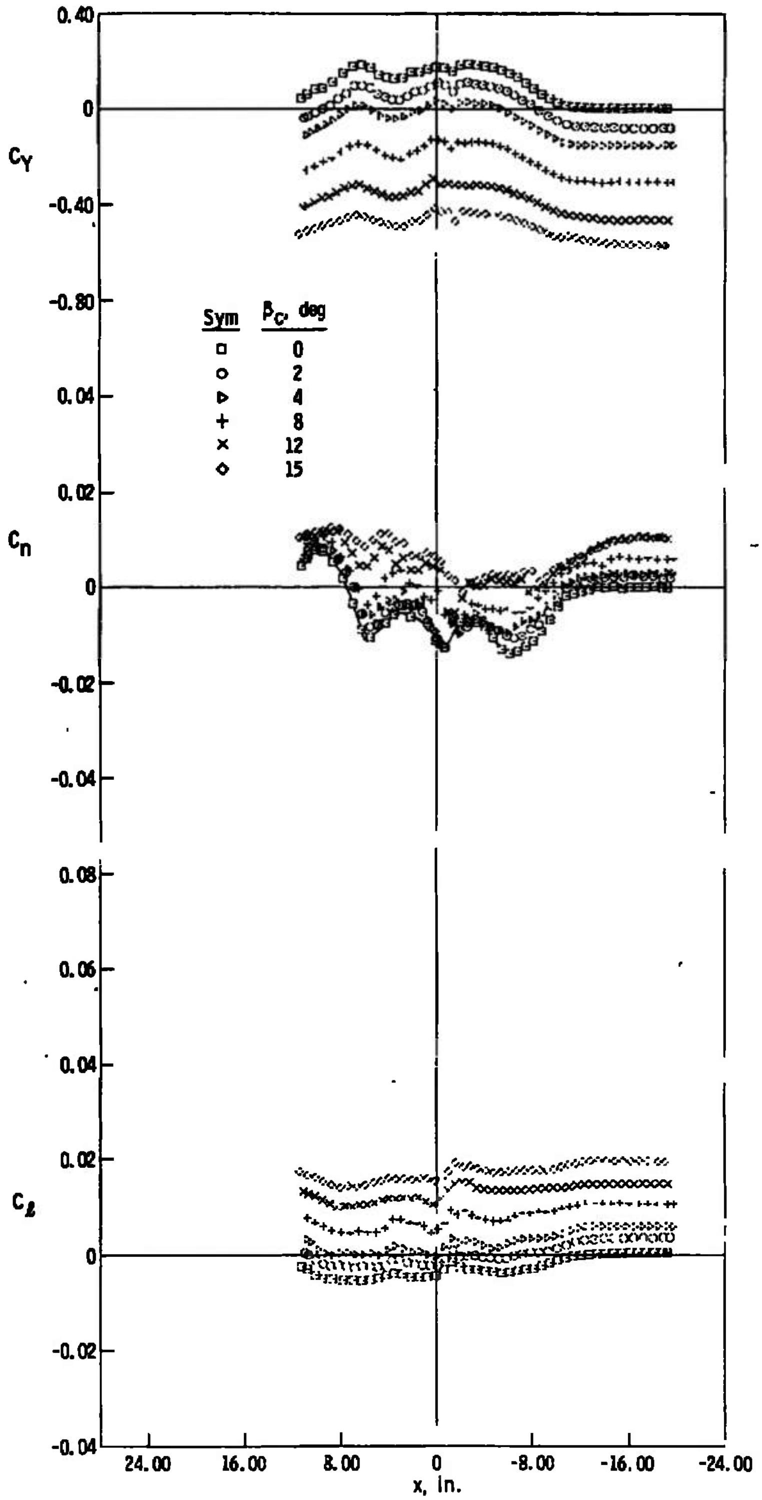

e. z = 3 in., y = -5 in.

Fig. 12 Concluded

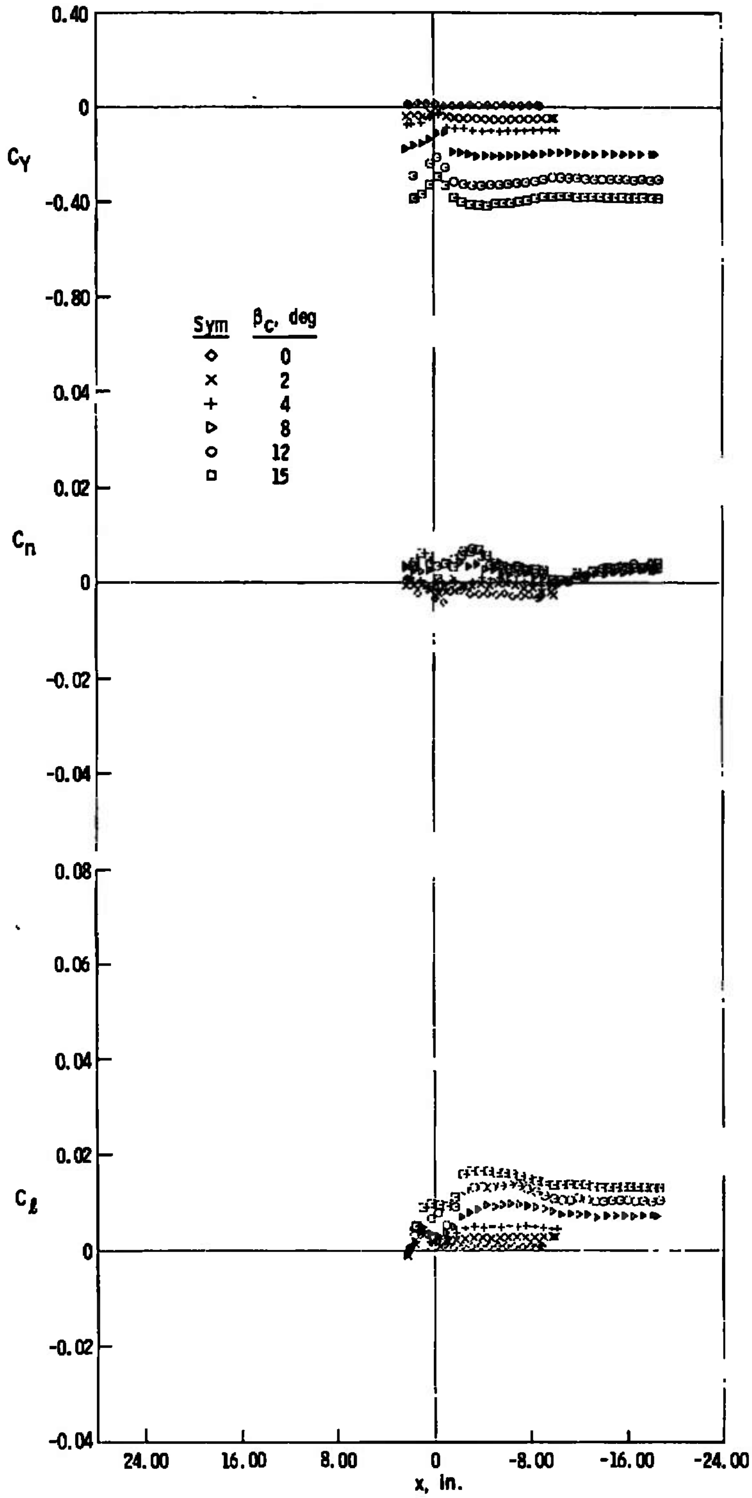

a. z = 3 in., y = 0

Fig. 13 Side-Force, Yawing-Moment, and Rolling-Moment Characteristics of the Capsule, Jet Off, M_∞ = 3

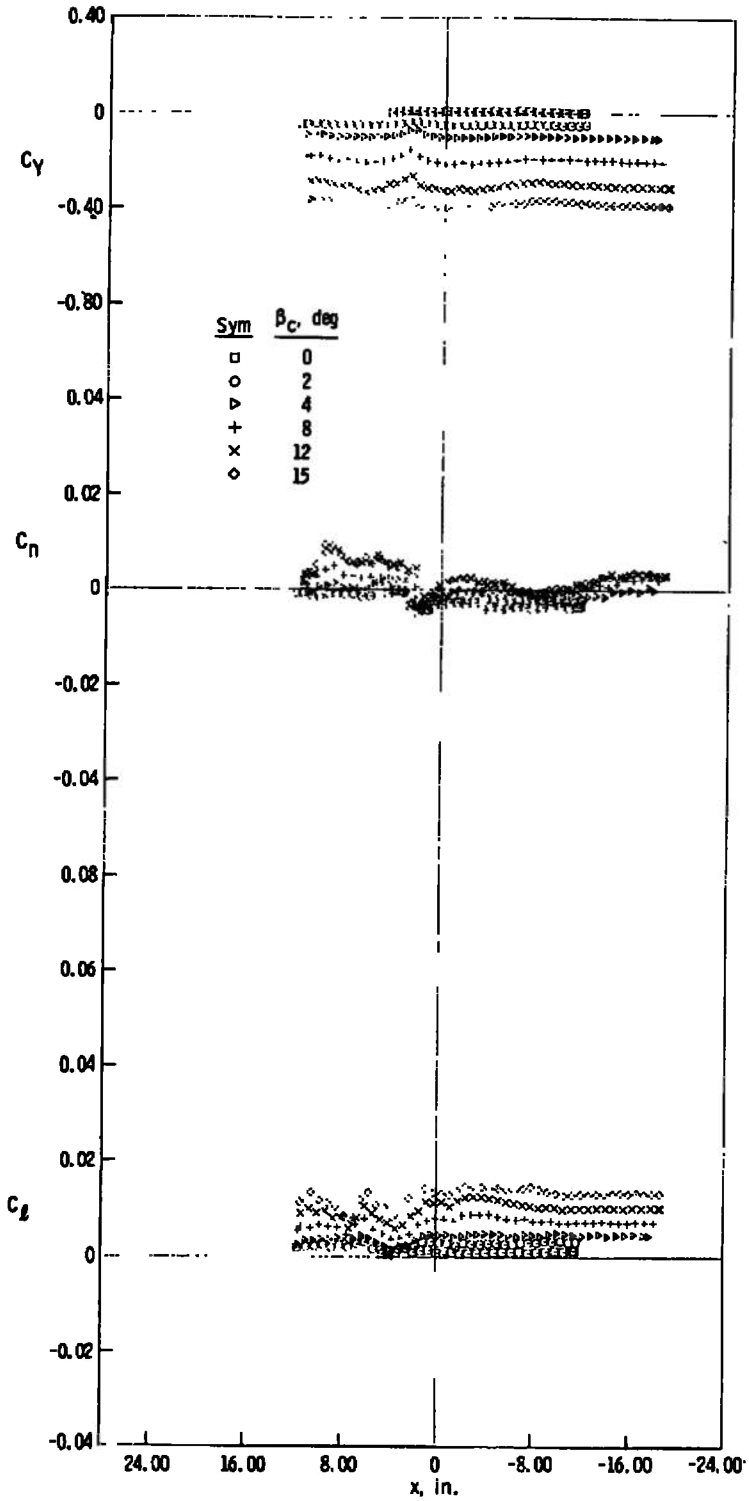

b. z = 4 in., y = 0
Fig. 13 Continued

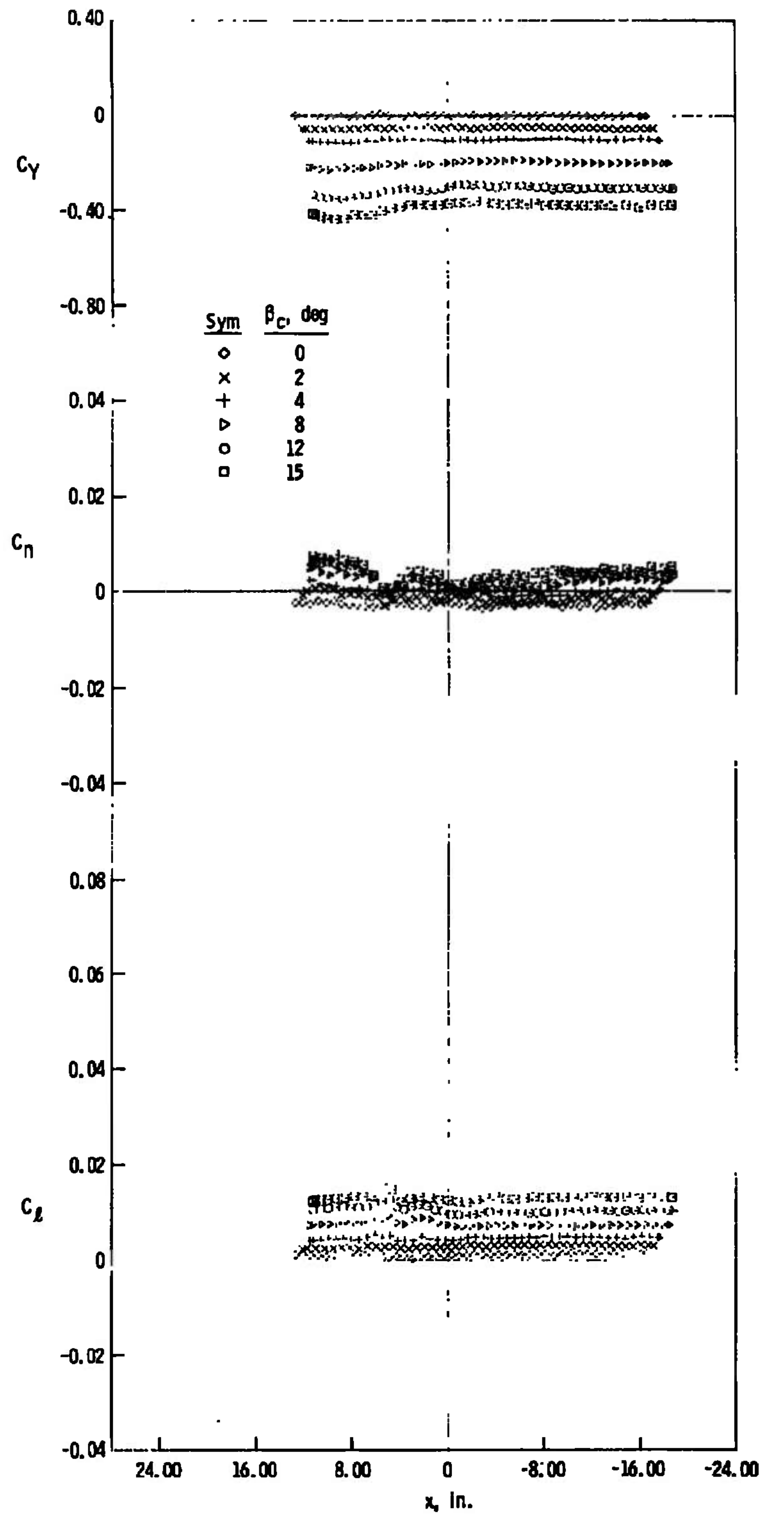

c. z = 6 in., y = 0

Fig. 13 Continued

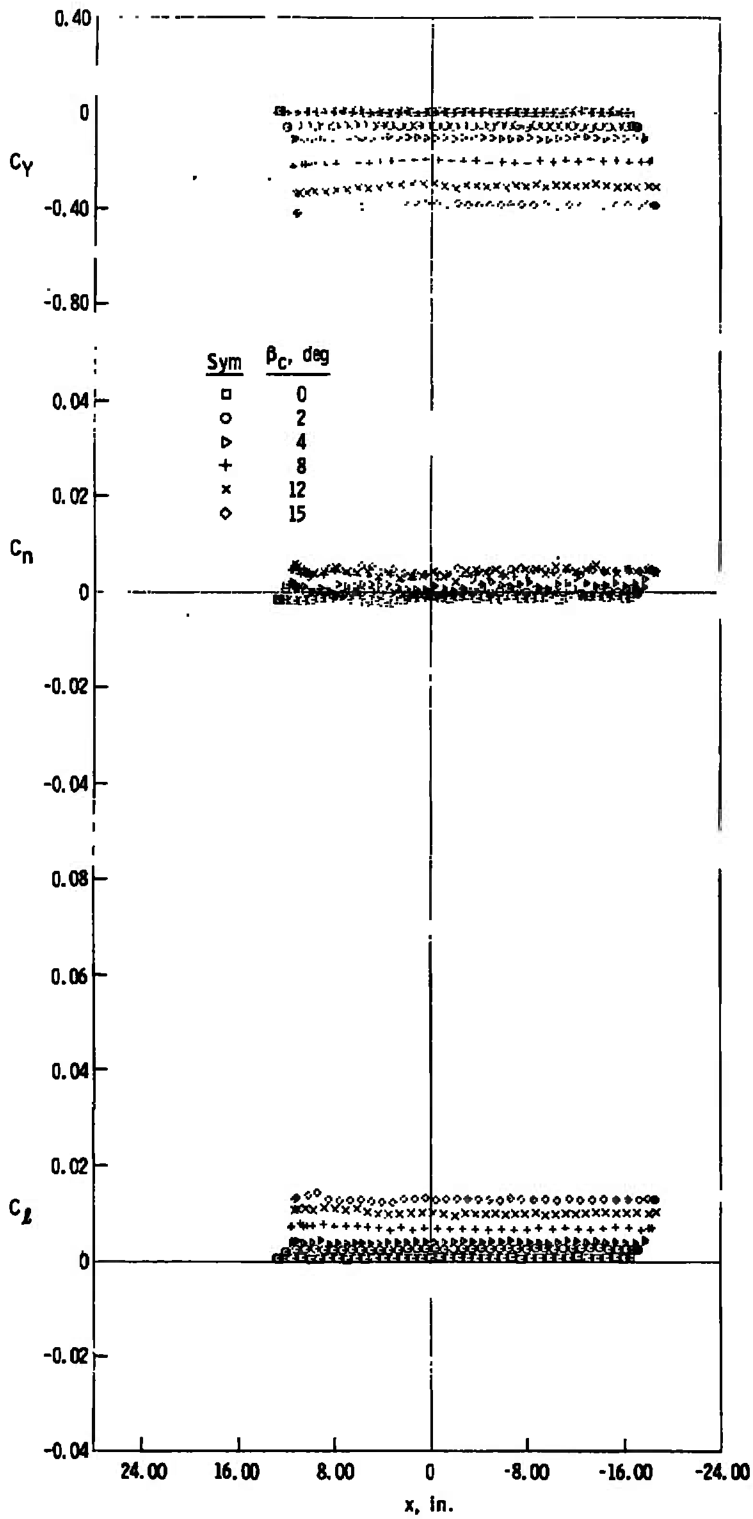

d. z = 8 in., y = 0

Fig. 13 Continued

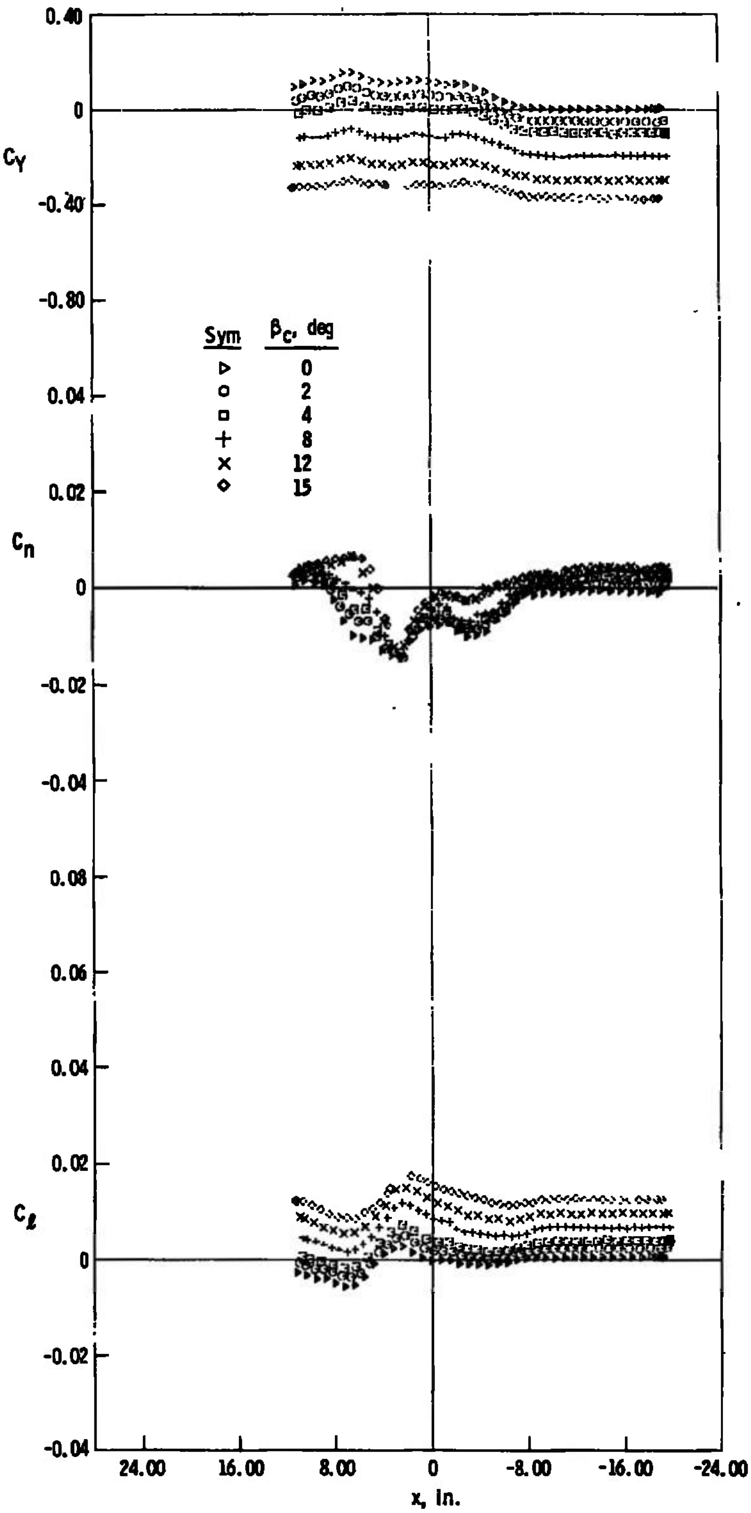

e. z = 3 in., y = –5 in.

Fig. 13 Concluded

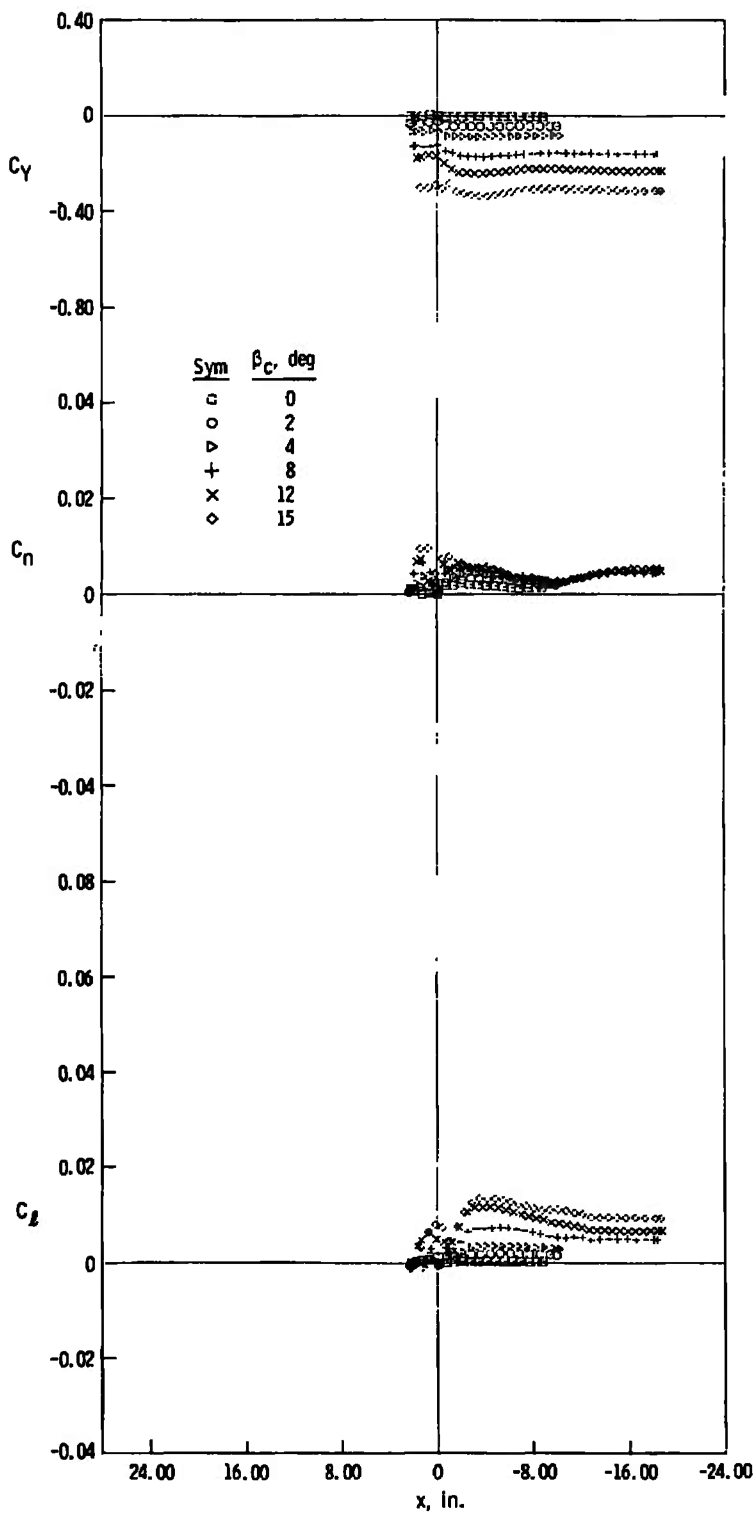

a. z = 3 in., y = 0

Fig. 14 Side-Force, Yawing-Moment, and Rolling-Moment Characteristics of the Capsule, Jet Off, M_∞ = 4

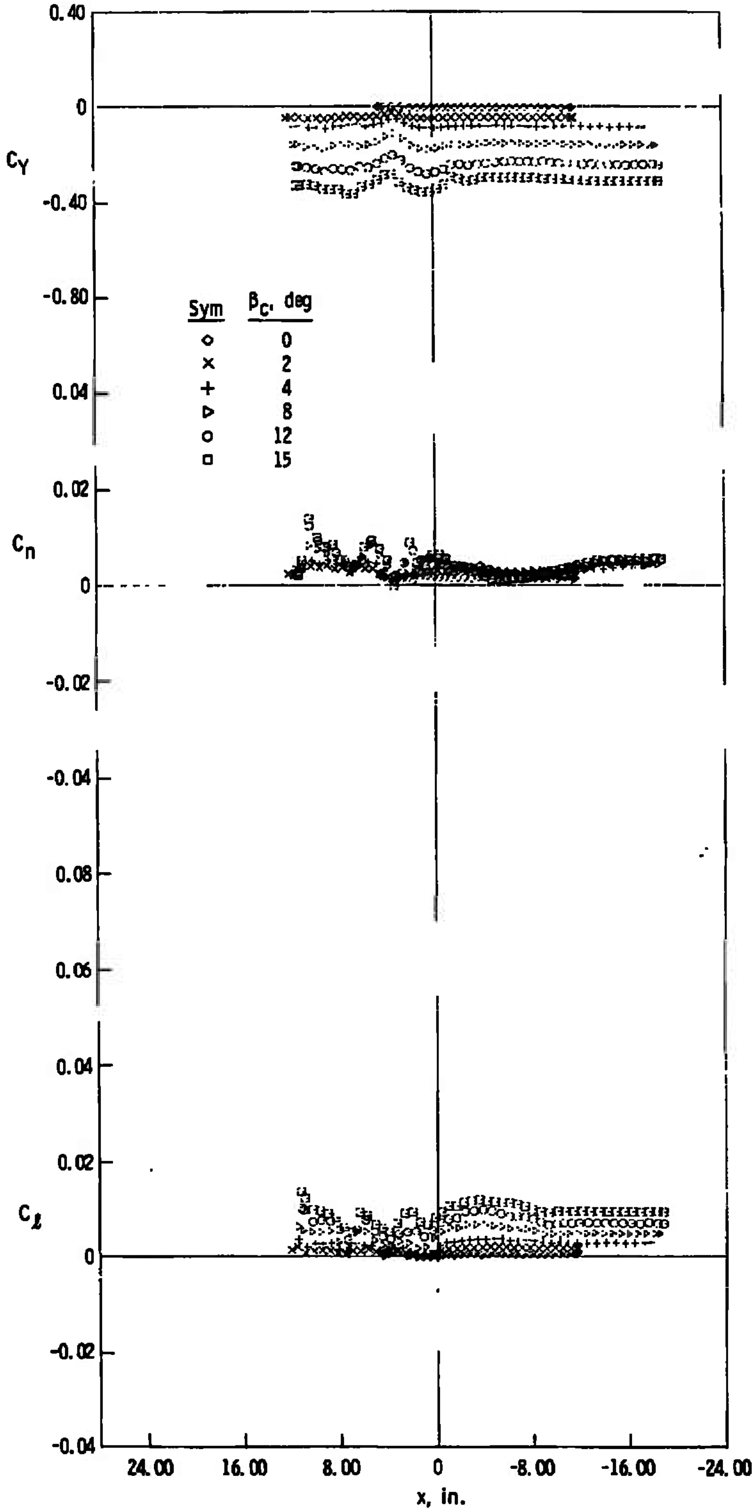

b. z = 4 in., y = 0

Fig. 14 Continued

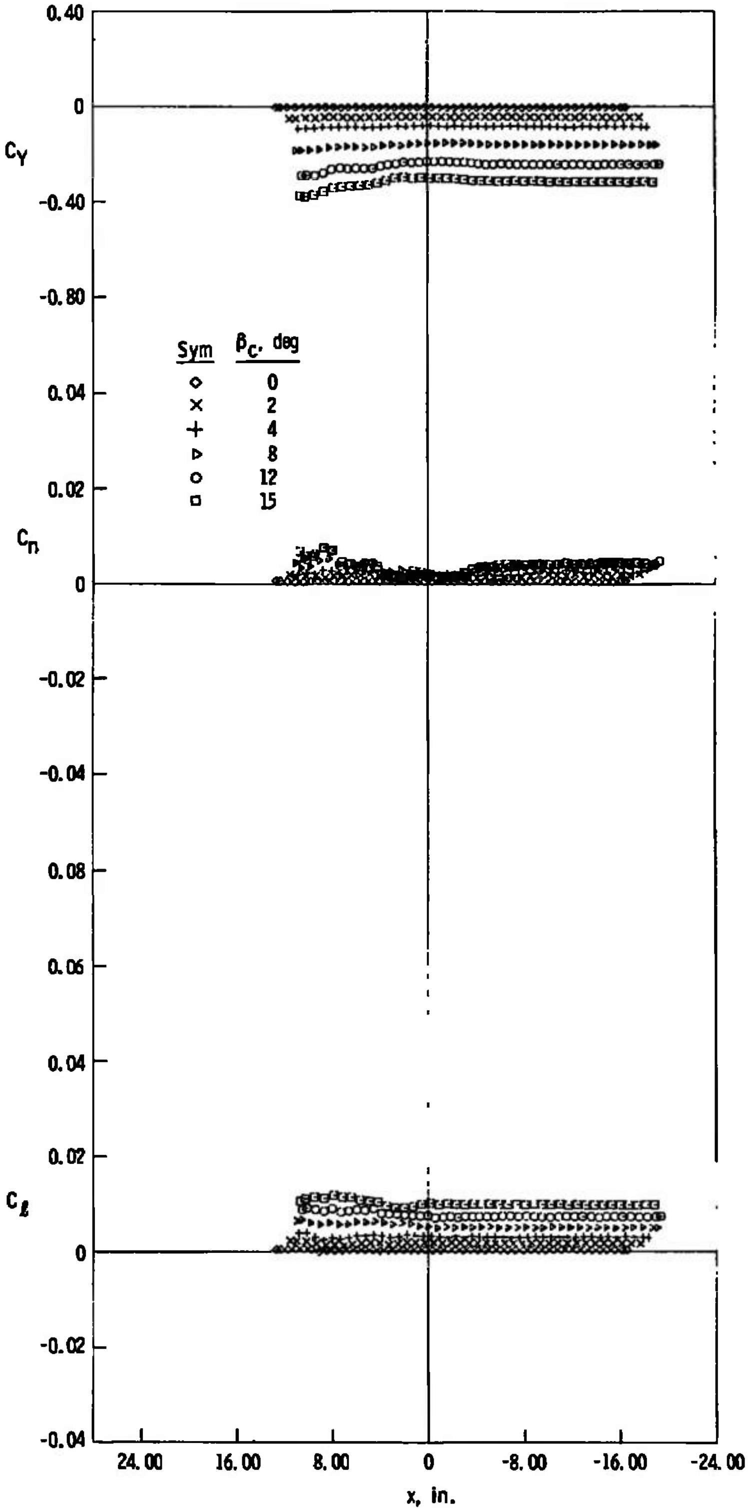

c. z = 6 in., y = 0

Fig. 14 Continued

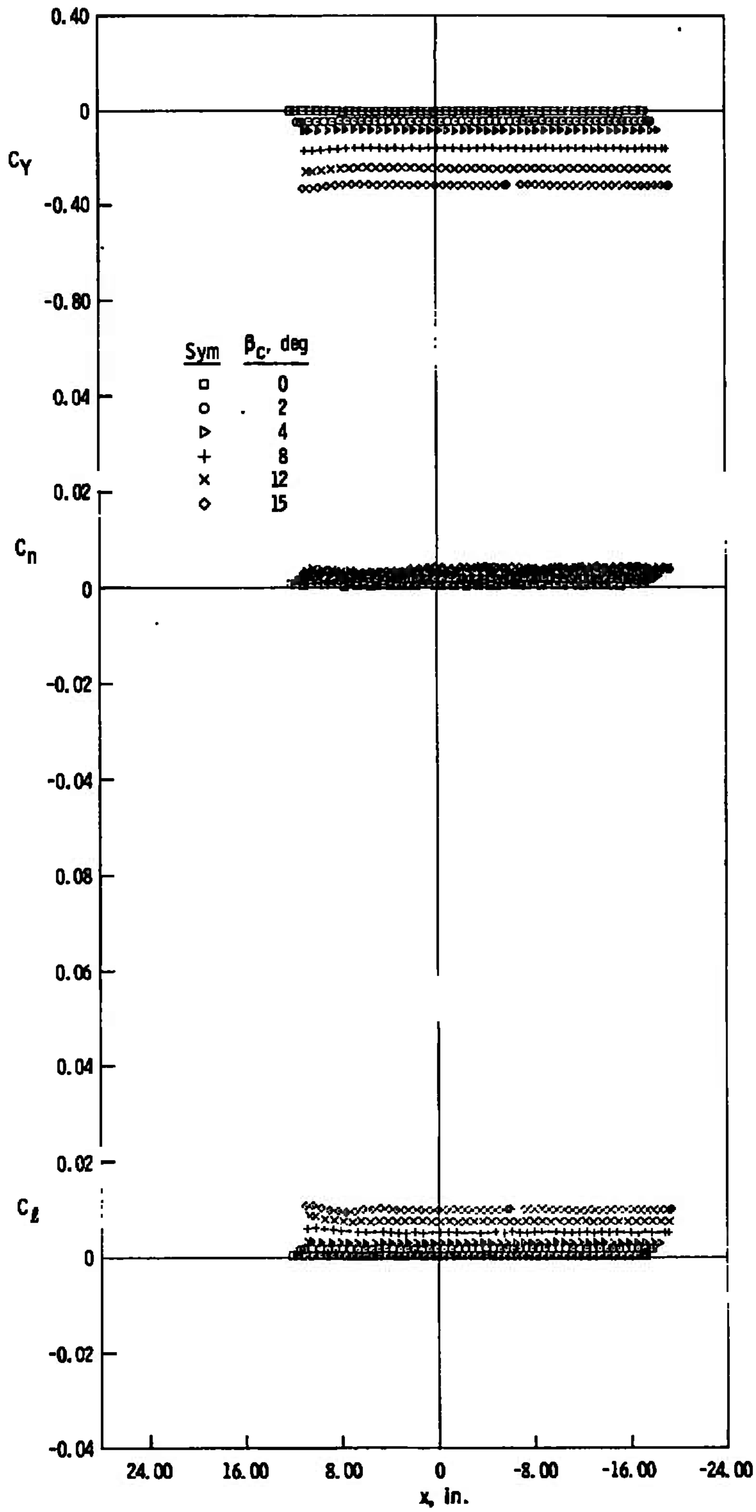

d. z = 8 in., y = 0

Fig. 14 Continued

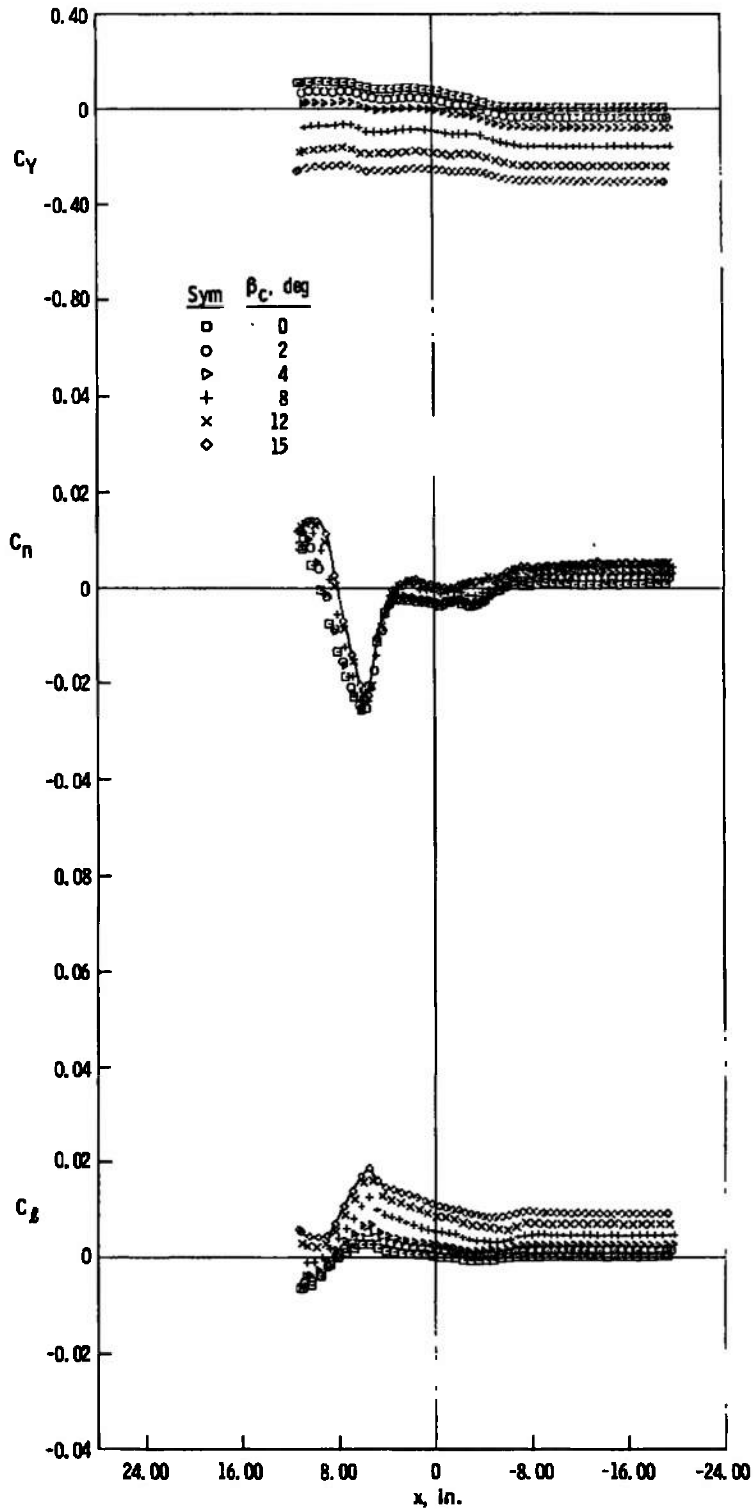

e. z = 3 in., y = -5 in.
Fig. 14 Concluded

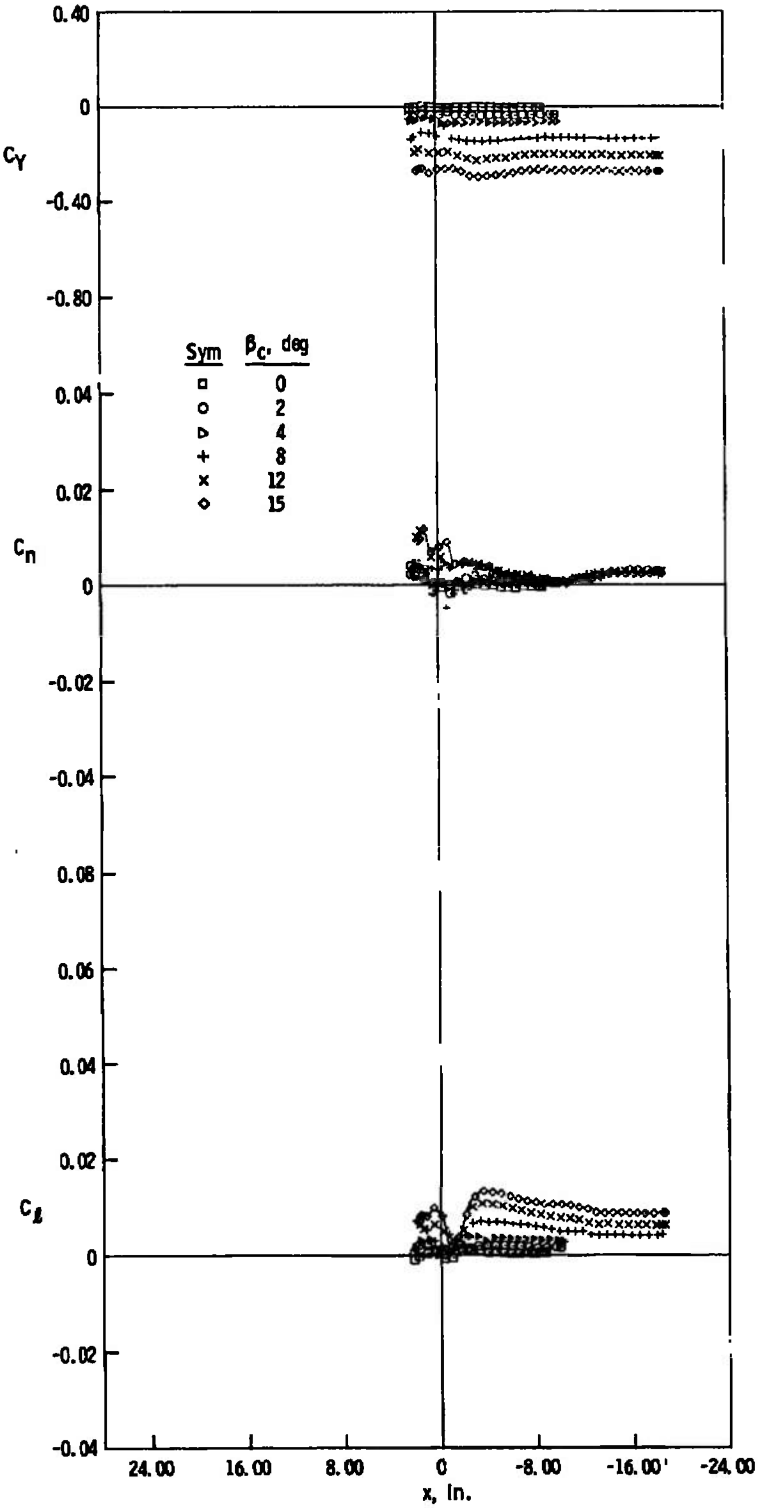

a. z = 3 in., y = 0

Fig. 15 Side-Force, Yawing-Moment, and Rolling-Moment Characteristics of the Capsule, Jet Off, M_∞ = 5

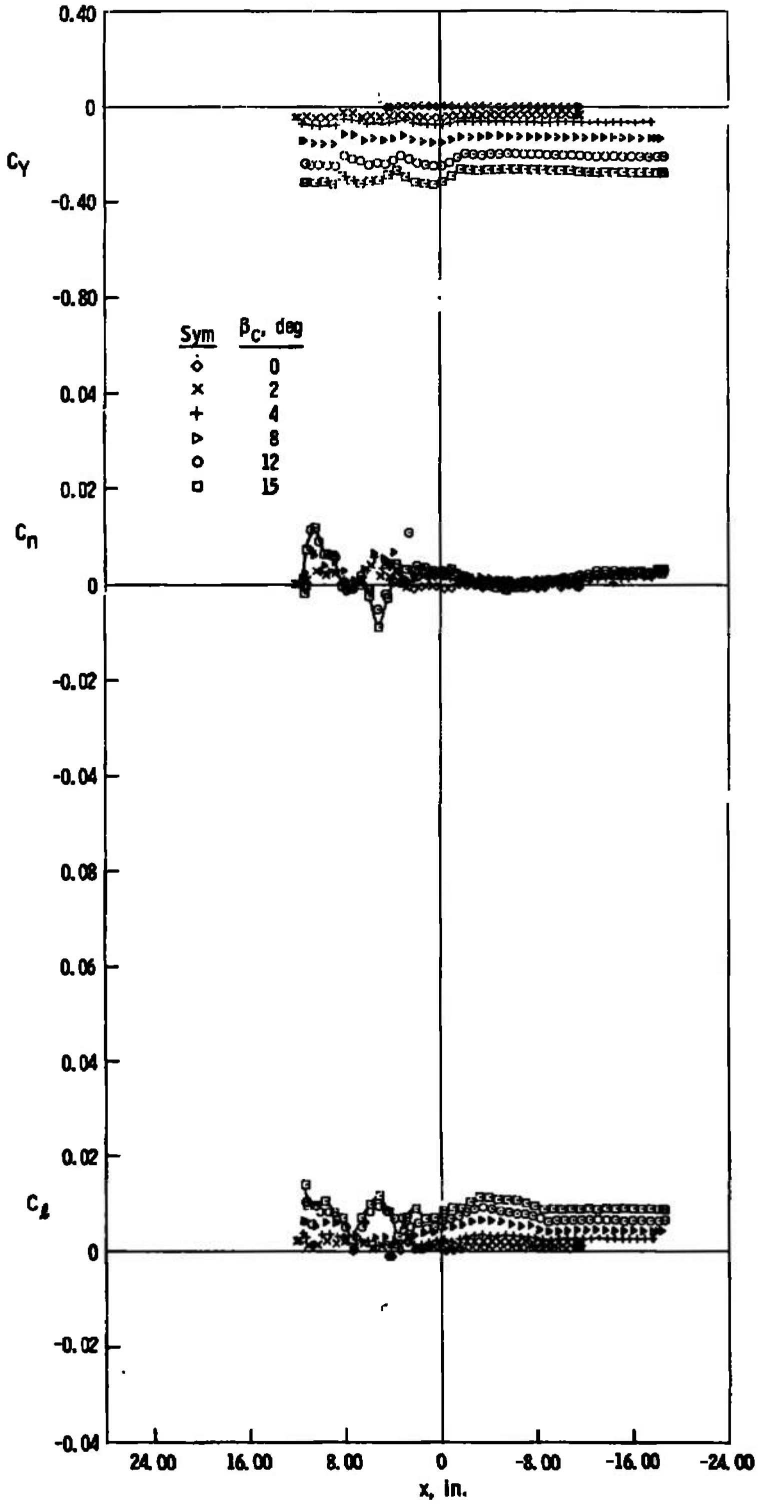

b. z = 4 in., y = 0
Fig. 15 Continued

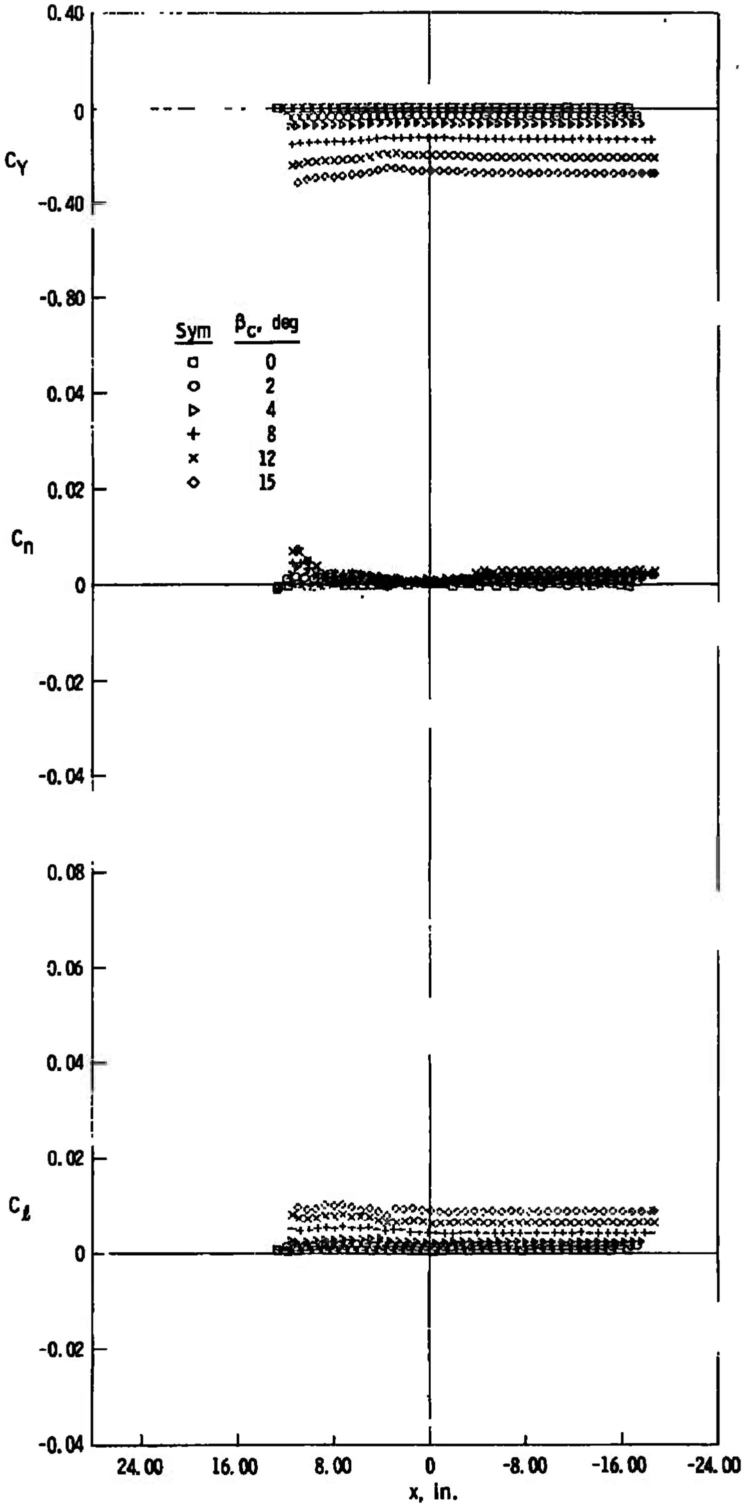

c. z = 6 in., y = 0

Fig. 15 Continued

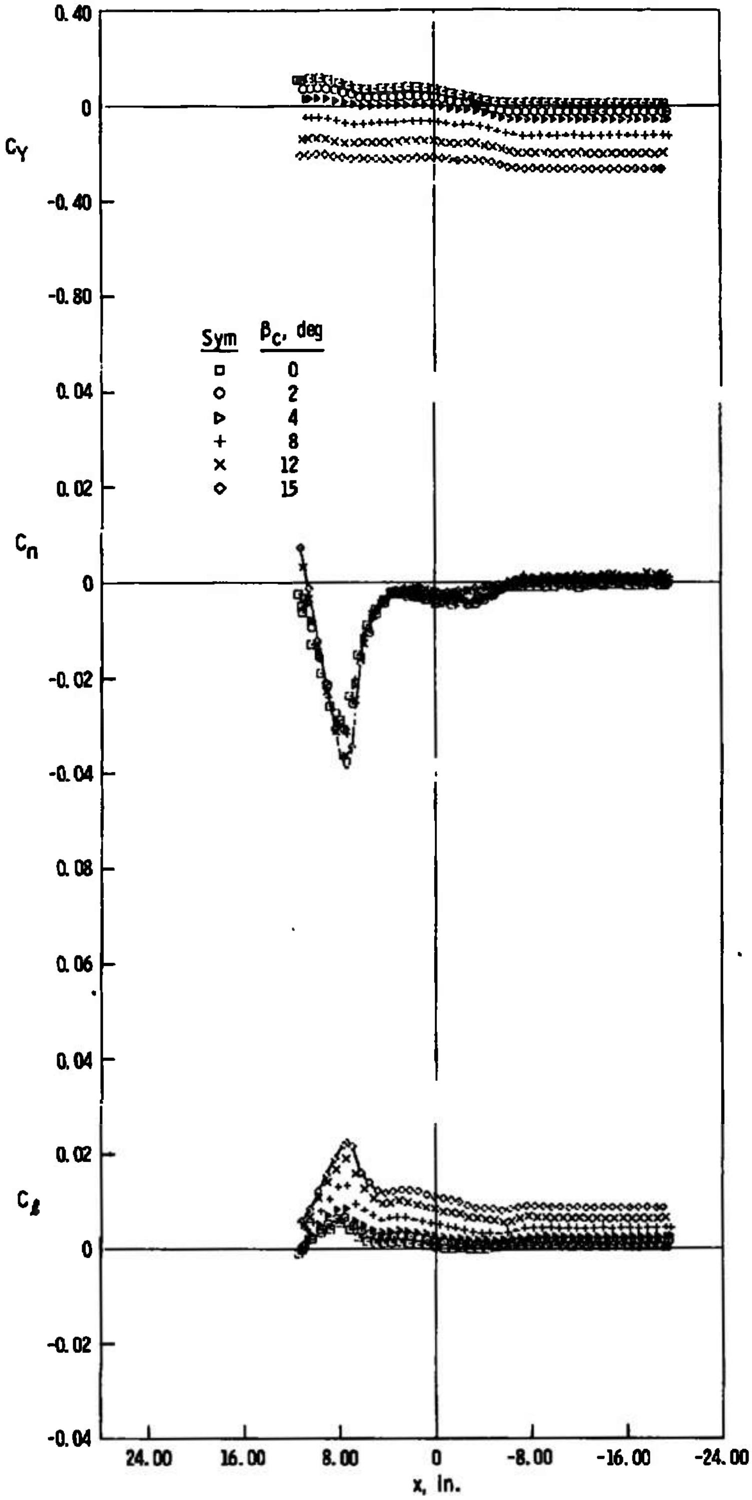

d. z = 3 in., y = -5 in.

Fig. 15 Concluded

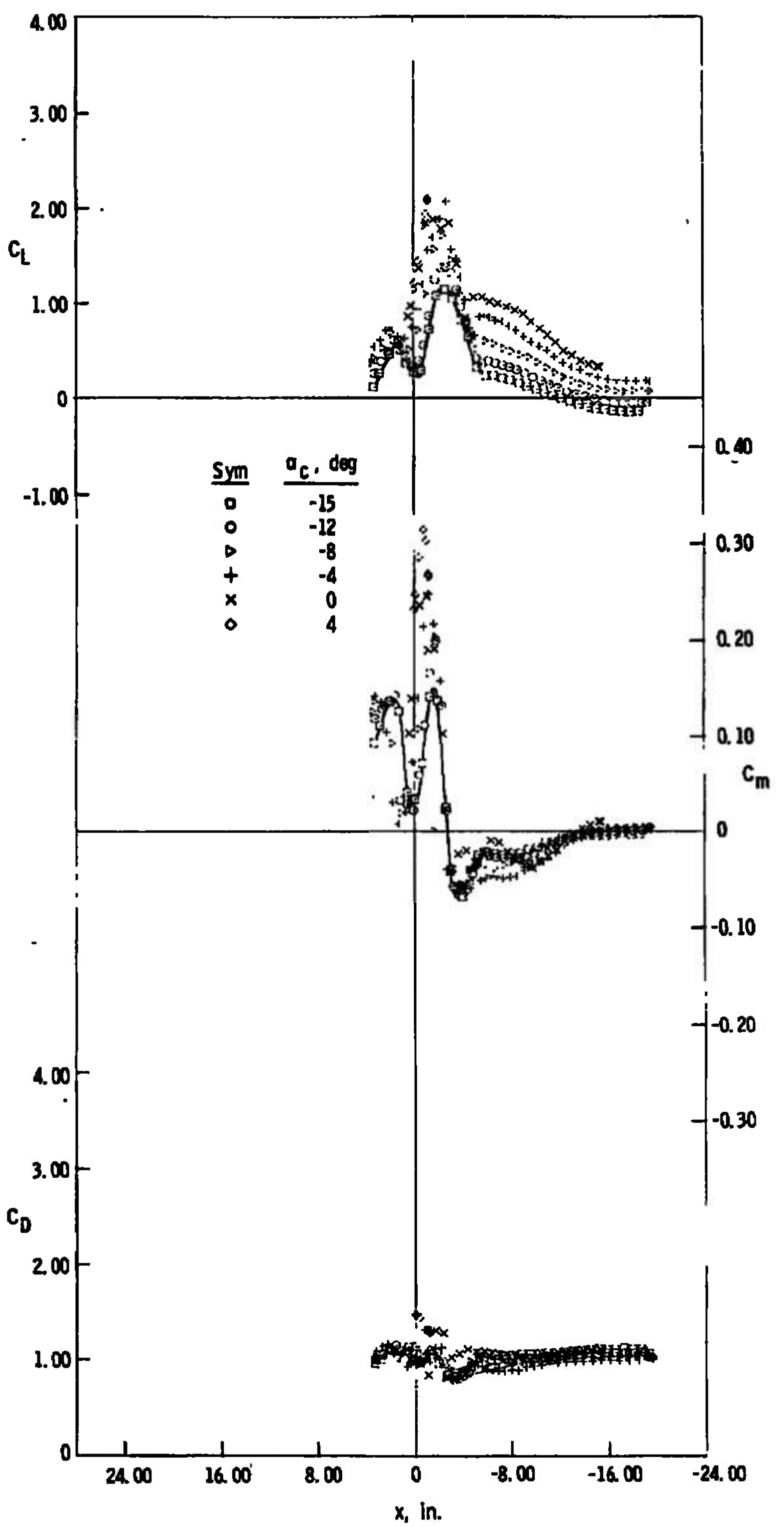

a. z = 3 in., y = 0

Fig. 16 Lift, Pitching-Moment, and Drag Characteristics of the Capsule, Jet On, $M_\infty = 2$, $p_c/p_\infty = 357$

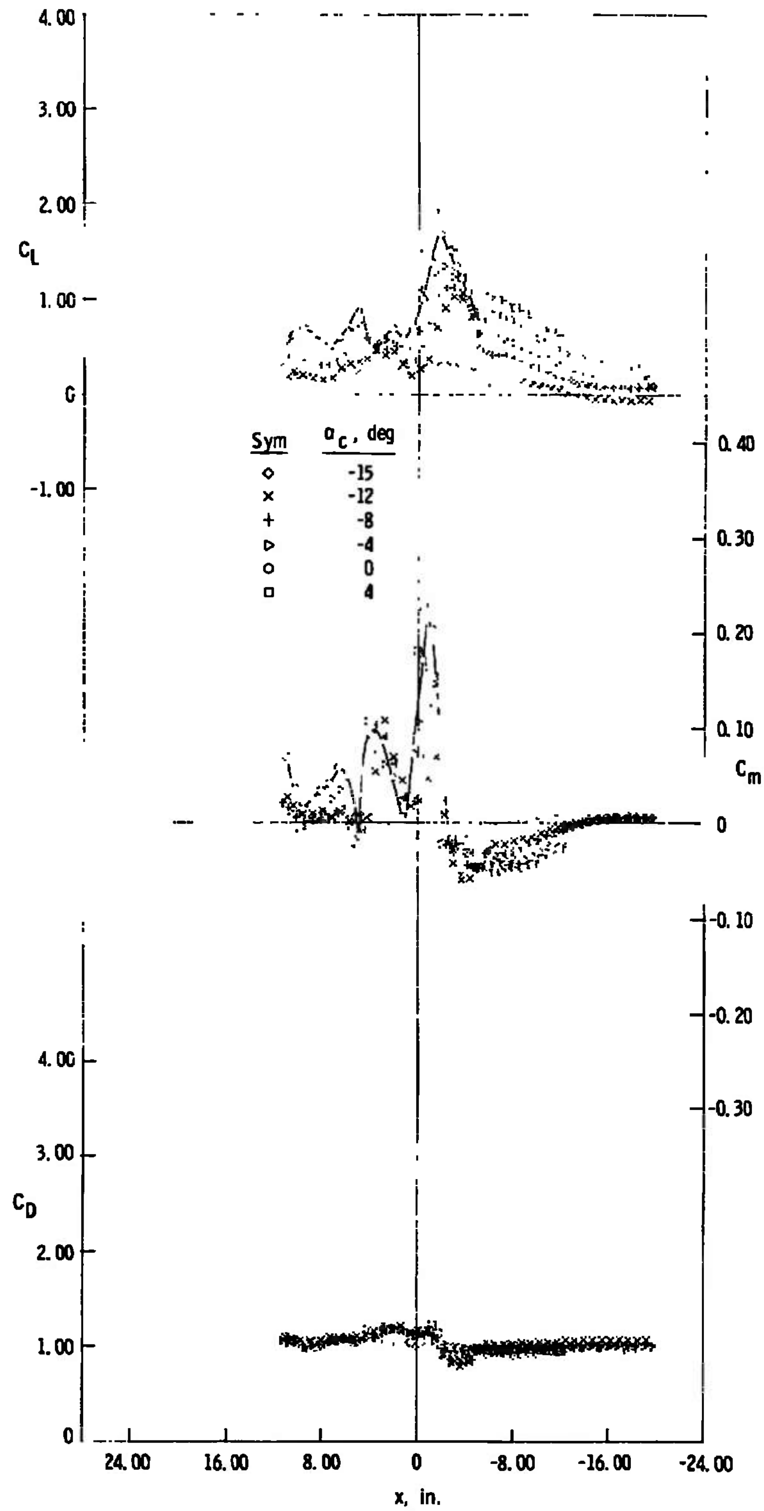

b. z = 4 in., y = 0
Fig. 16 Continued

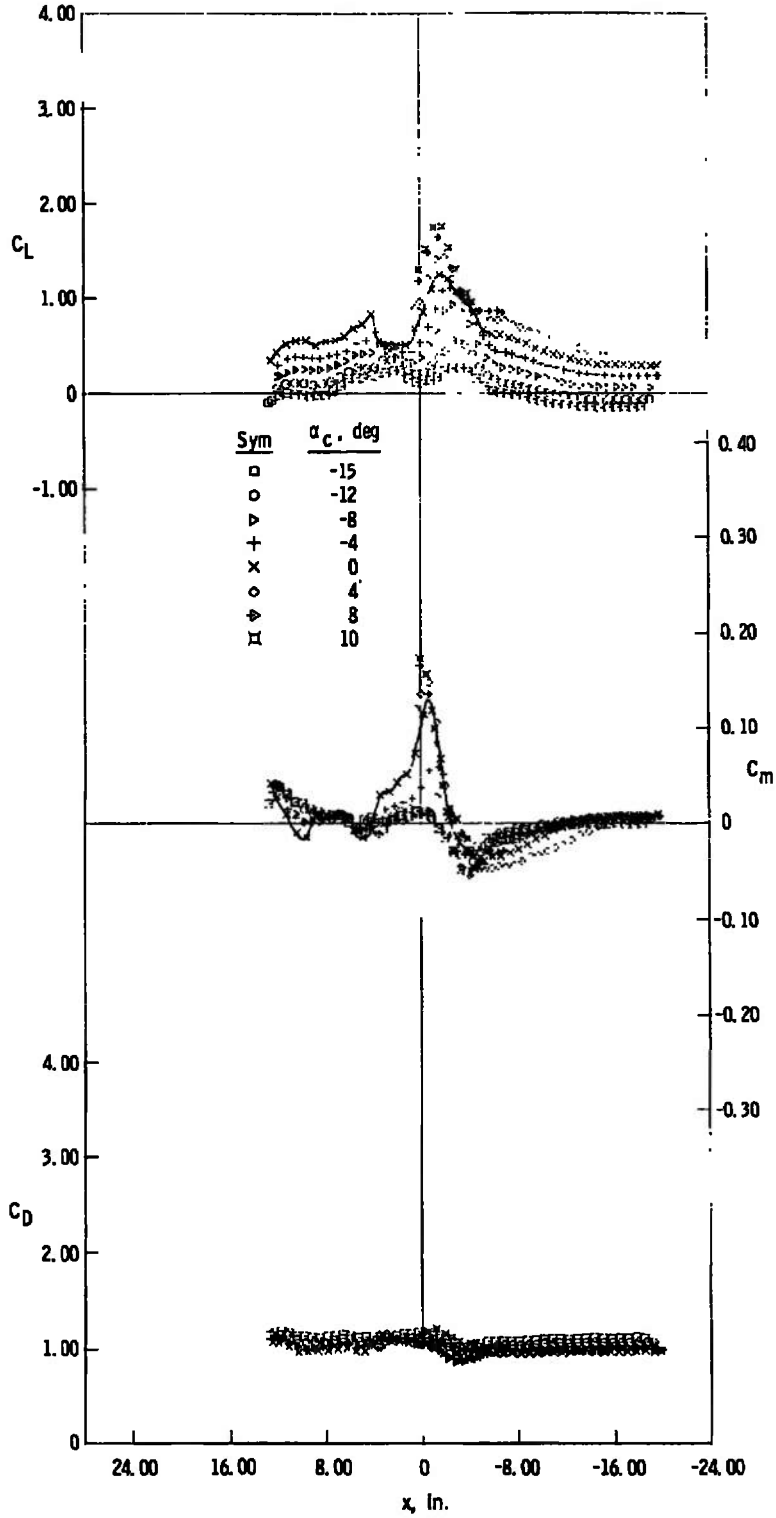

c. z = 5 in., y = 0

Fig. 16 Continued

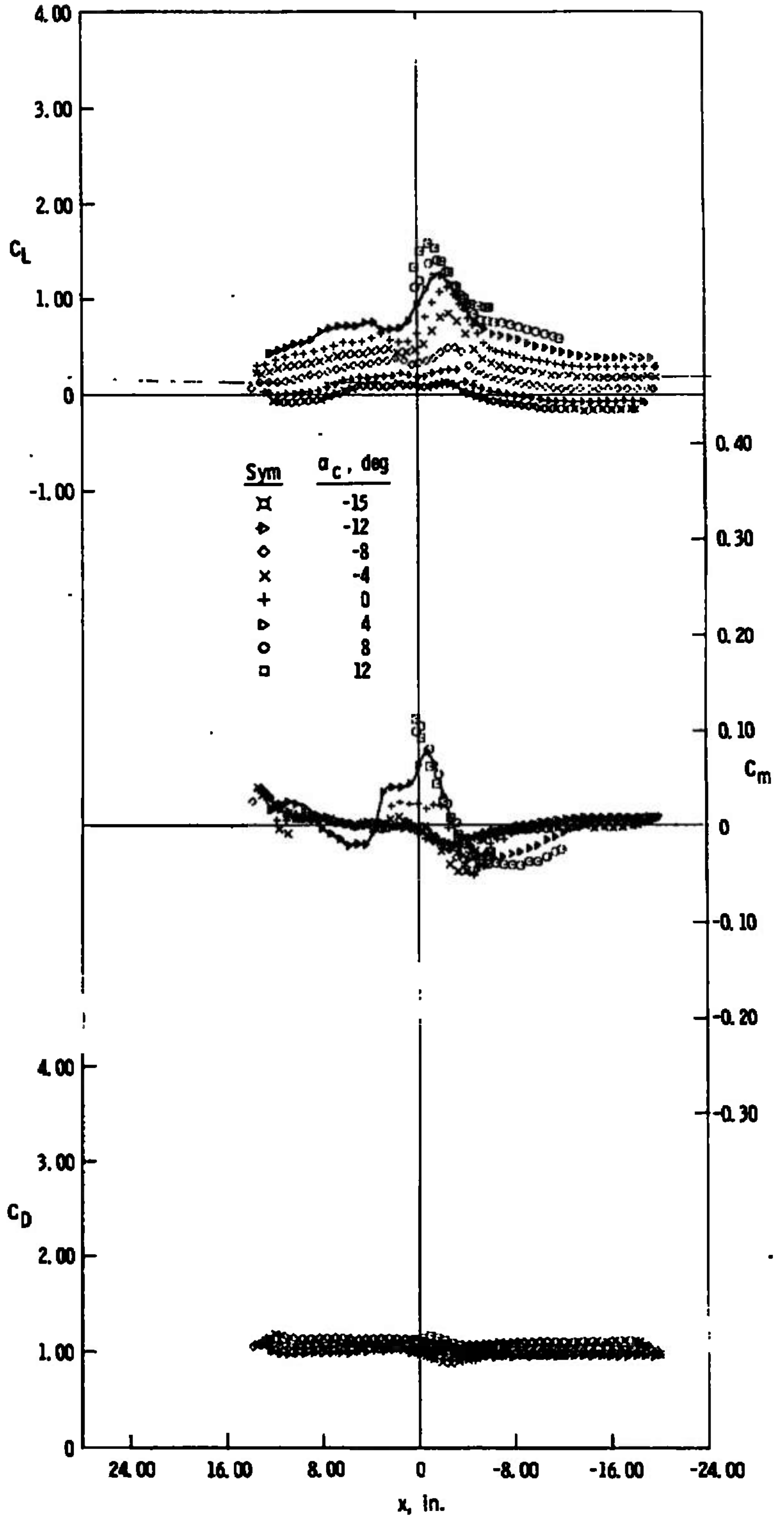

d. z = 6 in., y = 0

Fig. 16 Continued

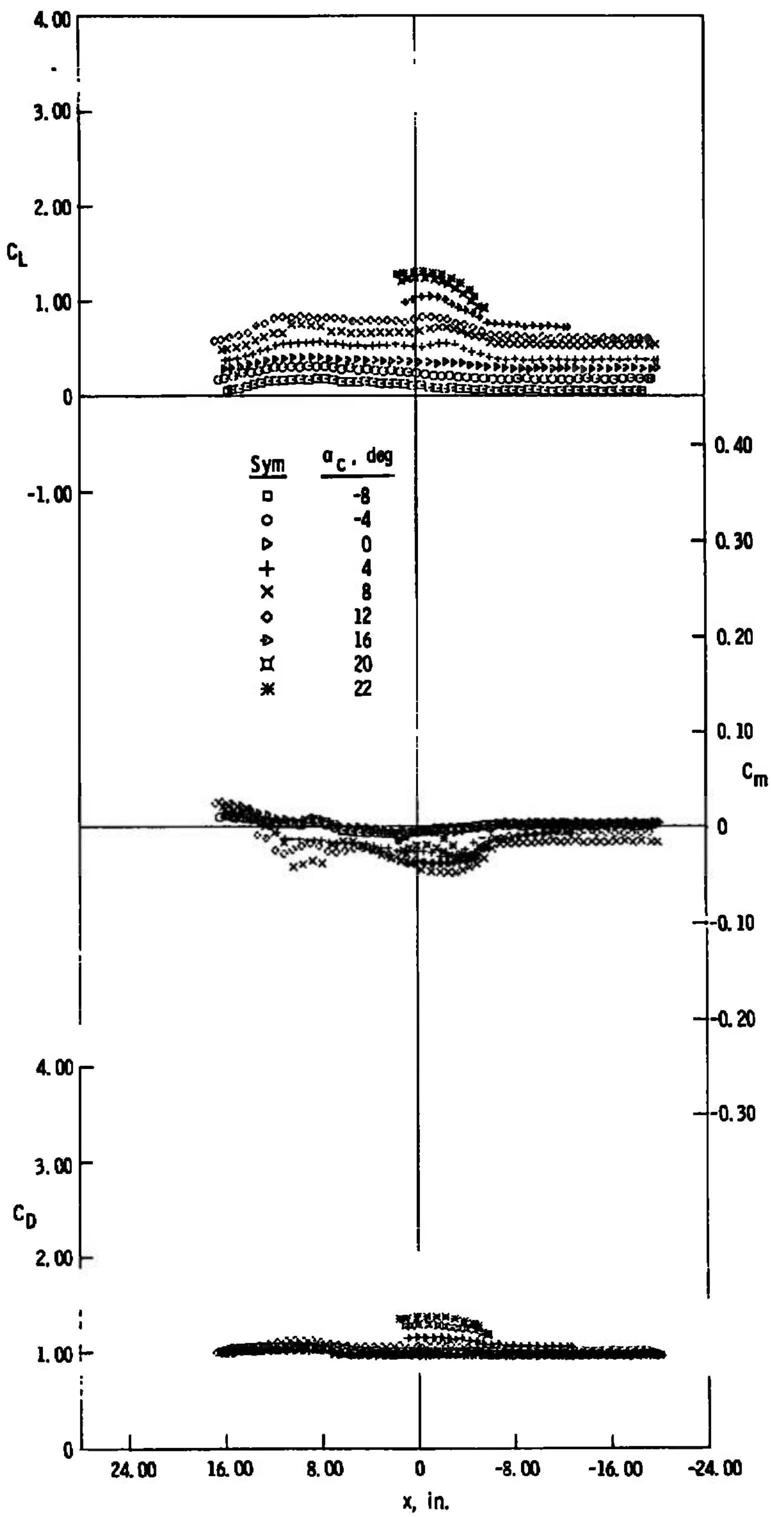

e. z = 10 in., y = 0

Fig. 16 Continued

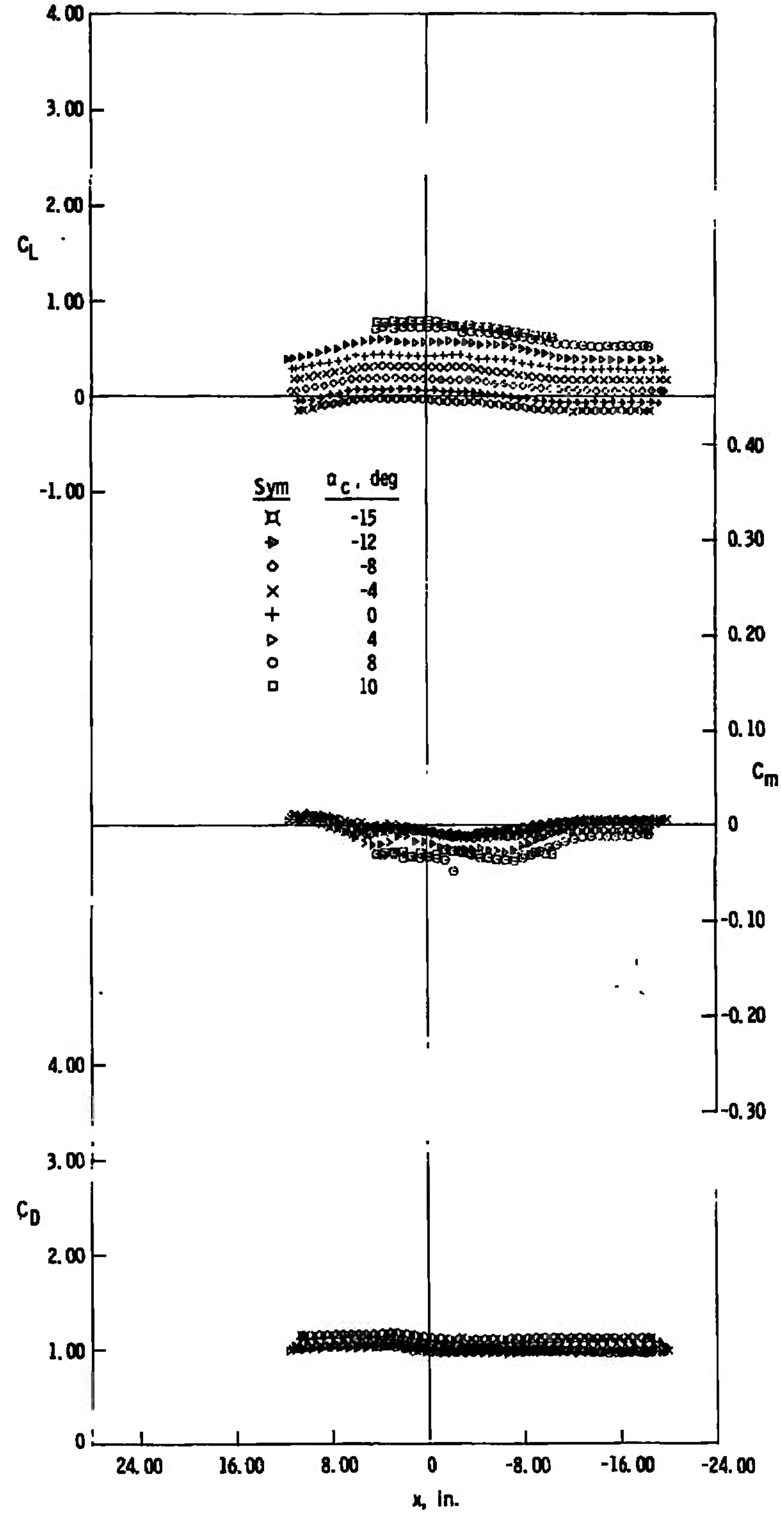

f. z = 5 in., y = 5 in.
Fig. 16 Concluded

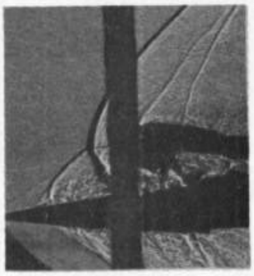

a. α_c = 4 deg
$y = 0$
$z = 3$ in.
$x = -1.0$ in.

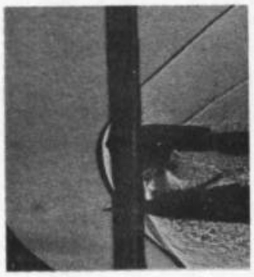

b. $\alpha_c = 0$
$y = 0$
$z = 3$ in.
$x = -11.5$ in.

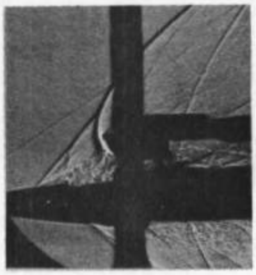

c. $\alpha_c = -4$ deg
$y = 0$
$z = 3$ in.
$x = 3.4$ in.

d. $\alpha_c = -8$ deg
$y = 0$
$z = 3$ in.
$x = -1.2$ in.

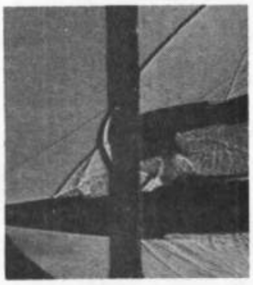

e. $\alpha_c = -15$ deg
$y = 0$
$z = 4$ in.
$x = 2.7$ in.

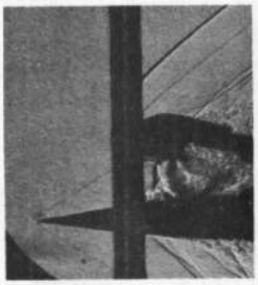

f. $\alpha_c = 10$ deg
$y = 0$
$z = 5$ in.
$x = -4.7$ in.

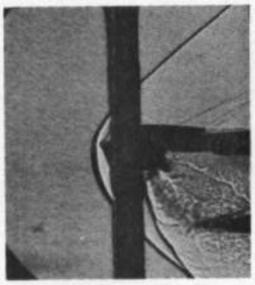

g. $\alpha_c = 0$
$y = 0$
$z = 5$ in.
$x = 19.7$ in.

h. $\alpha_c = -15$ deg
$y = 0$
$z = 5$ in.
$x = 8.5$ in.

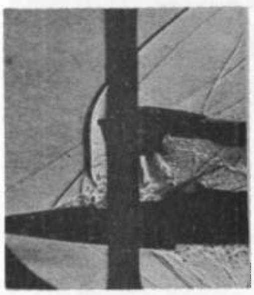

i. $\alpha_c = 4$ deg
$y = 0$
$z = 6$ in.
$x = 0.4$ in.

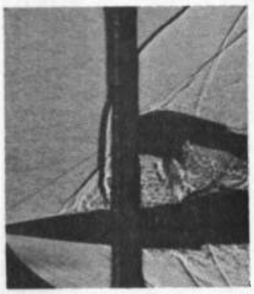

j. $\alpha_c = 12$ deg
$y = 0$
$z = 6$ in.
$x = 0.2$ in.

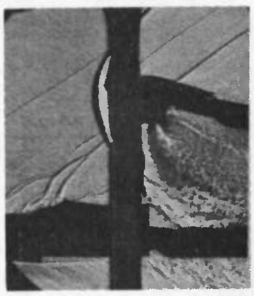

k. $\alpha_c = 12$ deg
$y = 0$
$z = 10$ in.
$x = 12.7$ in.

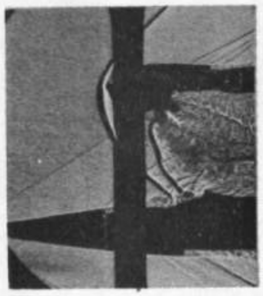

l. $\alpha_c = -4$ deg
$y = 0$
$z = 10$ in.
$x = 0.5$ in.

Fig. 17 Schlieren Photographs, Jet On, $M_\infty = 2$, $p_c/p_\infty = 357$

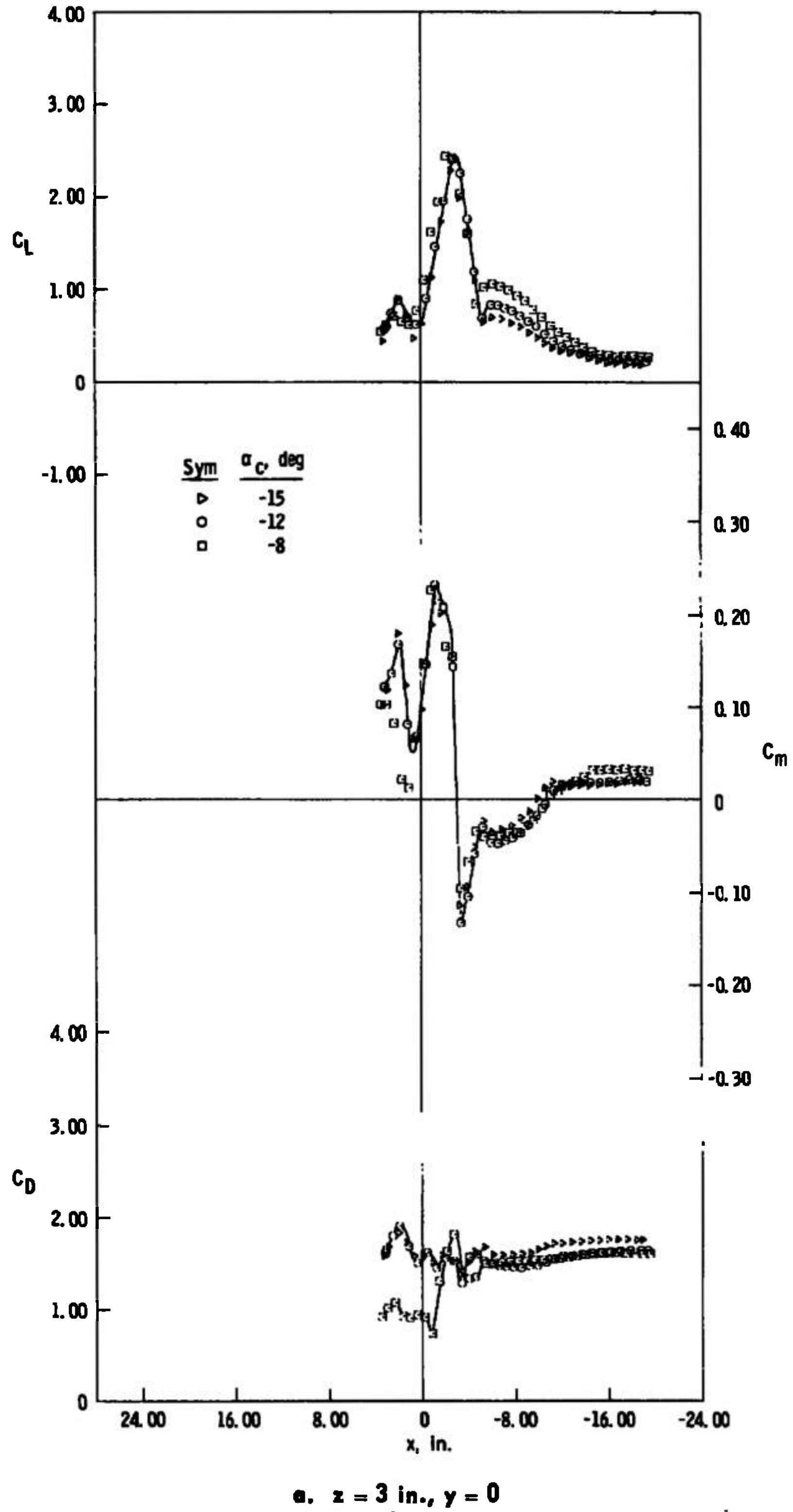

a. z = 3 in., y = 0

Fig. 18 Lift, Pitching-Moment, and Drag Characteristics of the Capsule, Jet On, $M_\infty = 3$, $p_c/p_\infty = 1206$

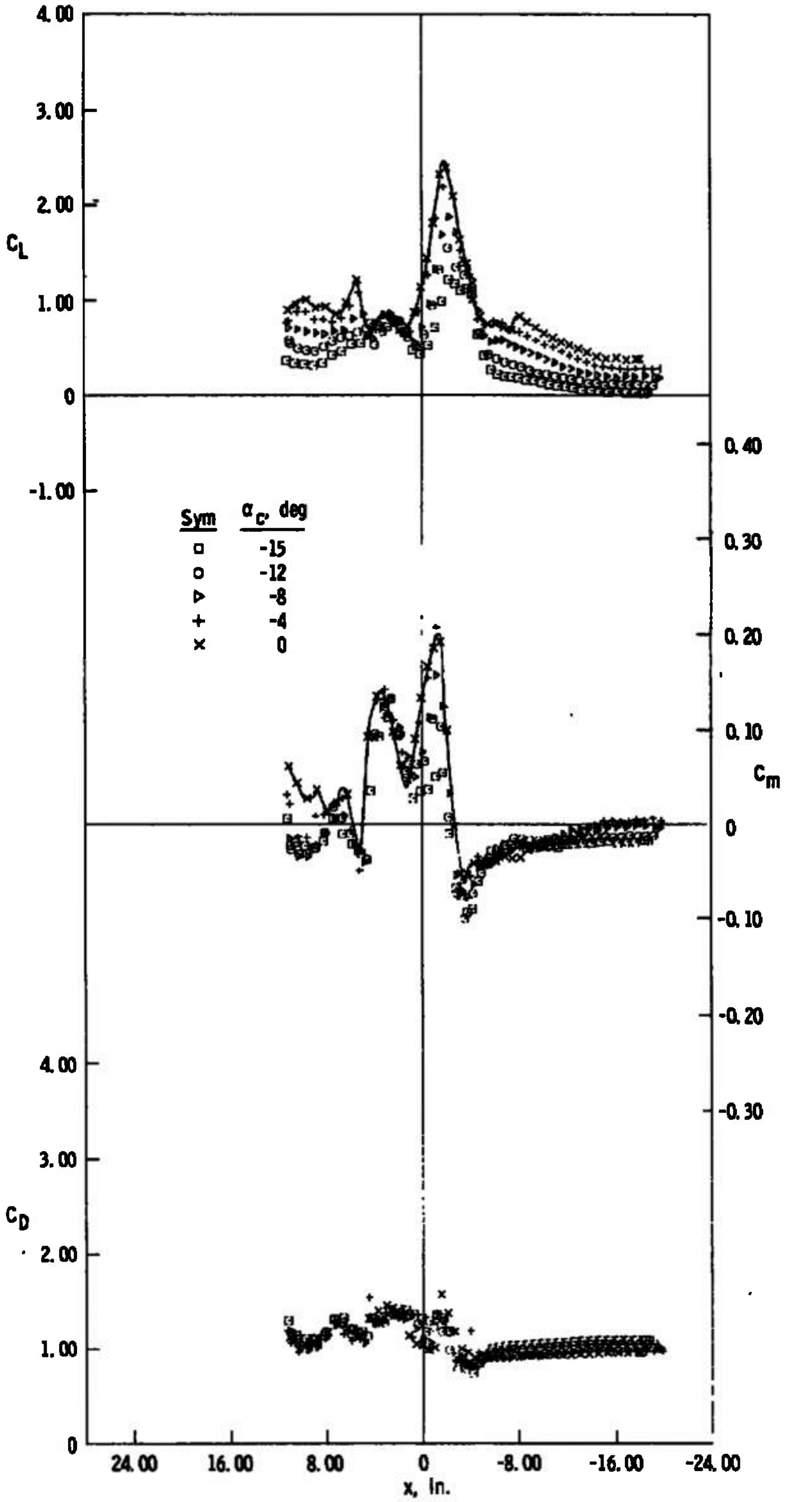

b. z = 4 in., y = 0
Fig. 18 Continued

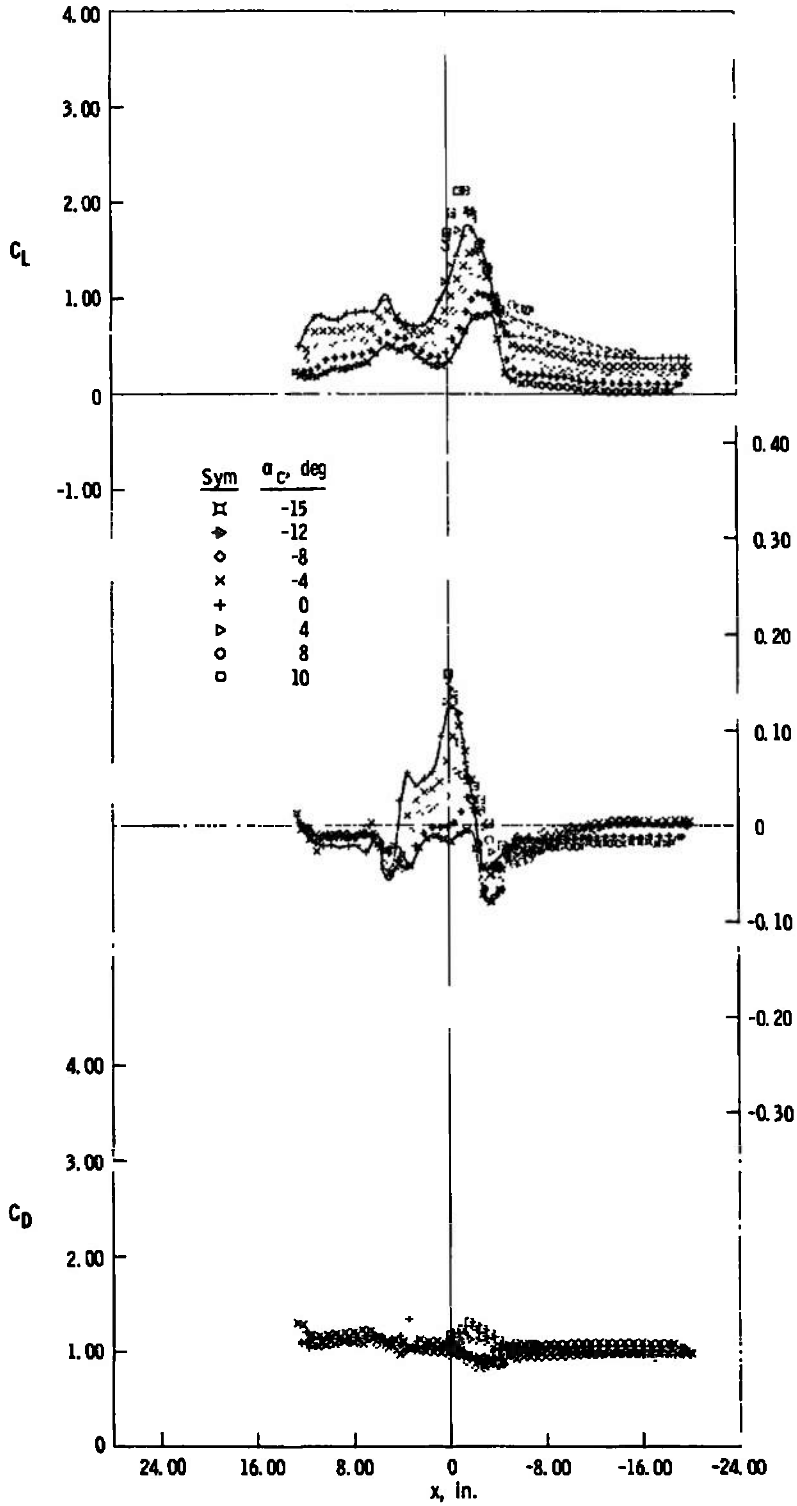

c. z = 5 in., y = 0
Fig. 18 Continued

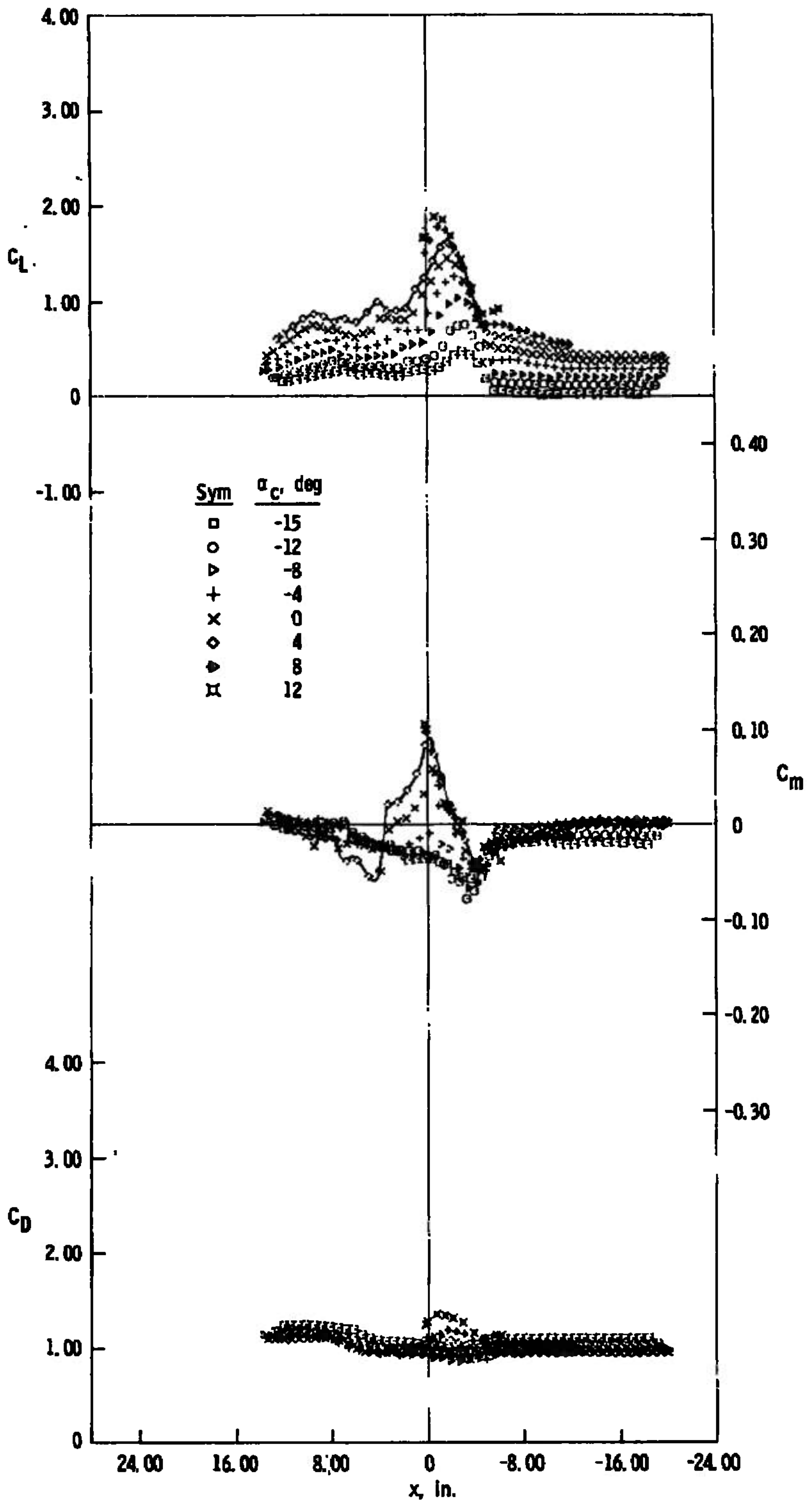

d. z = 6 in., y = 0

Fig. 18 Continued

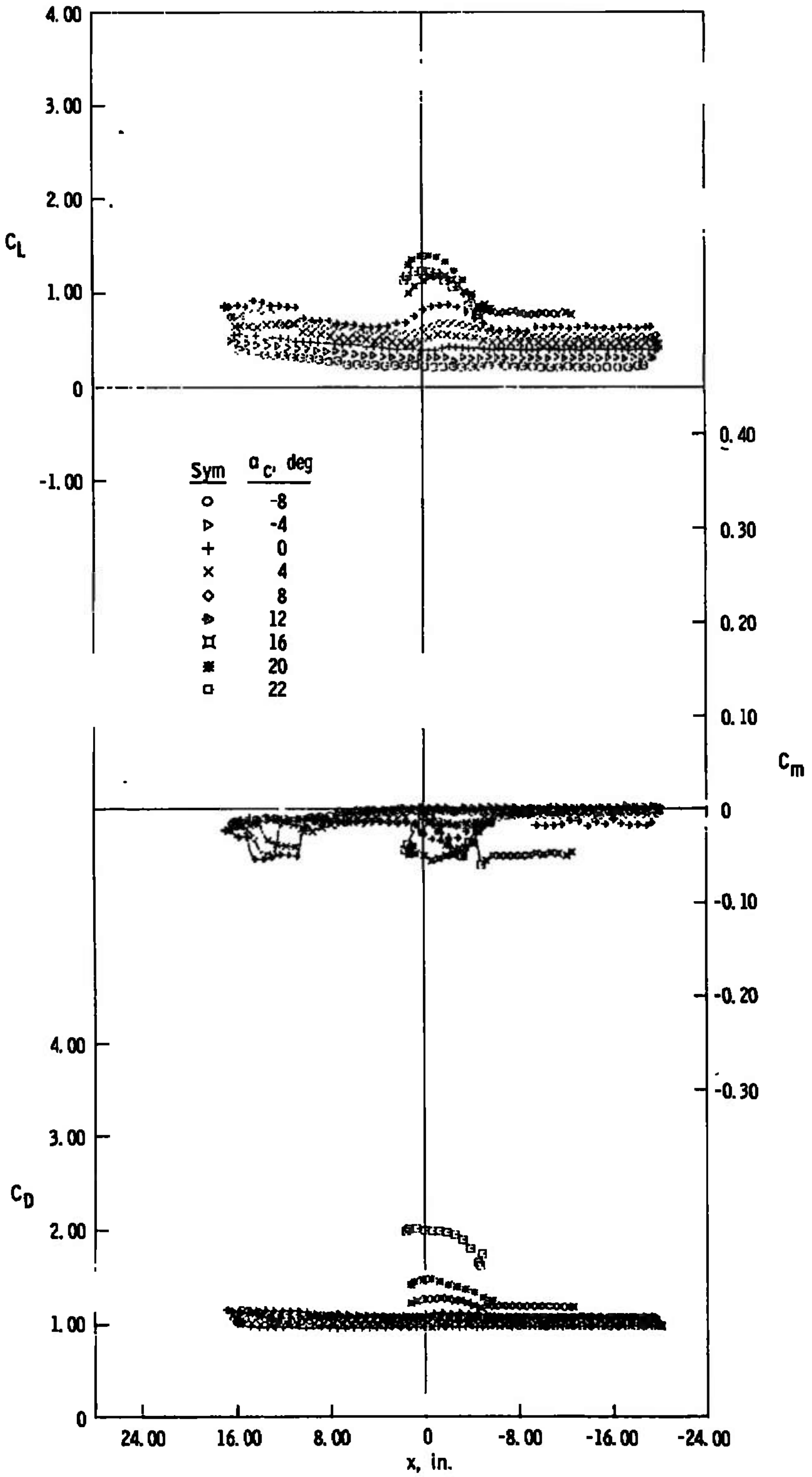

e. z = 10 in., y = 0

Fig. 18 Continued

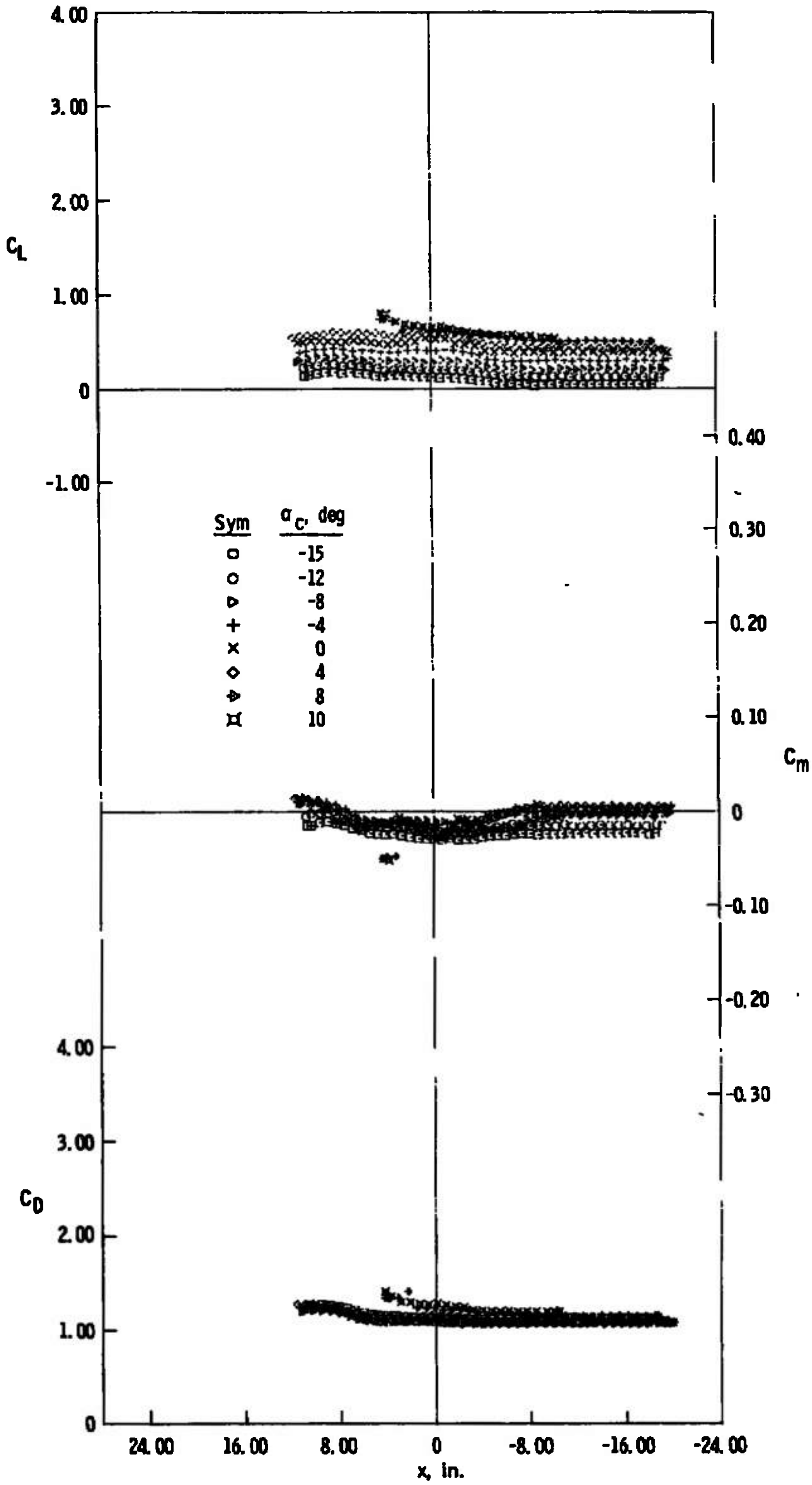

f. z = 5 in., y = 5 in.
Fig. 18 Concluded

a. α_c = −15 deg
y = 0
z = 3 in.
x = 3.1 in.

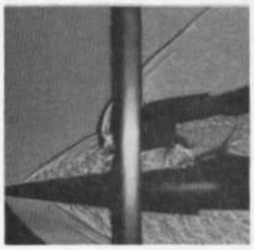

b. α_c = −15 deg
y = 0
z = 3 in.
x = −0.6 in.

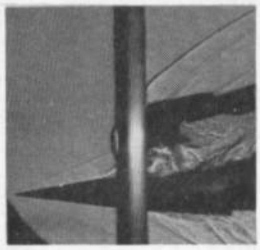

c. α_c = −15 deg
y = 0
z = 3 in.
x = −3.1 in.

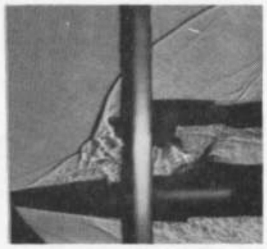

d. α_c = −4 deg
y = 0
z = 4 in.
x = 0.5 in.

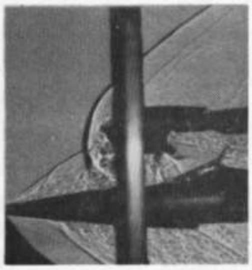

e. α_c = −4 deg
y = 0
z = 4 in.
x = −1.1 in.

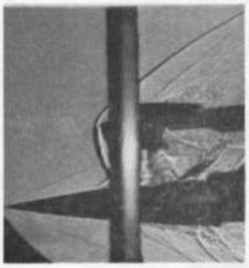

f. α_c = −4 deg
y = 0
z = 4 in.
x = −3.6 in.

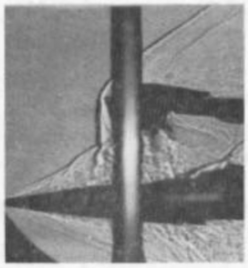

g. α_c = 4 deg
y = 0
z = 6 in.
x = −1.7 in.

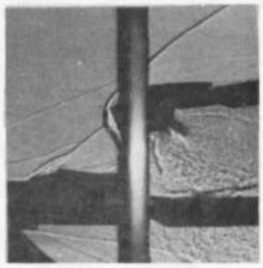

h. α_c = −8 deg
y = 0
z = 6 in.
x = 14.2 in.

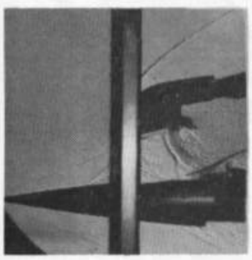

i. α_c = −15 deg
y = 0
z = 6 in.
x = −0.8 in.

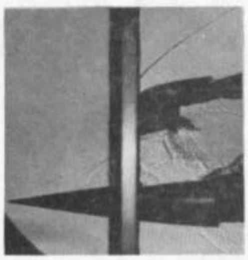

j. α_c = −15 deg
y = 0
z = 6 in.
x = −2.0 in.

k. α_c = 16 deg
y = 0
z = 10 in.
x = −8.8 in.

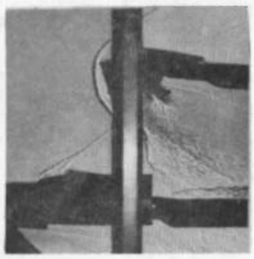

l. α_c = 4 deg
y = 0
z = 10 in.
x = 12.0 in.

Fig. 19 Schlieren Photographs, Jet On, $M_\infty = 3$, p_c/p_∞ = 1206

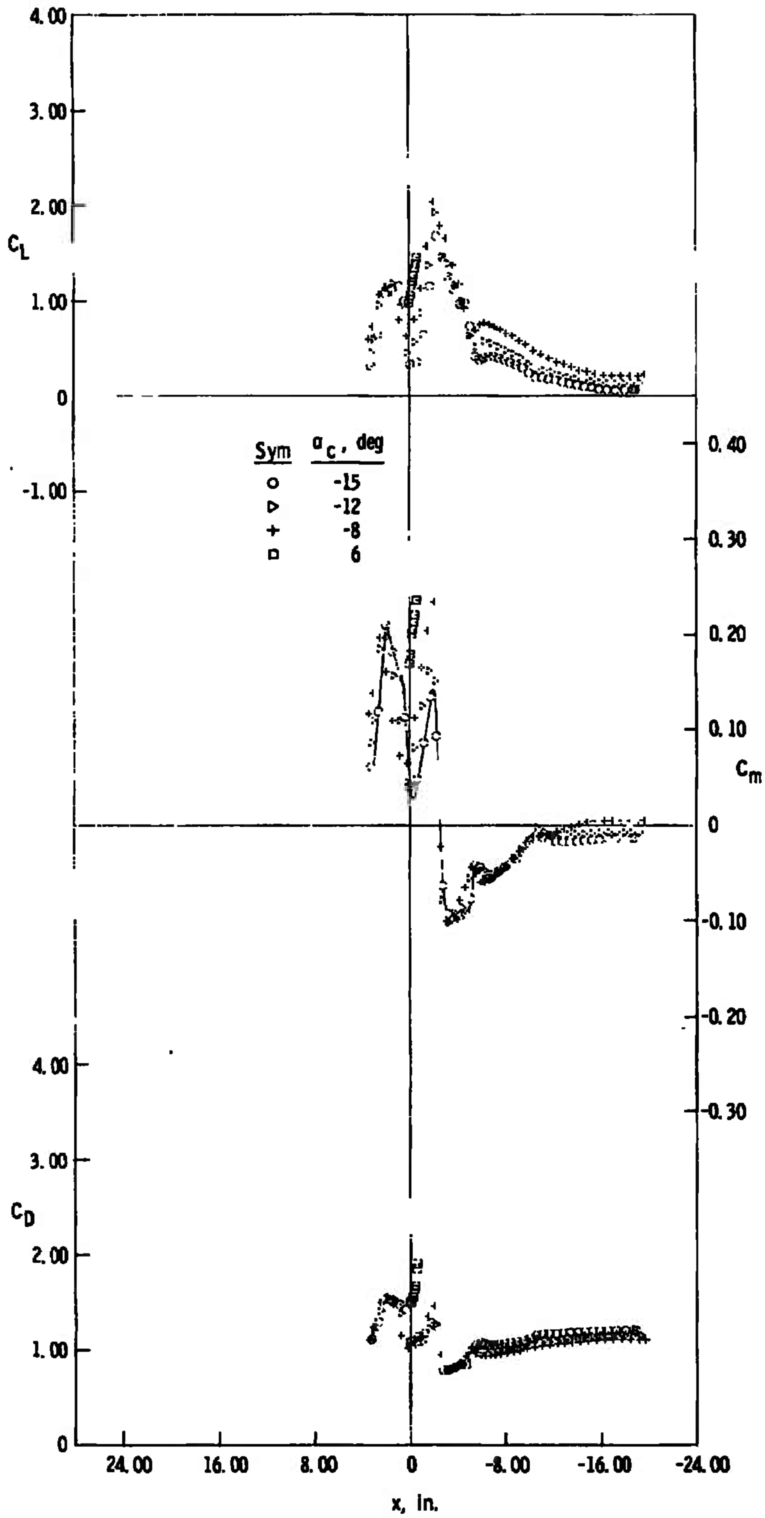

a. z = 3 in., y = 0

Fig. 20 Lift, Pitching-Moment, and Drag Characteristics of the Capsule, Jet On, $M_\infty = 4$, $p_c/p_\infty = 1303$

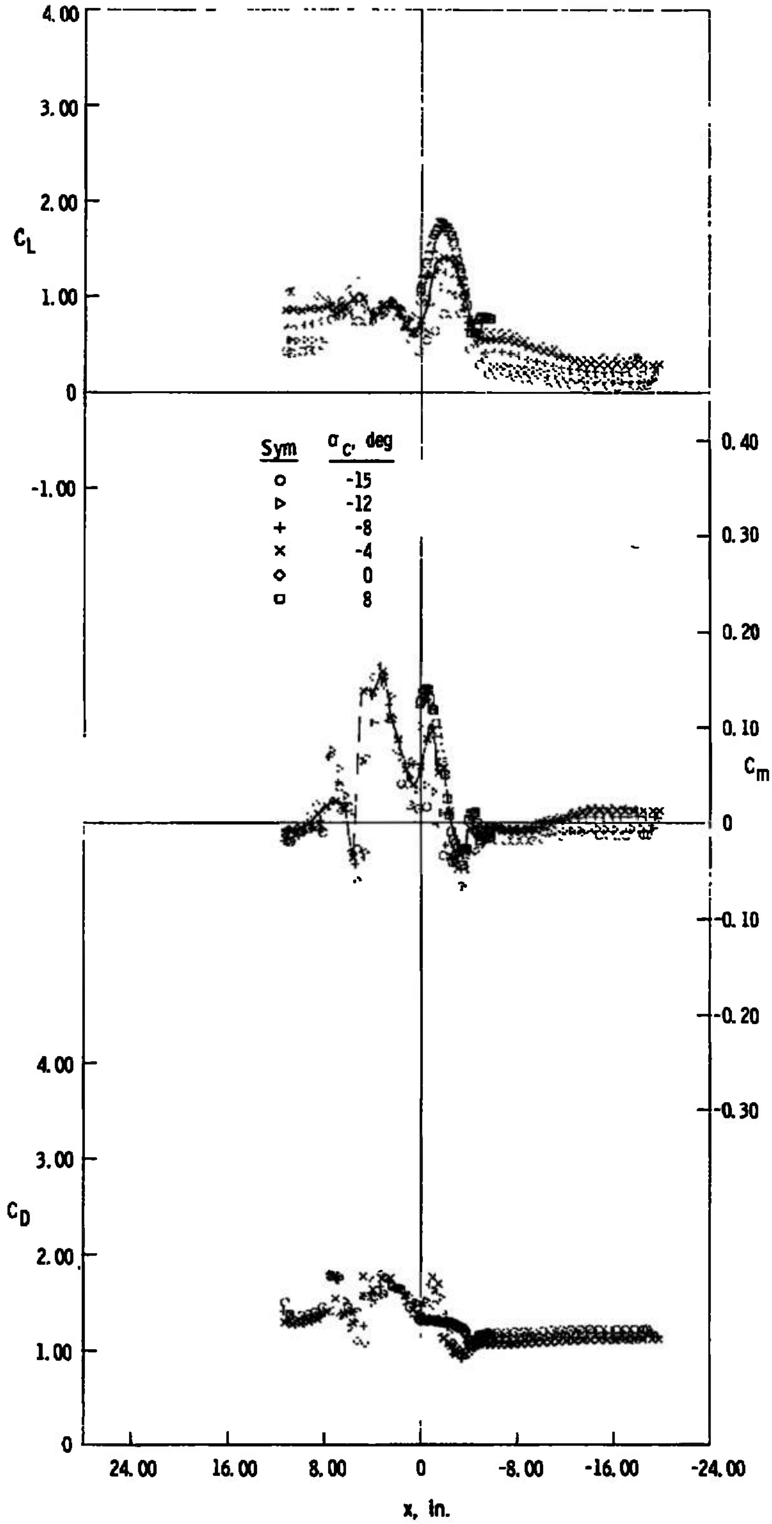

b. z = 4 in., y = 0
Fig. 20 Continued

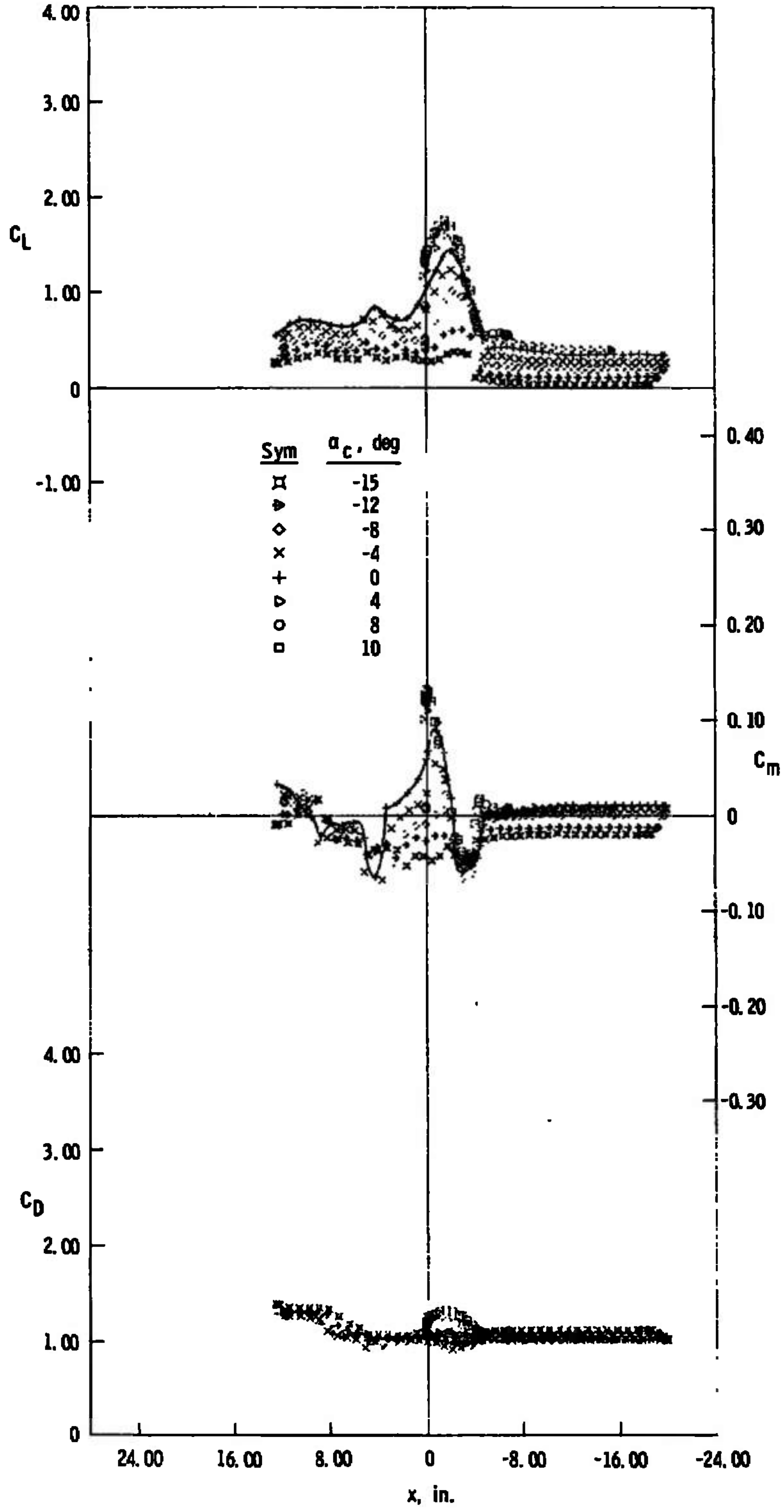

c. z = 5 in., y = 0
Fig. 20 Continued

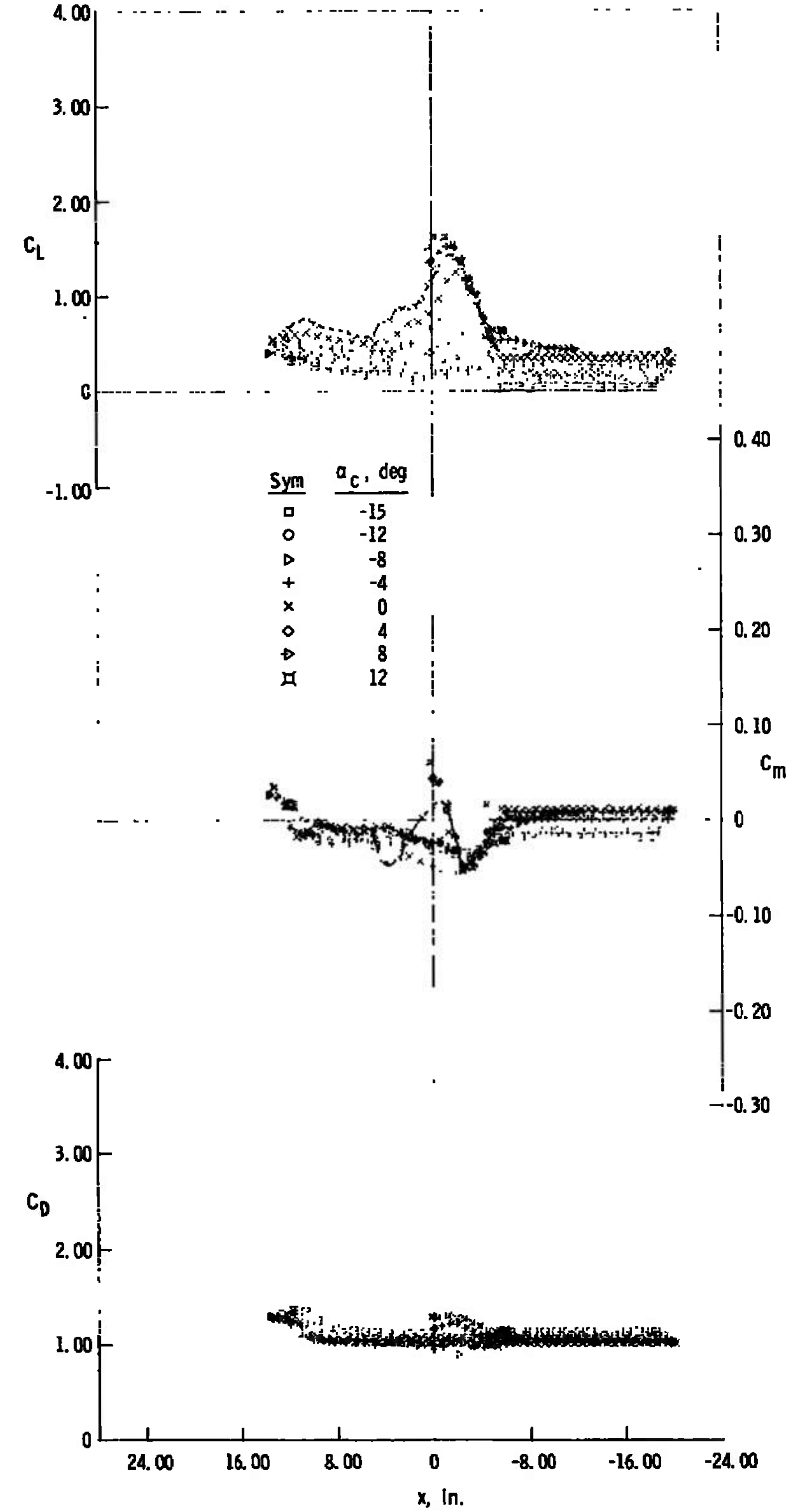

d. z = 6 in., y = 0
Fig. 20 Continued

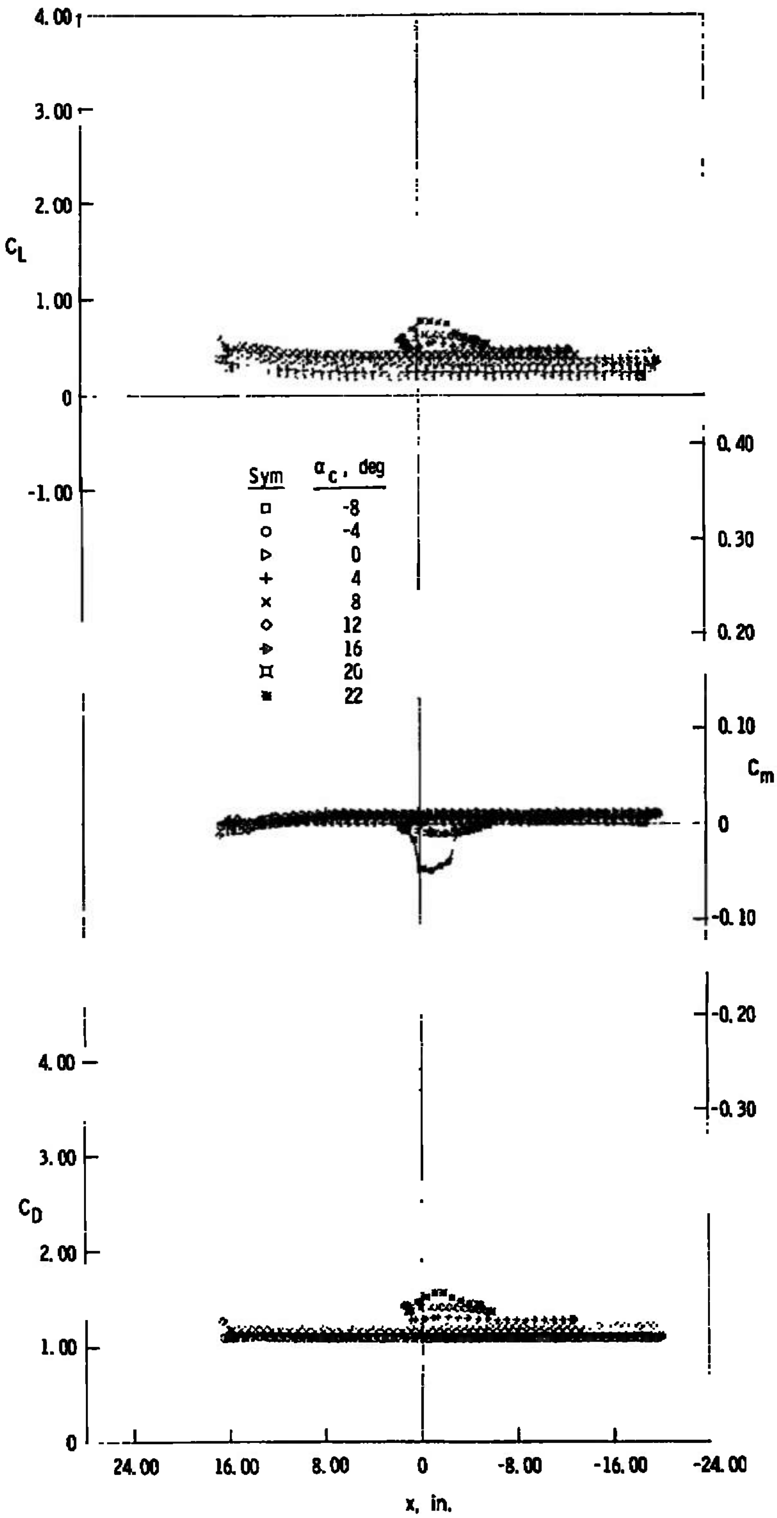

e. z = 10 in., y = 0
Fig. 20 Continued

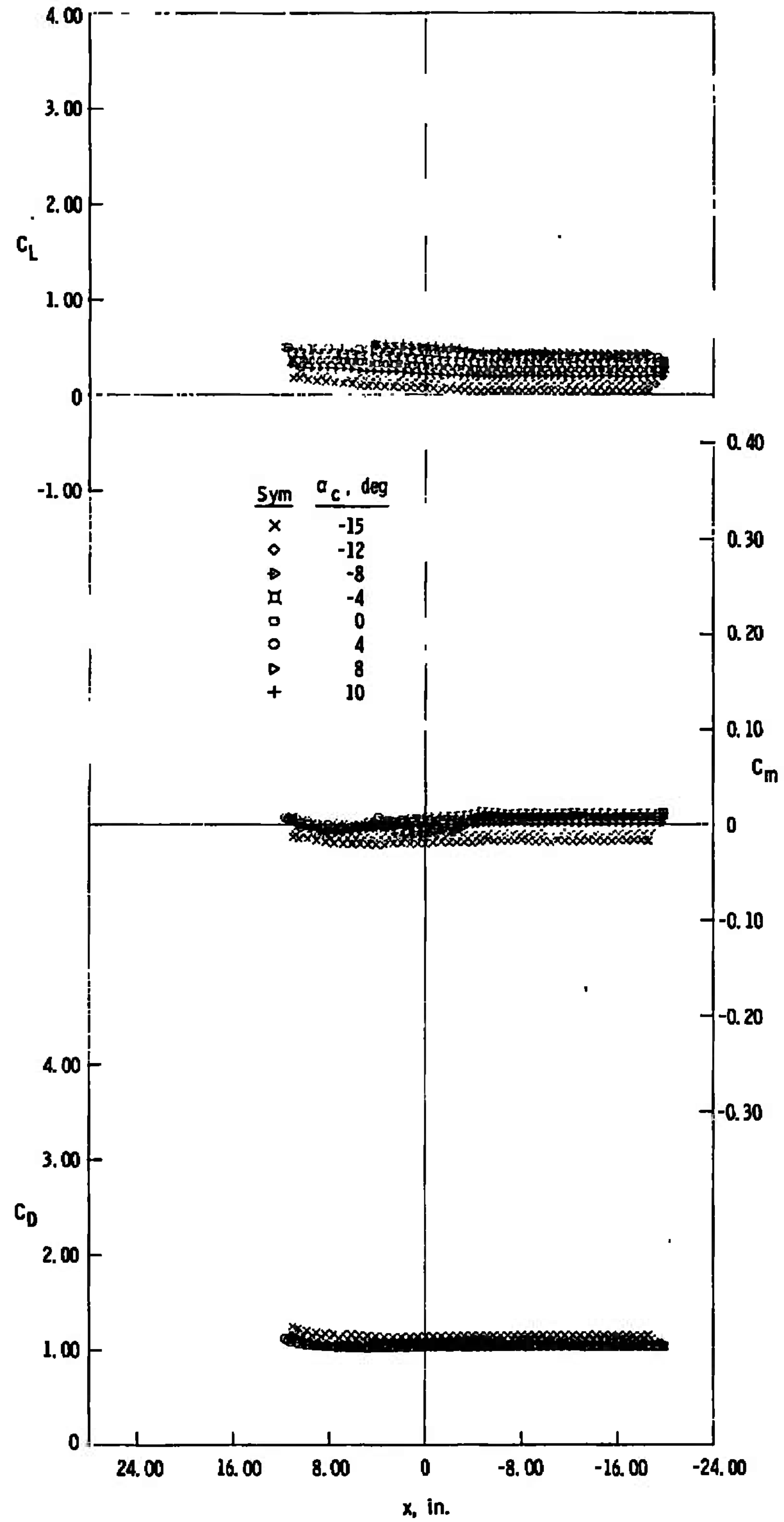

f. z = 5 in., y = 5 in.

Fig. 20 Concluded

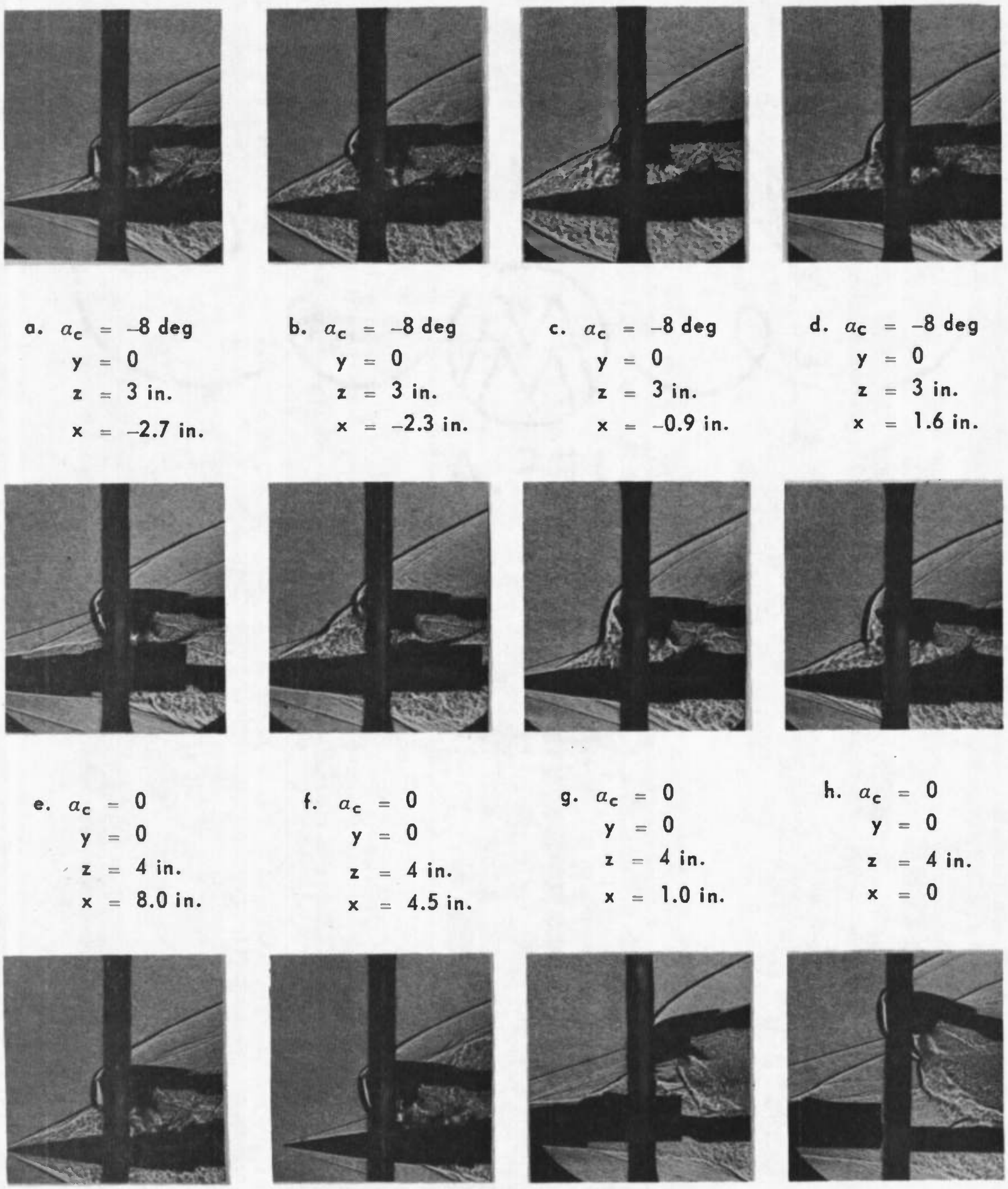

a. α_c = –8 deg
y = 0
z = 3 in.
x = –2.7 in.

b. α_c = –8 deg
y = 0
z = 3 in.
x = –2.3 in.

c. α_c = –8 deg
y = 0
z = 3 in.
x = –0.9 in.

d. α_c = –8 deg
y = 0
z = 3 in.
x = 1.6 in.

e. α_c = 0
y = 0
z = 4 in.
x = 8.0 in.

f. α_c = 0
y = 0
z = 4 in.
x = 4.5 in.

g. α_c = 0
y = 0
z = 4 in.
x = 1.0 in.

h. α_c = 0
y = 0
z = 4 in.
x = 0

i. α_c = 0
y = 0
z = 4 in.
5 = –2.5 in.

j. α_c = 0
y = 0
z = 4 in.
x = –3.9 in.

k. α_c = –15 deg
y = 0
z = 6 in.
x = 11.7 in.

l. α_c = 12 deg
y = 0
z = 10 in.
x = 16.2 in.

Fig. 21 Schlieren Photographs, Jet On, M_∞ = 4, p_c/p_∞ = 1303

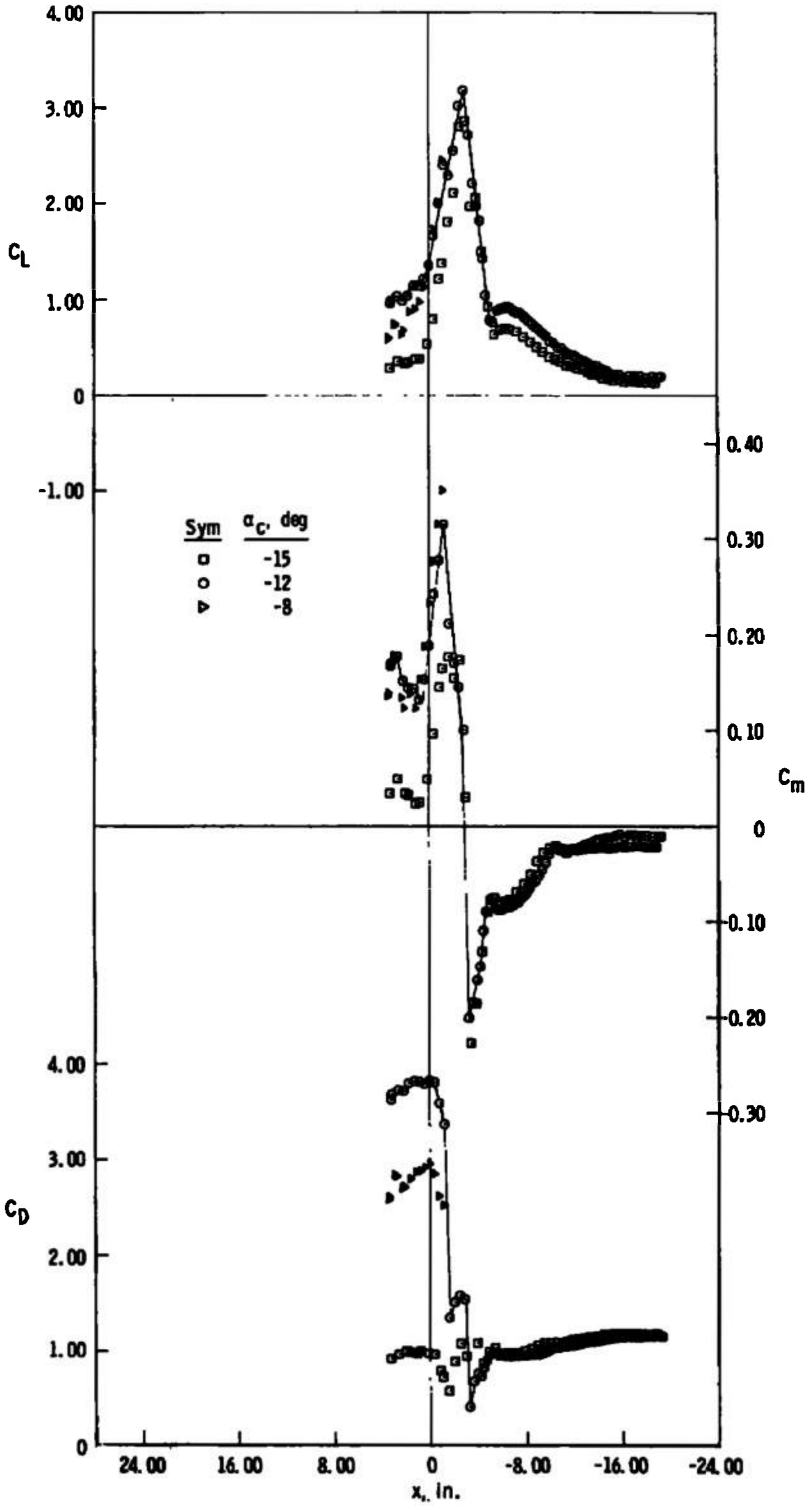

a. z = 3 in., y = 0

Fig. 22 Lift, Pitching-Moment, and Drag Characteristics of the Capsule, Jet On, $M_\infty = 5$, $p_c/p_\infty = 4204$

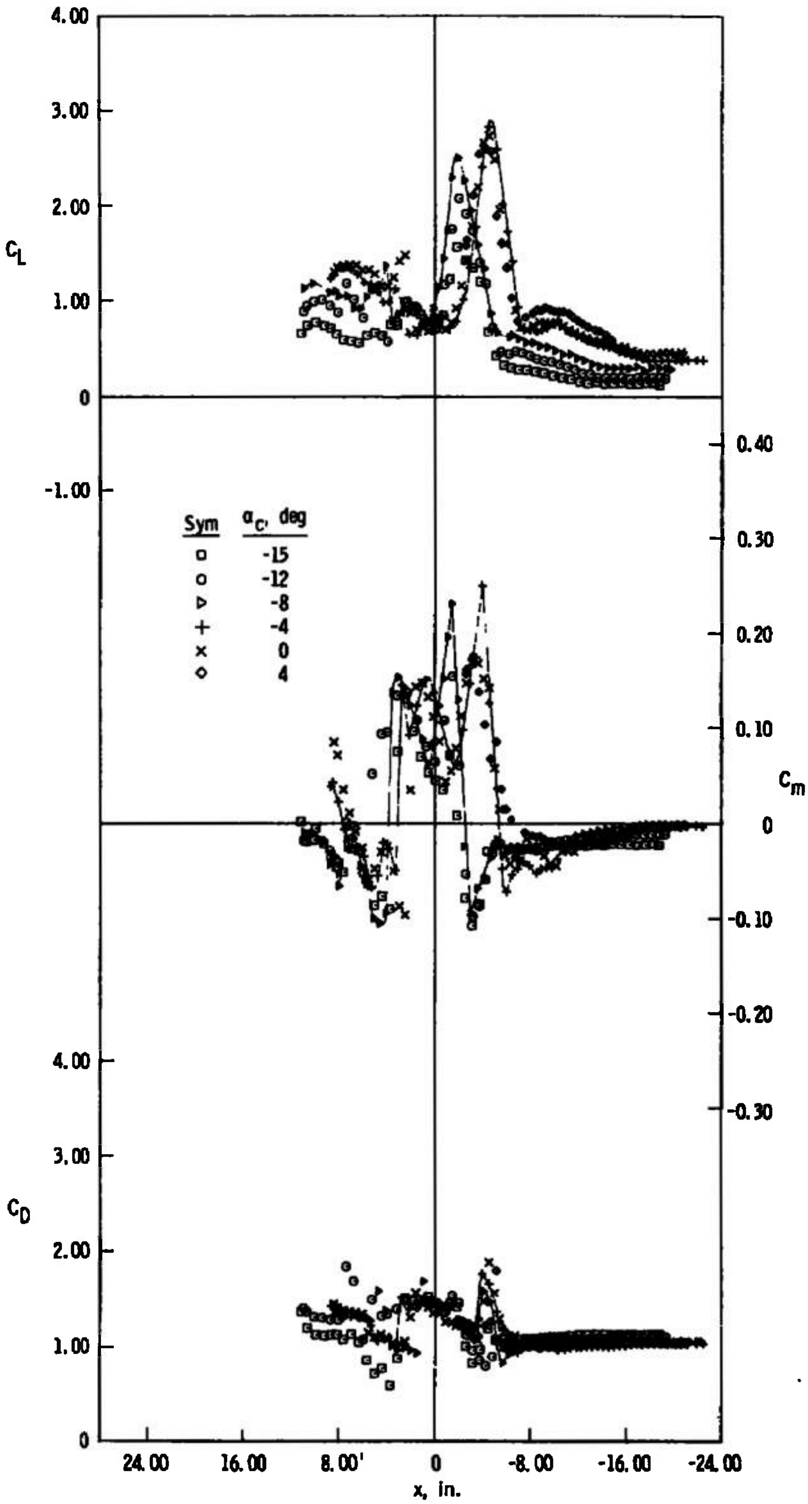

b. z = 4 in., y = 0
Fig. 22 Continued

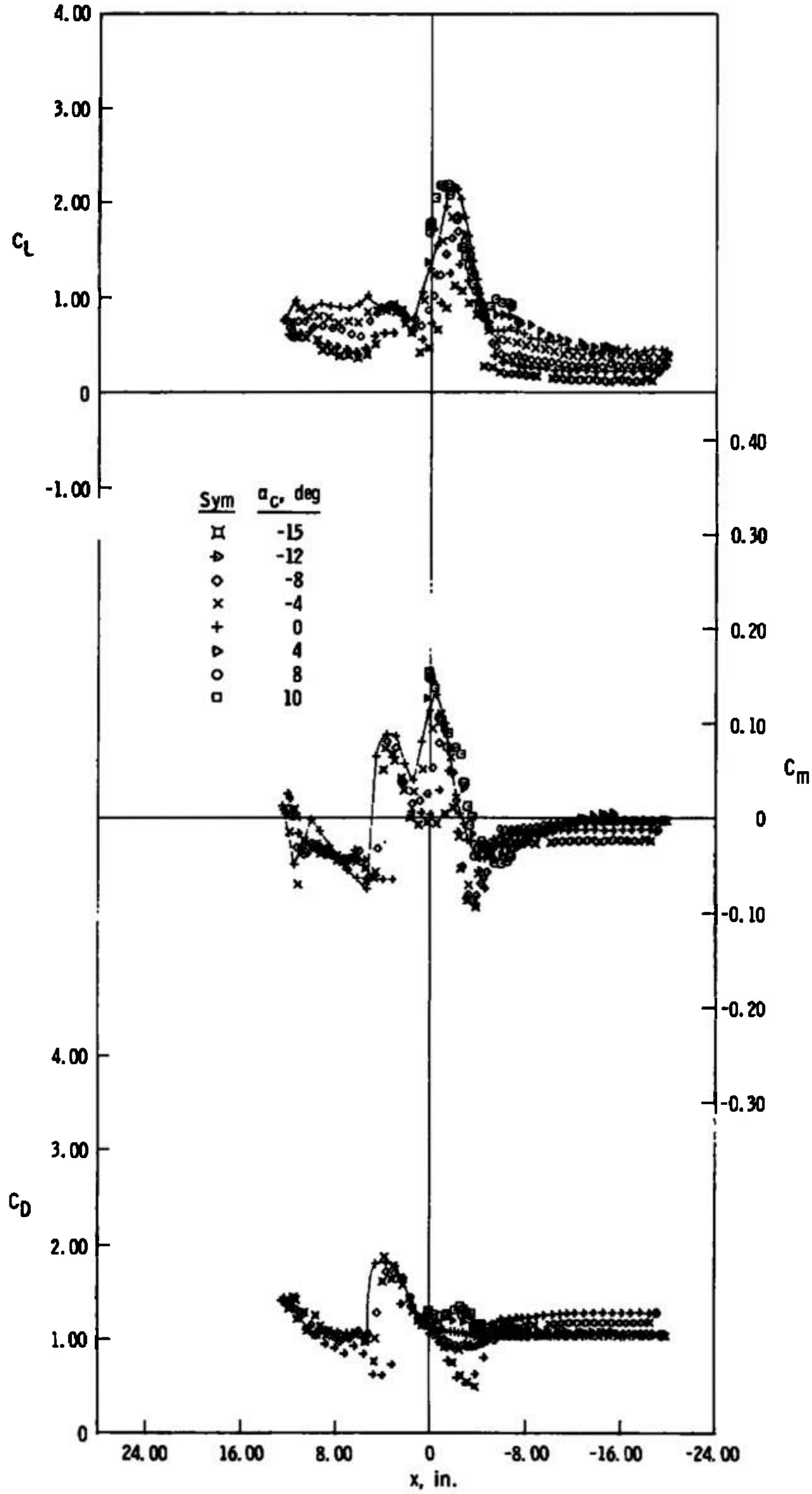

c. z = 5 in., y = 0
Fig. 22 Continued

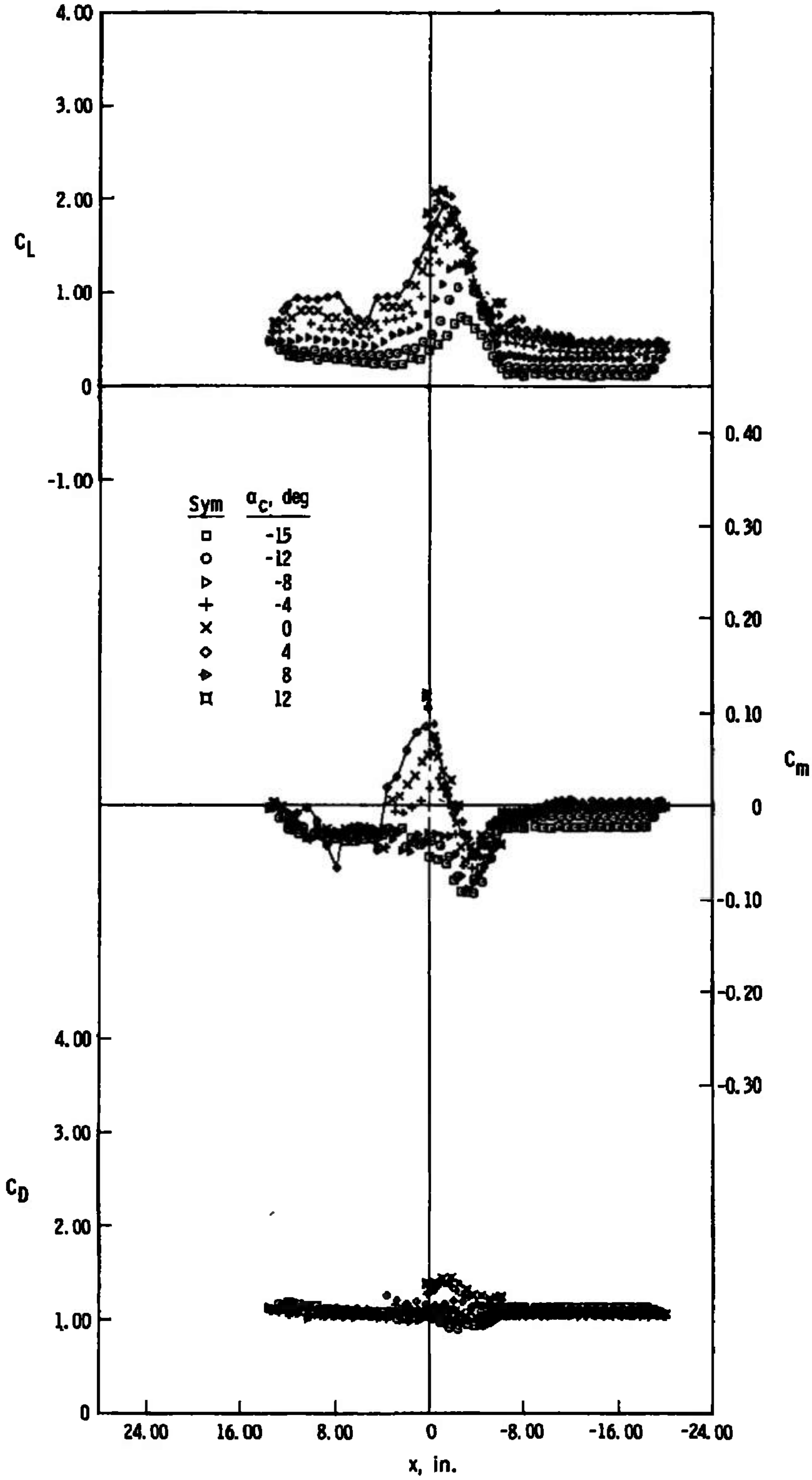

d. z = 6 in., y = 0
Fig. 22 Continued

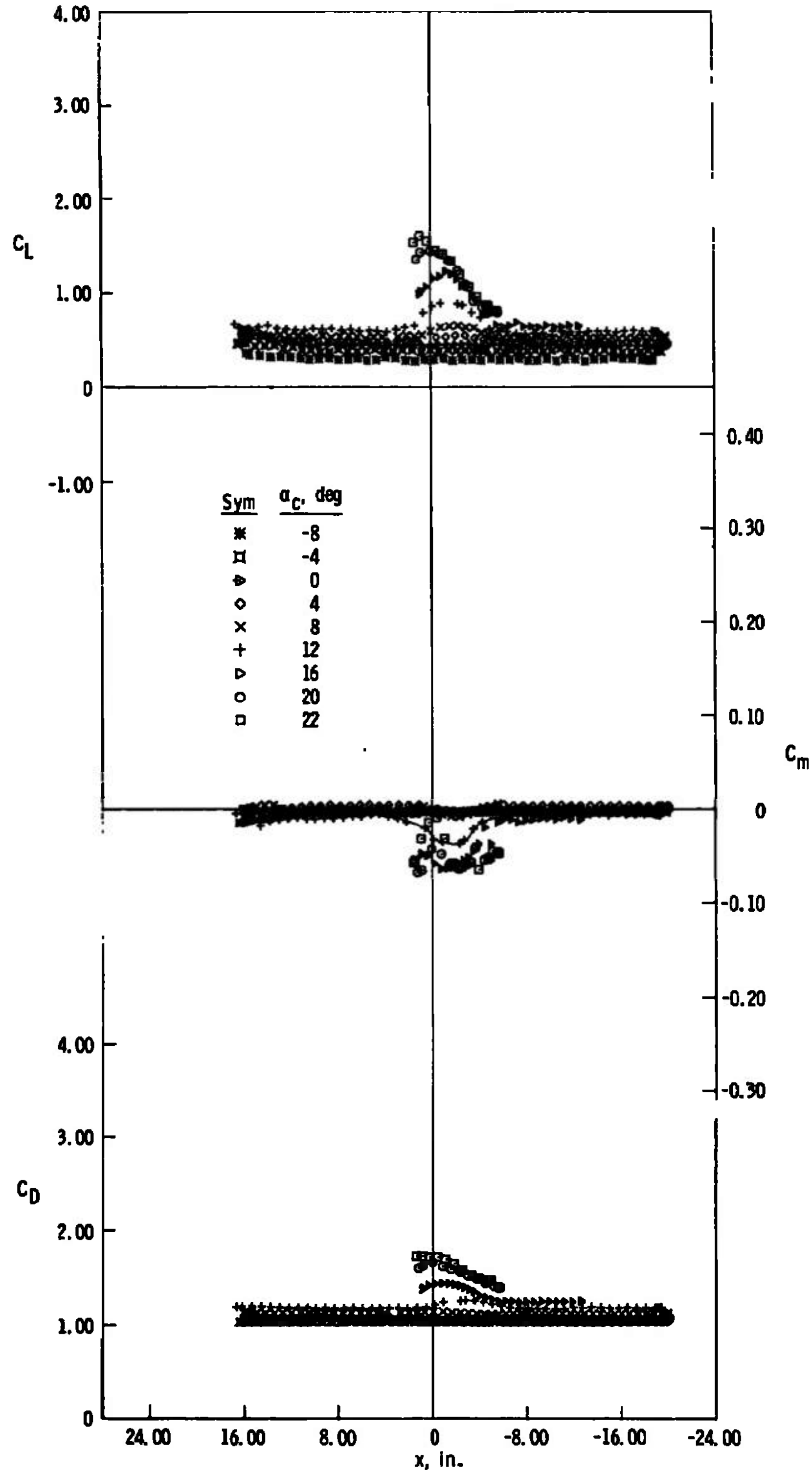

e. z = 10 in., y = 0

Fig. 22 Continued

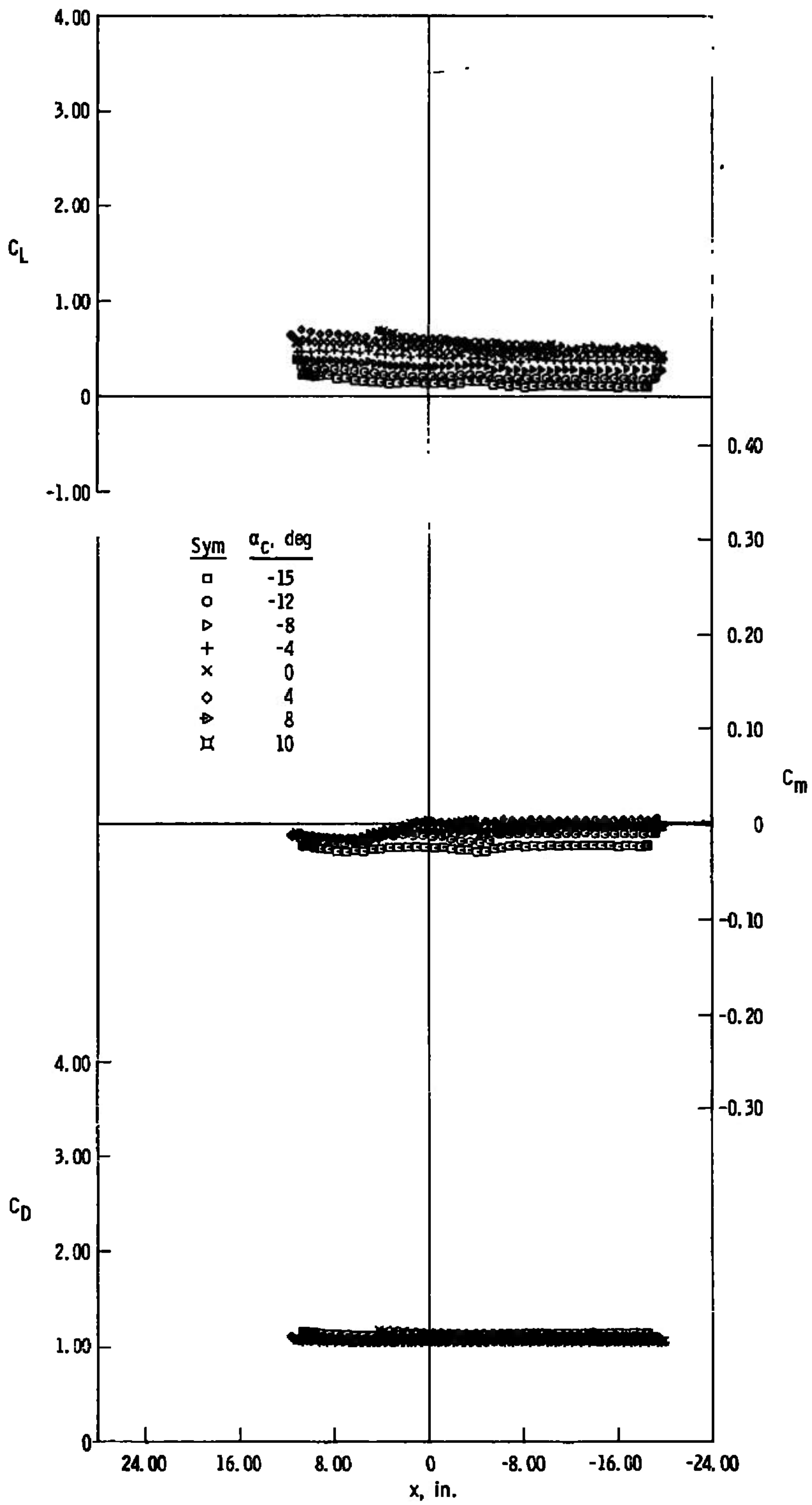

f. z = 5 in., y = 5 in.
Fig. 22 Concluded

a. α_c = –12 deg
y = 0
z = 3 in.
x = –2.9 in.

b. α_c = –12 deg
y = 0
z = 3 in.
x = –2.2 in.

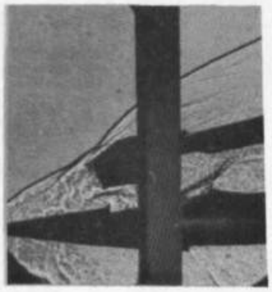

c. α_c = –12 deg
y = 0
z = 3 in.
x = –1.6 in.

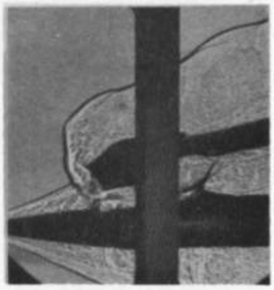

d. α_c = –12 deg
y = 0
z = 3 in.
x = –0.9 in.

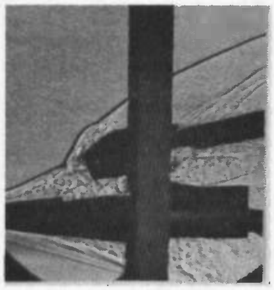

e. α_c = –12 deg
y = 0
z = 3 in.
x = 1.6 in.

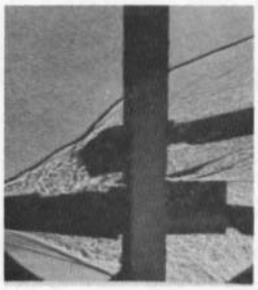

f. α_c = –12 deg
y = 0
z = 3 in.
x = 3.2 in.

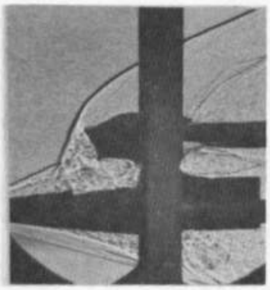

g. α_c = 0
y = 0
z = 4 in.
x = 1.3 in.

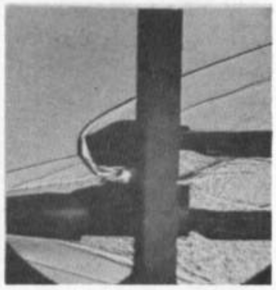

h. α_c = 0
y = 0
z = 4 in.
x = 7.1 in.

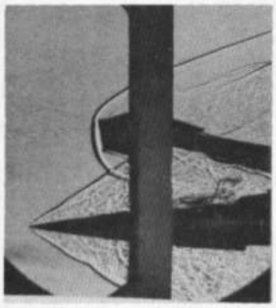

i. α_c = 12 deg
y = 0
z = 6 in.
x = –5.9 in.

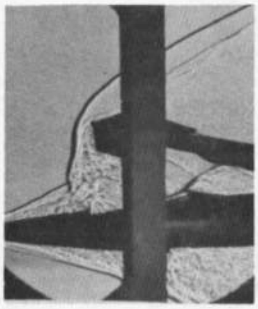

j. α_c = 12 deg
y = 0
z = 6 in.
x = 0.3 in.

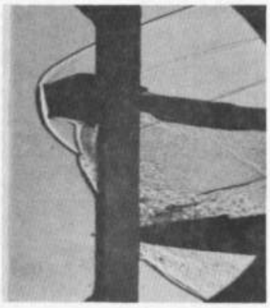

k. α_c = 8 deg
y = 0
z = 10 in.
x = –16.2 in.

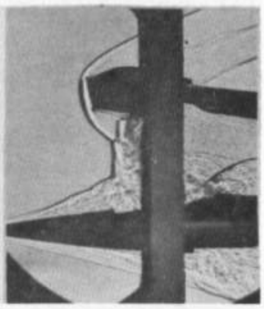

l. α_c = 8 deg
y = 0
z = 10 in.
x = –2.3 in.

Fig. 23 Schlieren Photographs, Jet On, M_∞ = 5, p_c/p_∞ = 4204

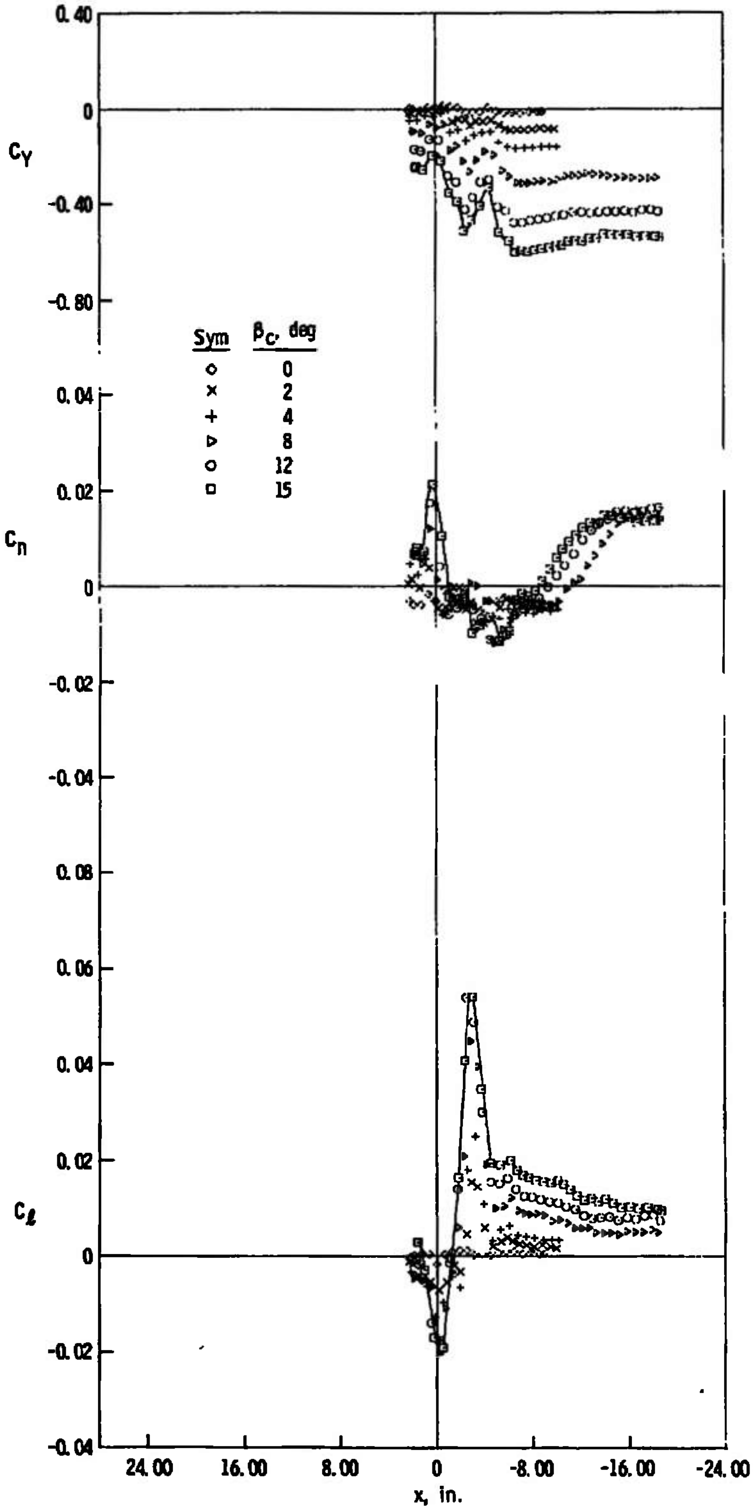

a. z = 3 in., y = 0

Fig. 24 Side-Force, Yawing-Moment, and Rolling-Moment Characteristics of the Capsule, Jet On, $M_\infty = 2$, $p_c/p_\infty = 357$

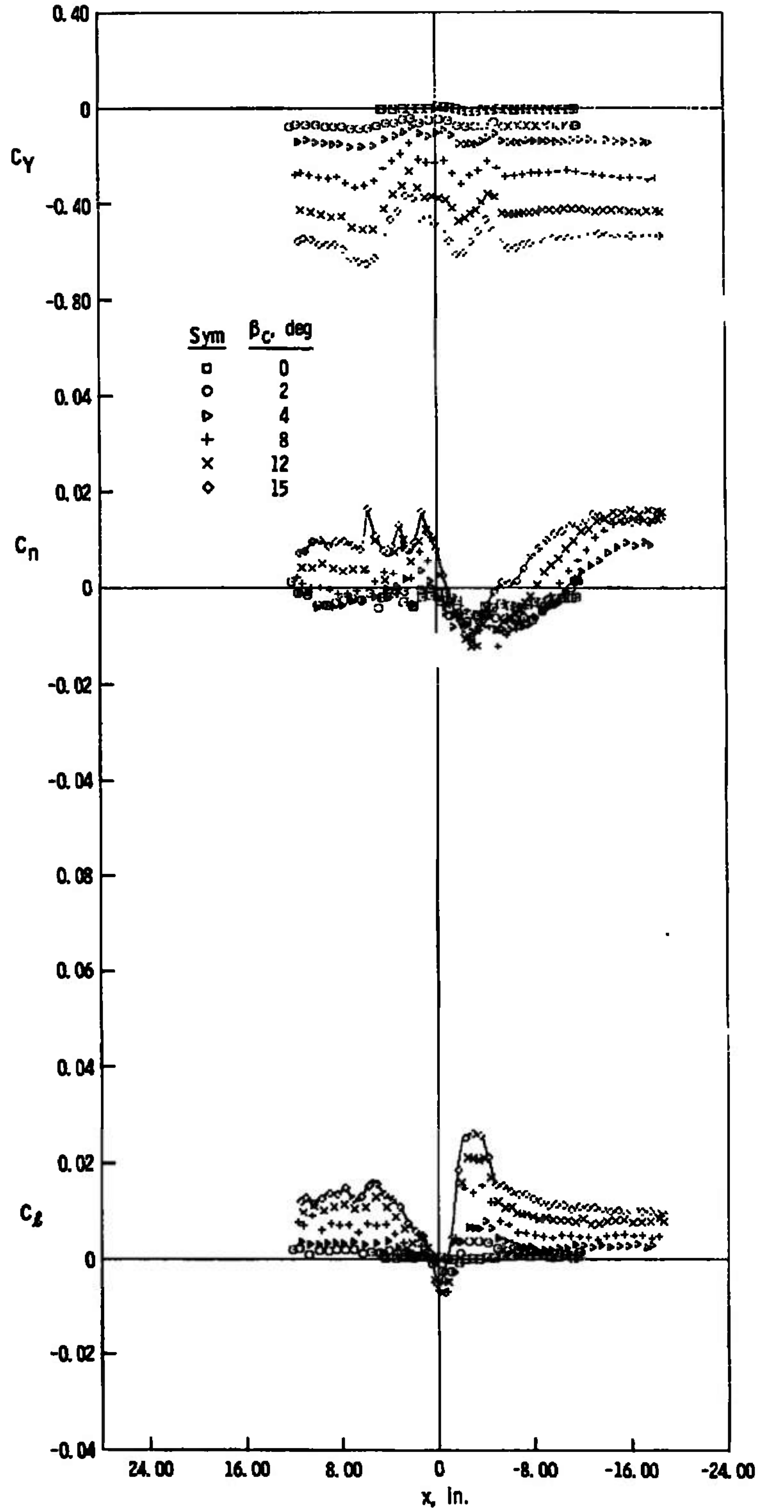

b. z = 4 in., y = 0
Fig. 24 Continued

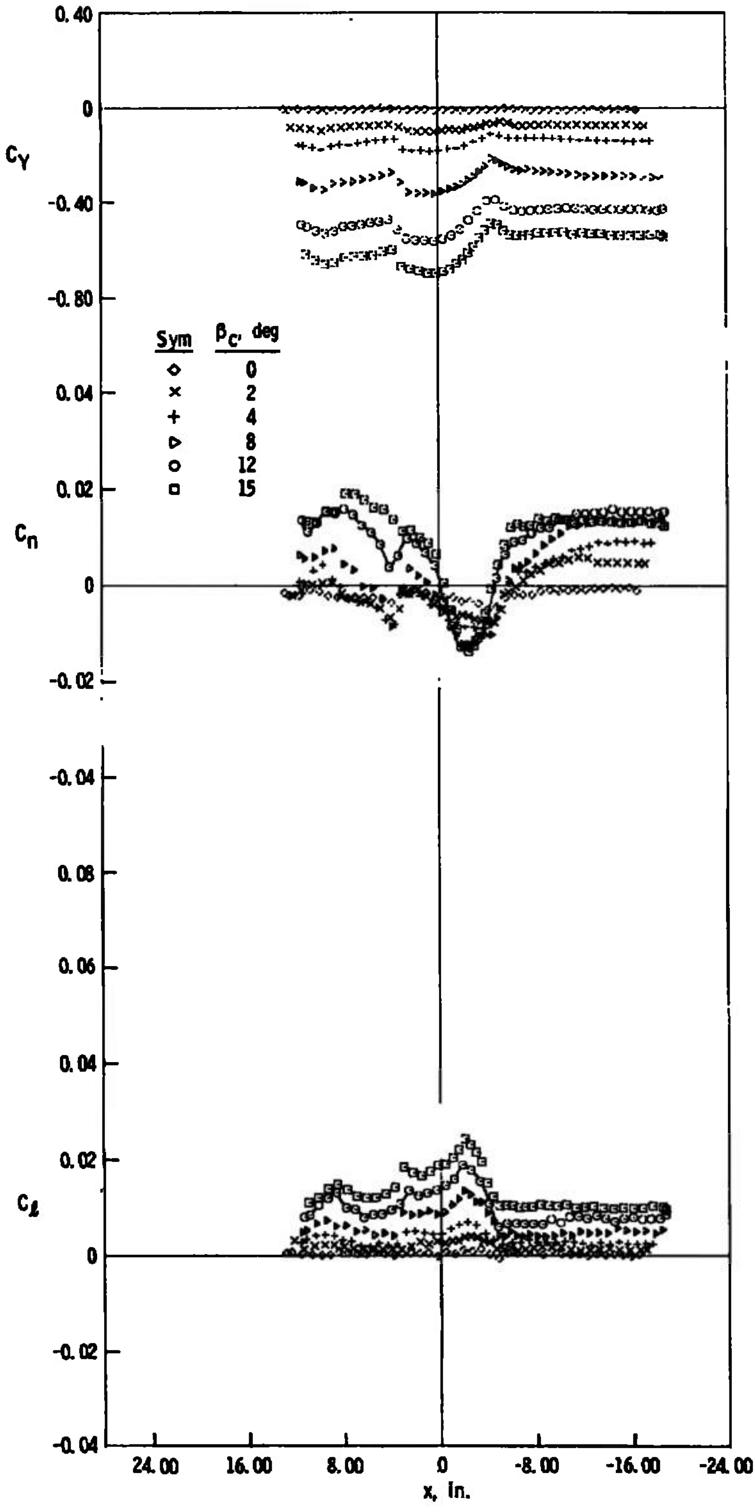

c. z = 6 in., y = 0

Fig. 24 Continued

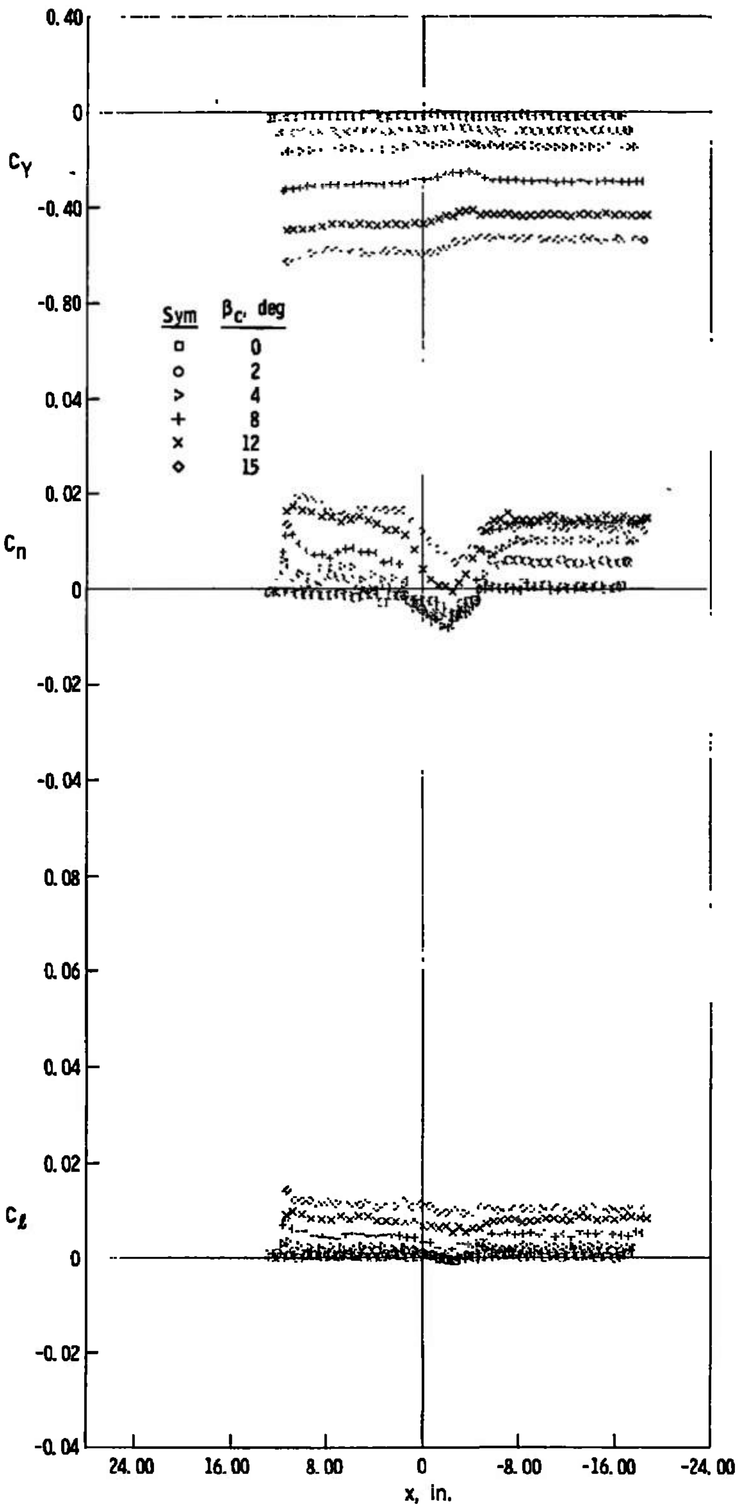

d. z = 8 in., y = 0
Fig. 24 Continued

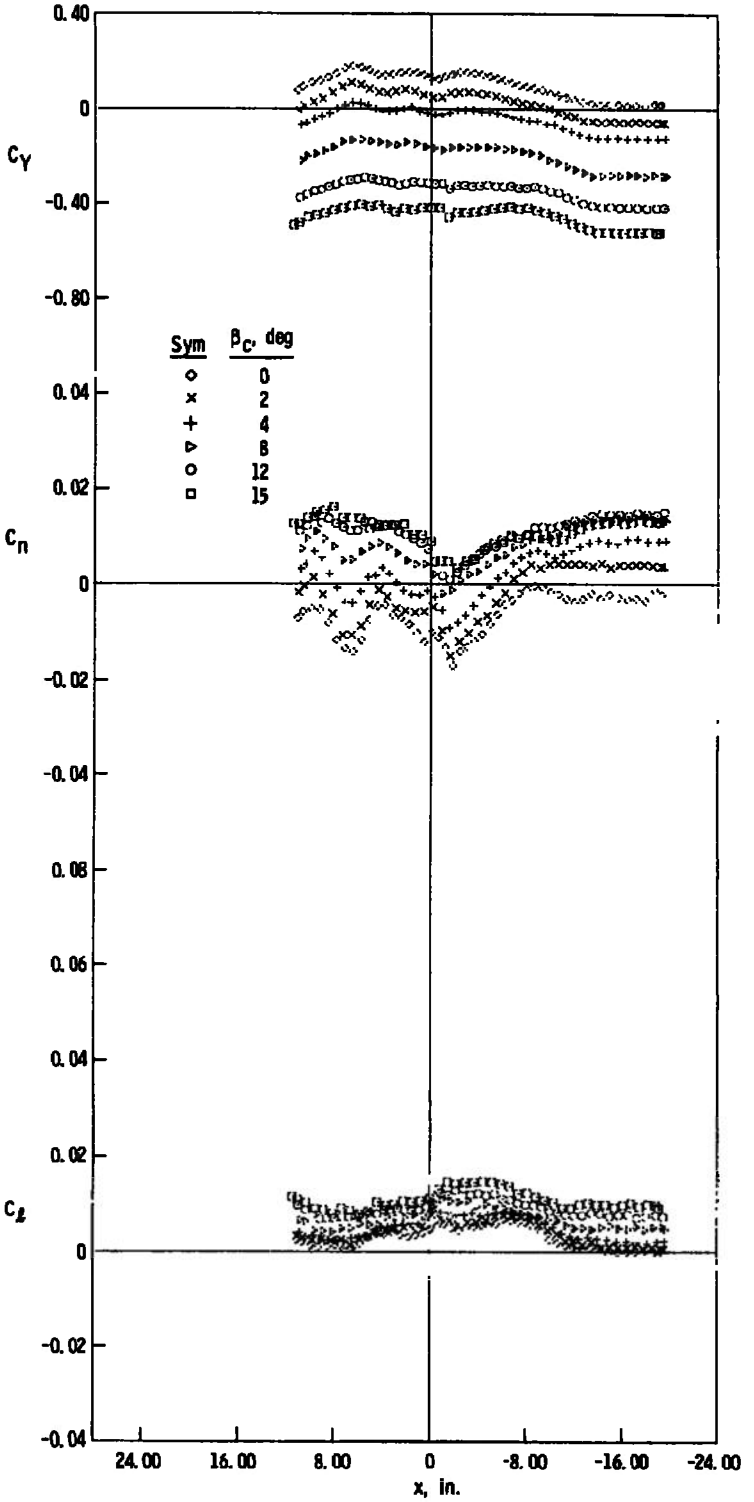

e. z = 3 in., y = -5 in.

Fig. 24 Concluded

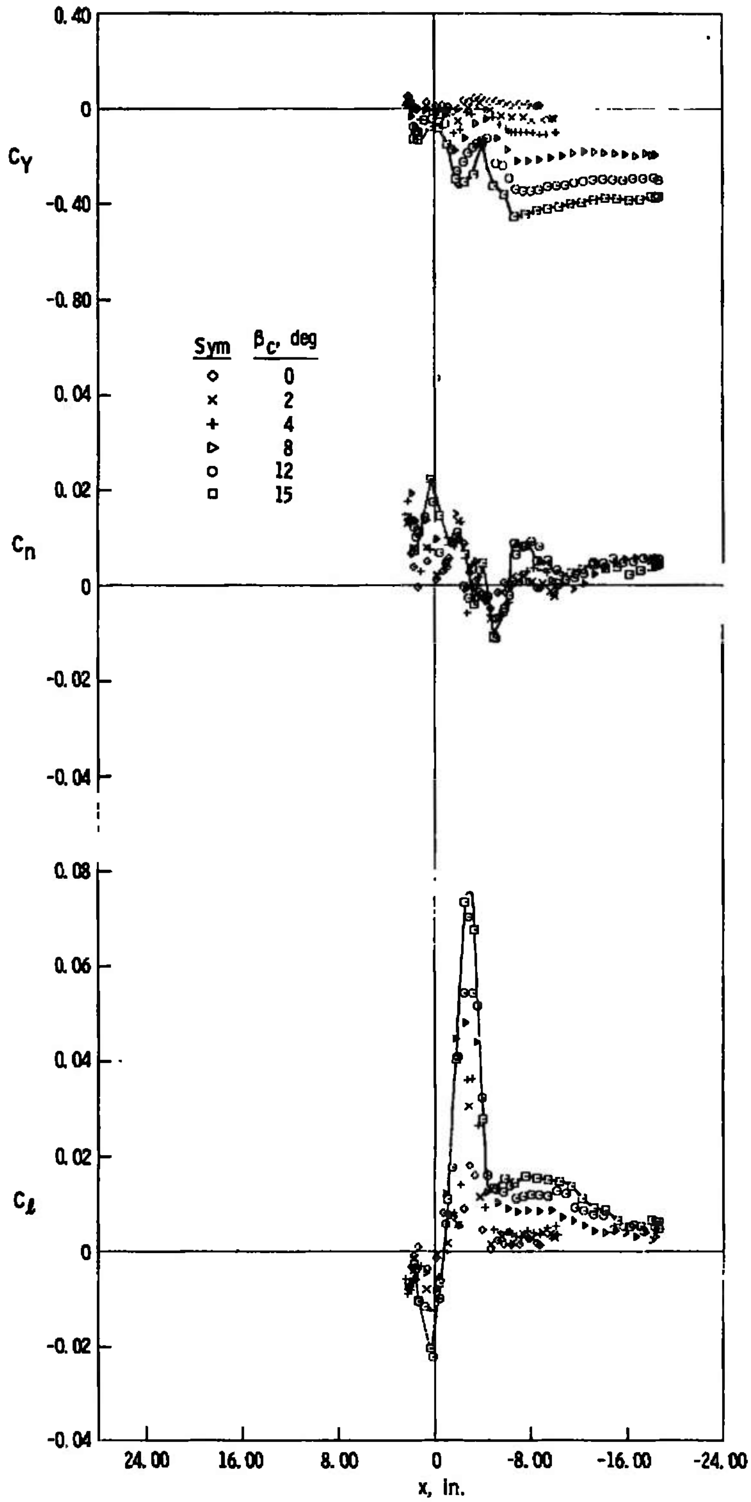

a. z = 3 in., y = 0

Fig. 25 Side-Force, Yawing-Moment, and Rolling-Moment Characteristics of the Capsule, Jet On, M_∞ = 3, p_c/p_∞ = 1206

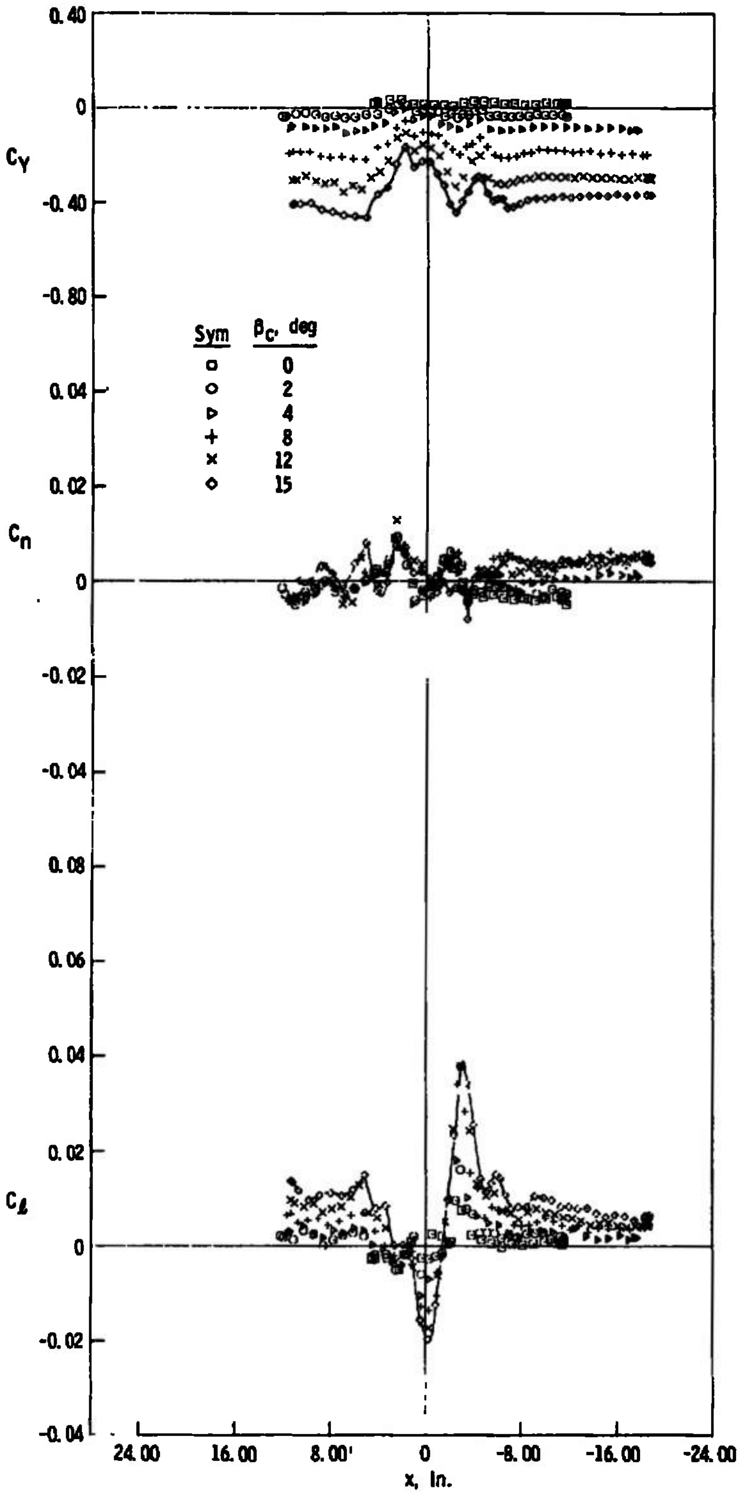

b. z = 4 in., y = 0

Fig. 25 Continued

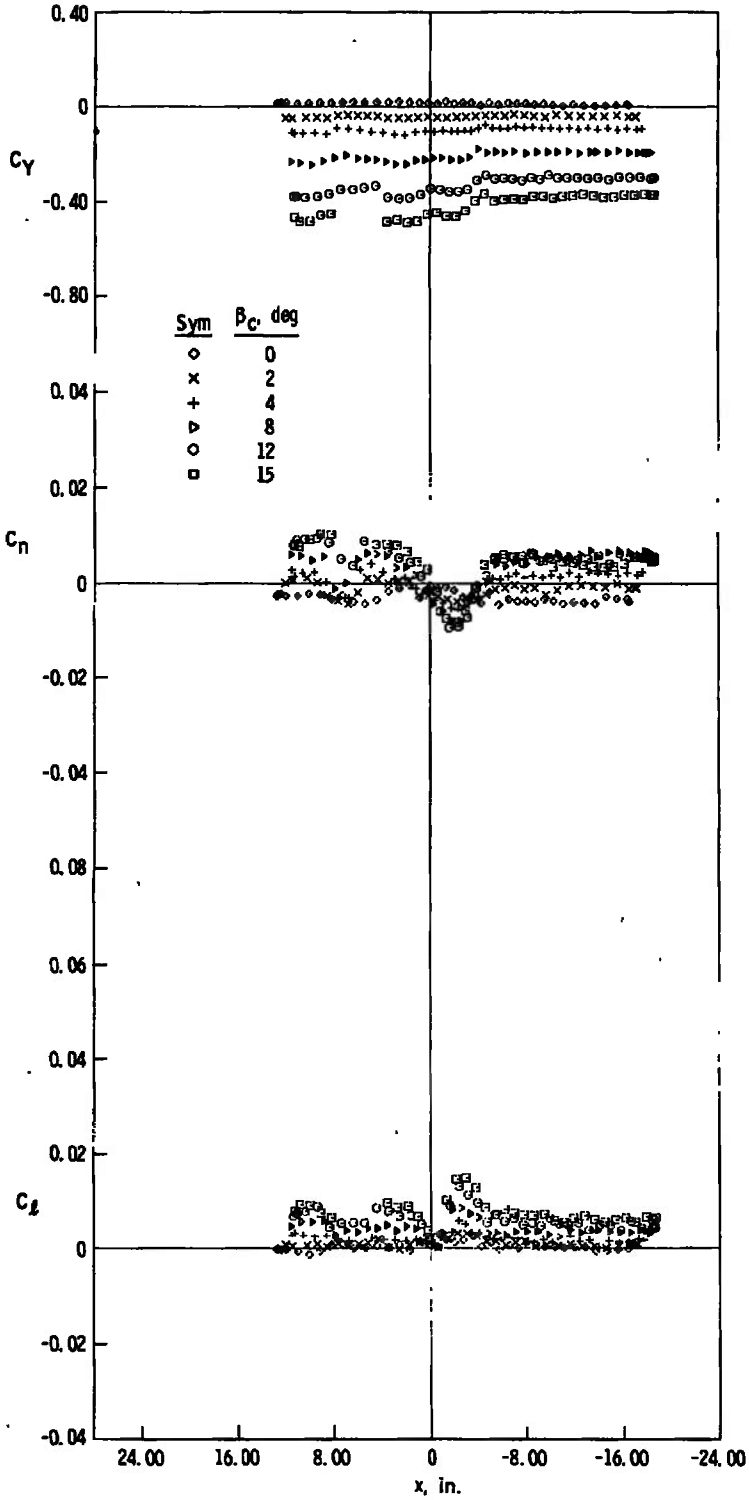

c. z = 6 in., y = 0

Fig. 25 Continued

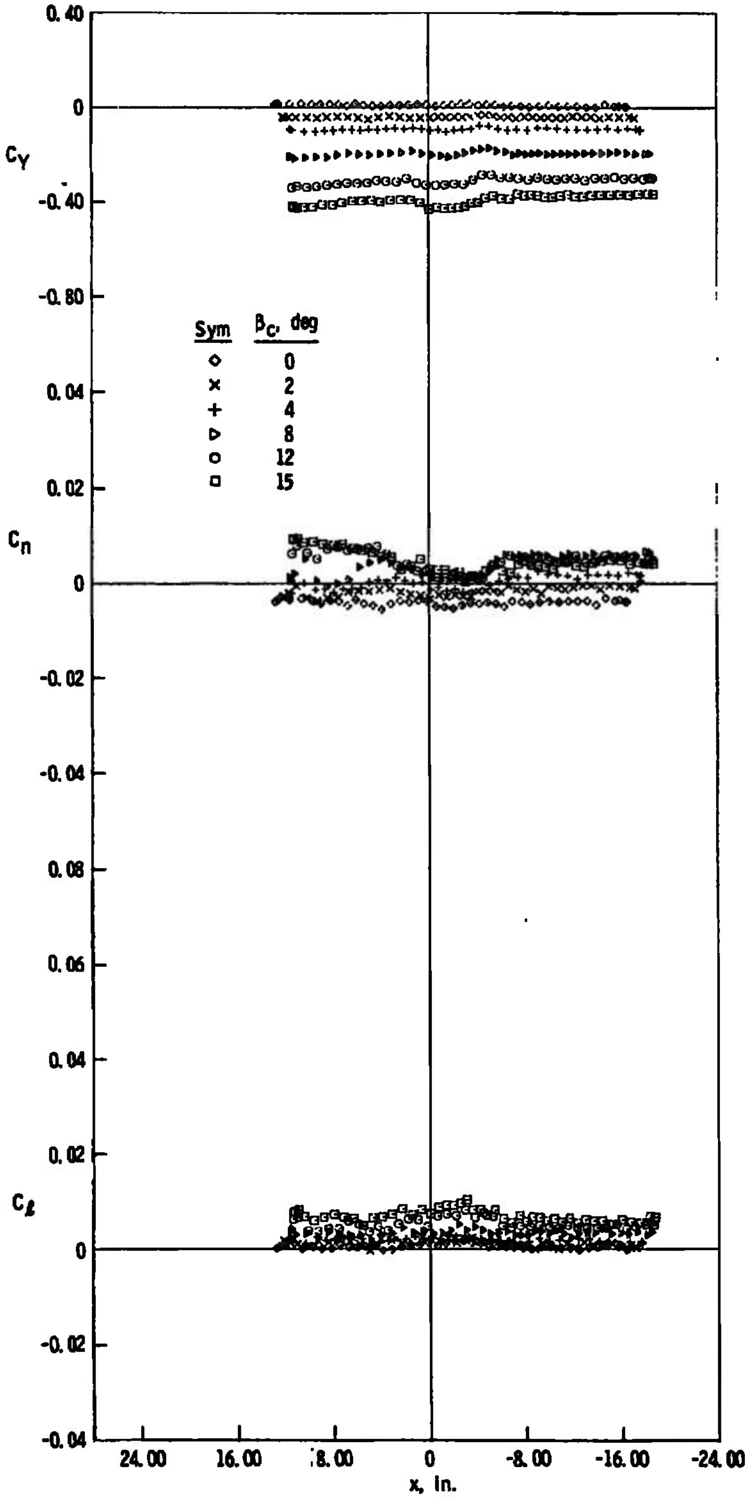

d. z = 8 in., y = 0
Fig. 25 Continued

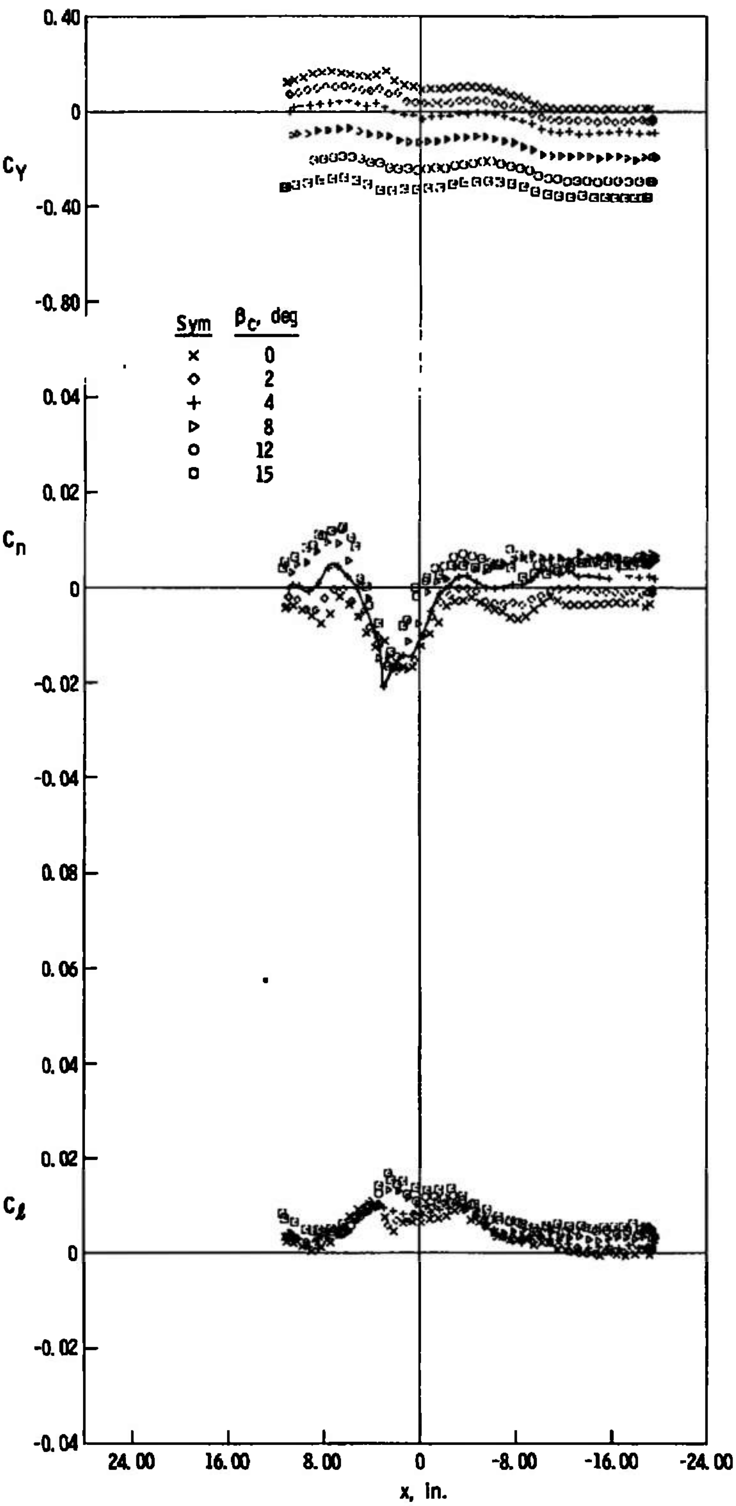

e. z = 3 in., y = -5 in.

Fig. 25 Concluded

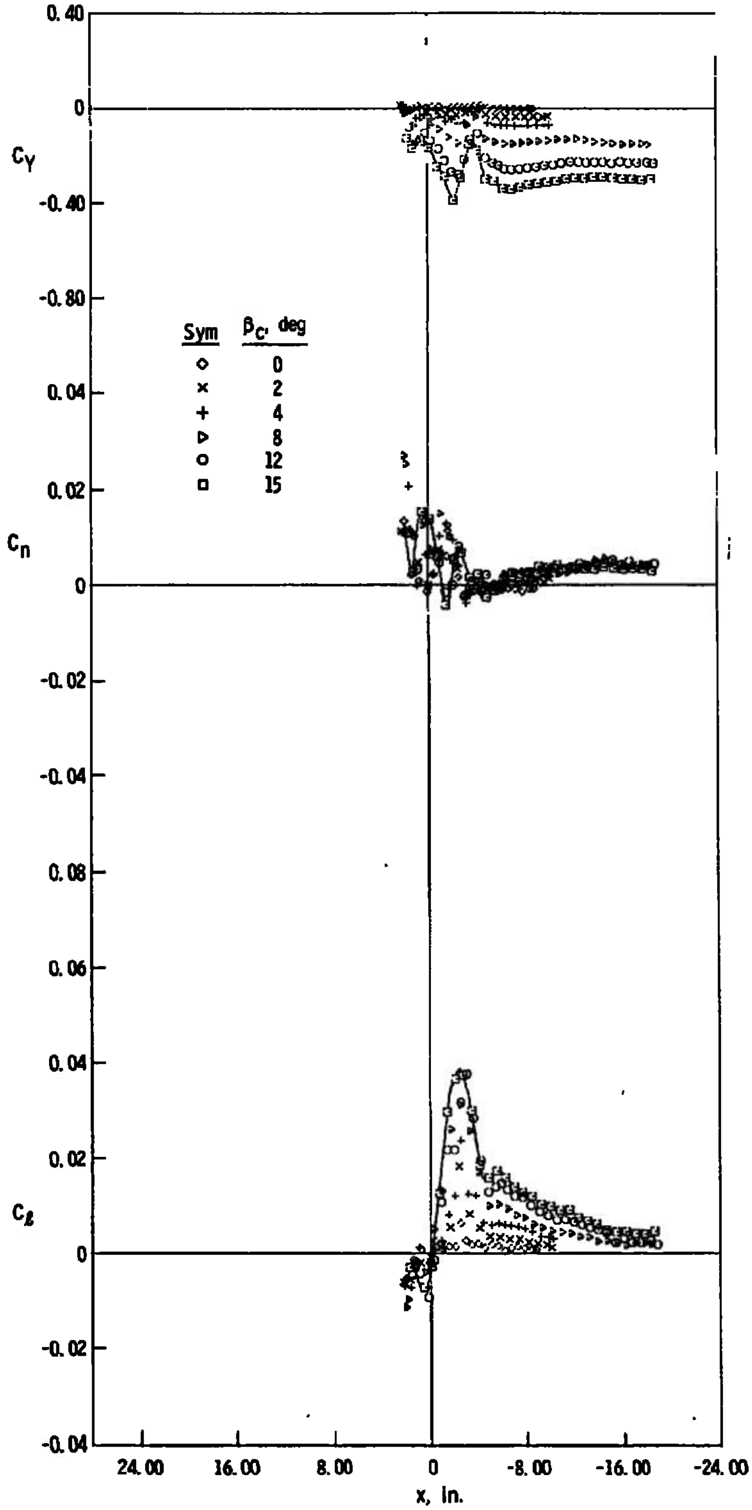

a. z = 3 in., y = 0

Fig. 26 Side-Force, Yawing-Moment, and Rolling-Moment Characteristics of the Capsule, Jet On, $M_\infty = 4$, $p_c/p_\infty = 1303$

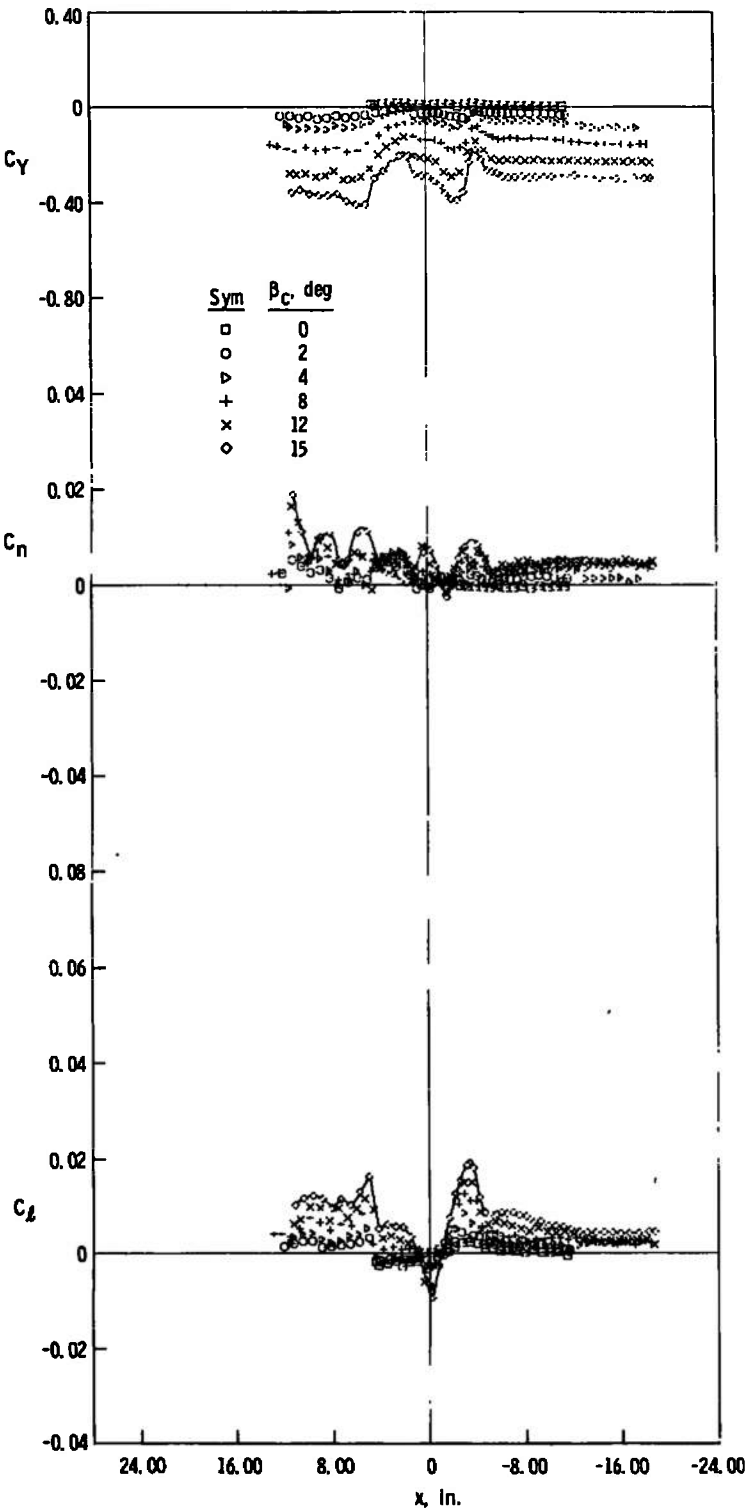

b. z = 4 in., y = 0

Fig. 26 Continued

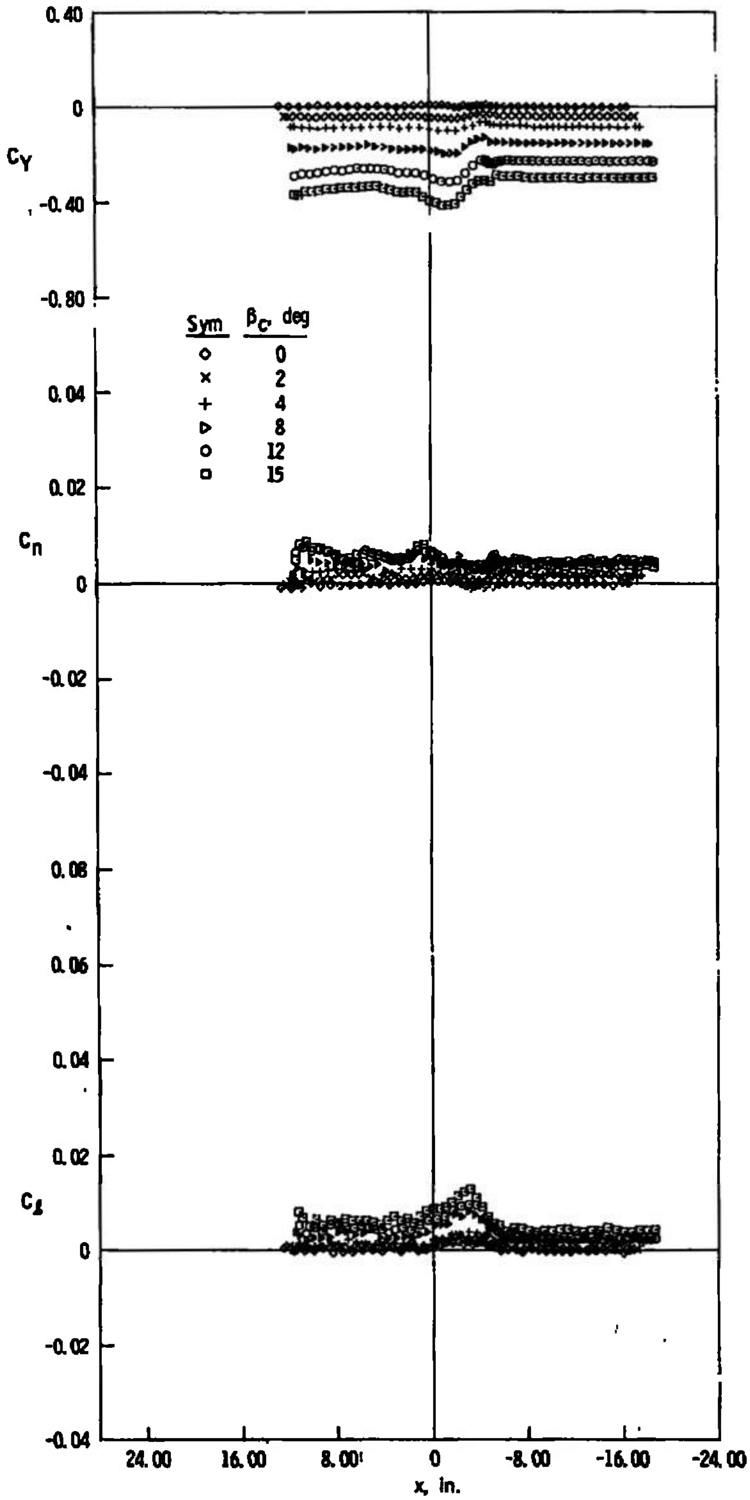

c. z = 6 in., y = 0

Fig. 26 Continued

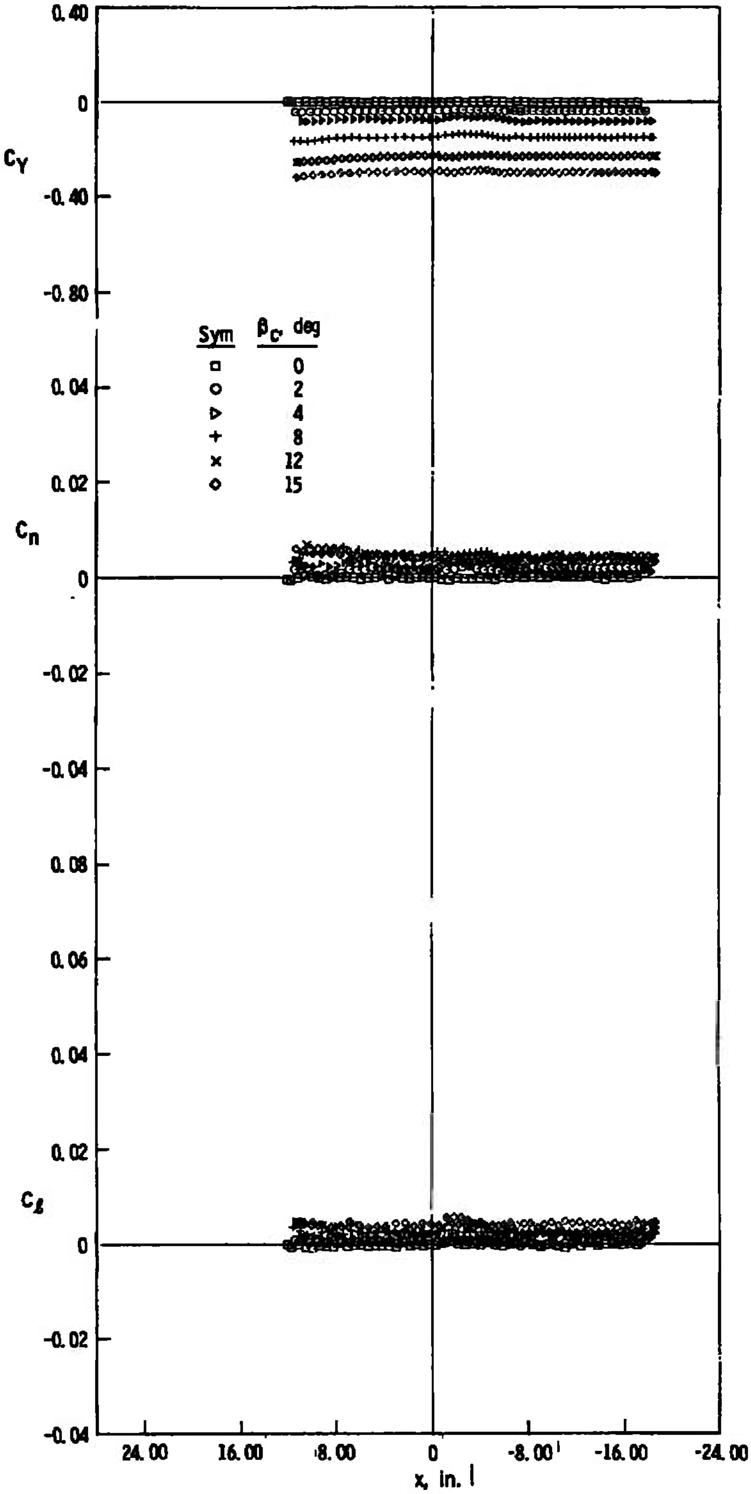

d. z = 8 in., y = 0
Fig. 26 Continued

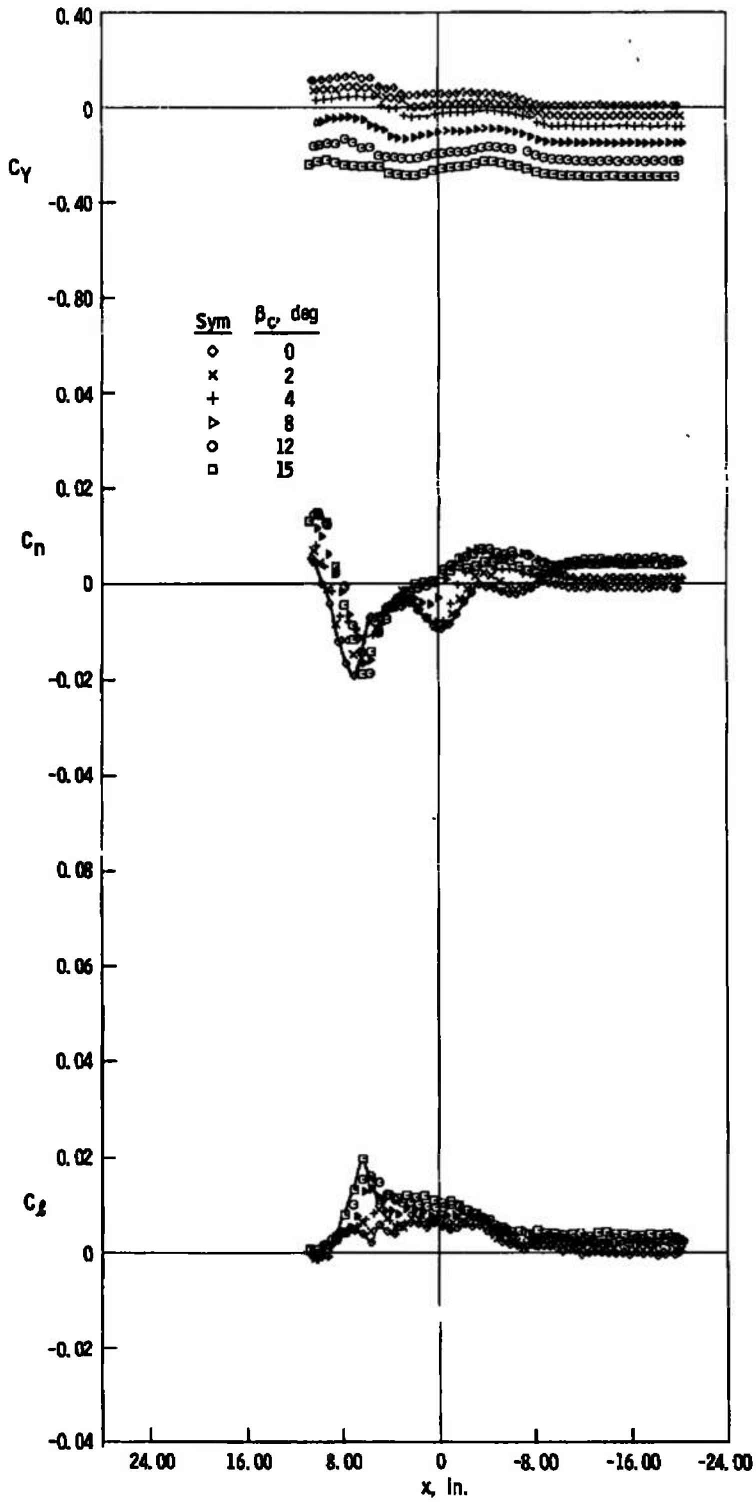

e. z = 3 in., y = –5 in.
Fig. 26 Concluded

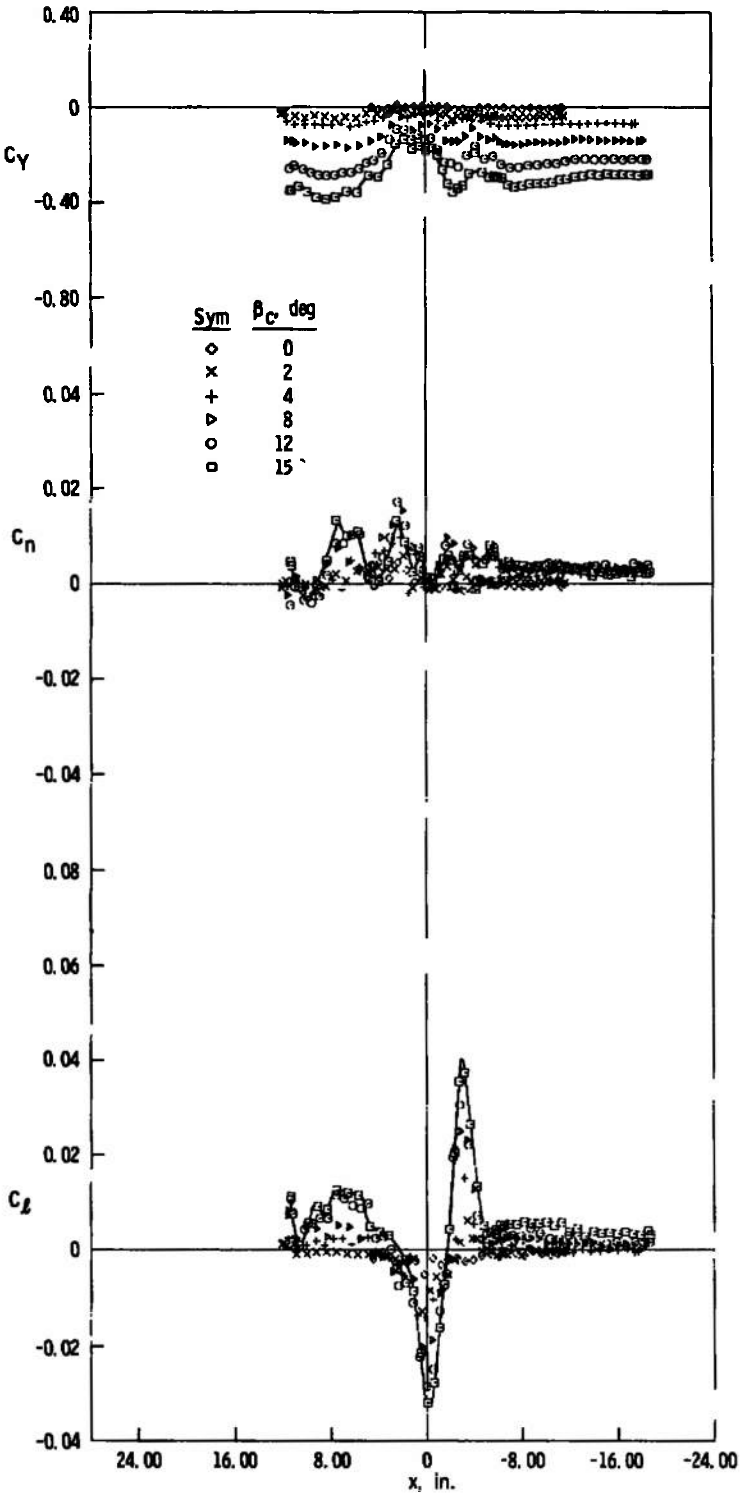

a. z = 4 in., y = 0

Fig. 27 Side-Force, Yawing-Moment, and Rolling-Moment Characteristics of the Capsule, Jet On, M_∞ = 5, p_c/p_∞ = 4204

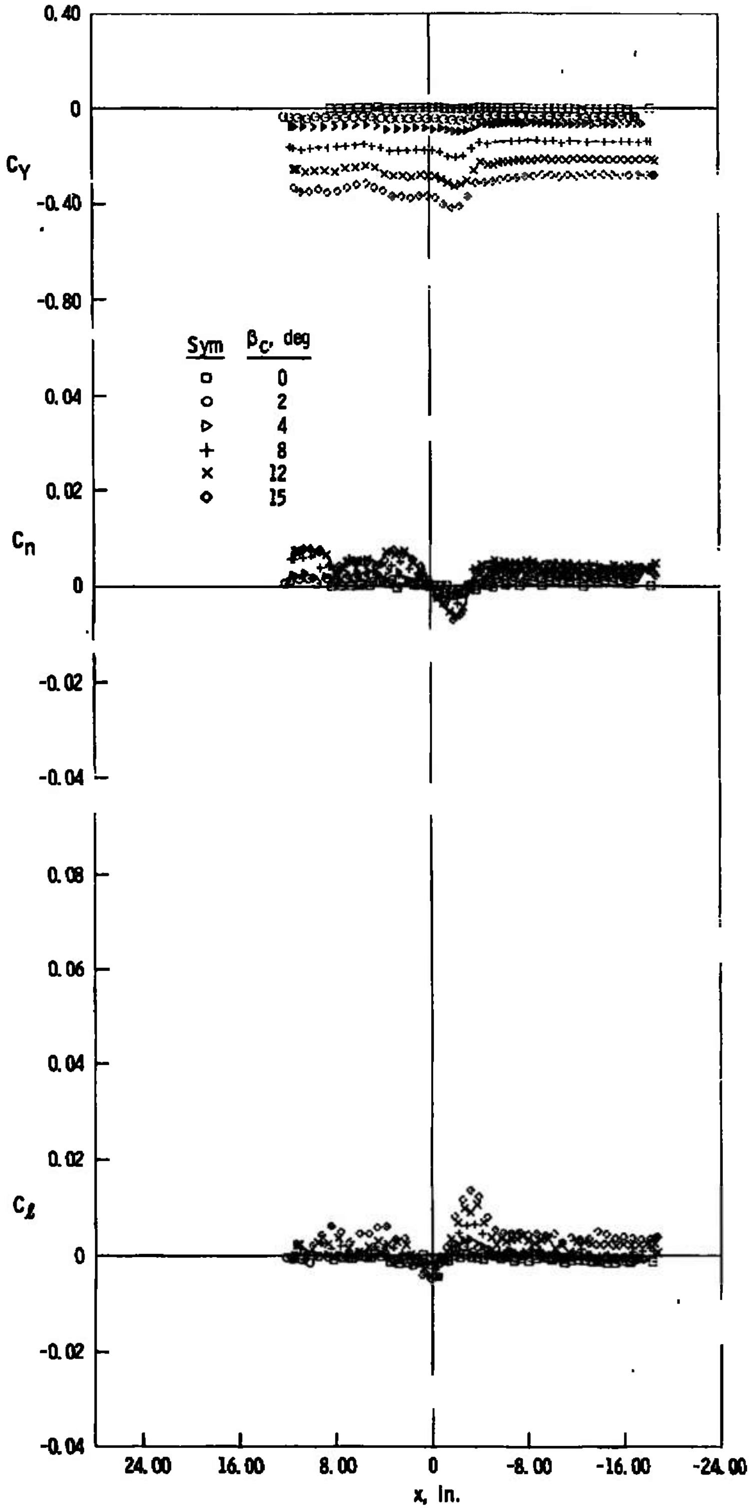

b. z = 6 in., y = 0

Fig. 27 Continued

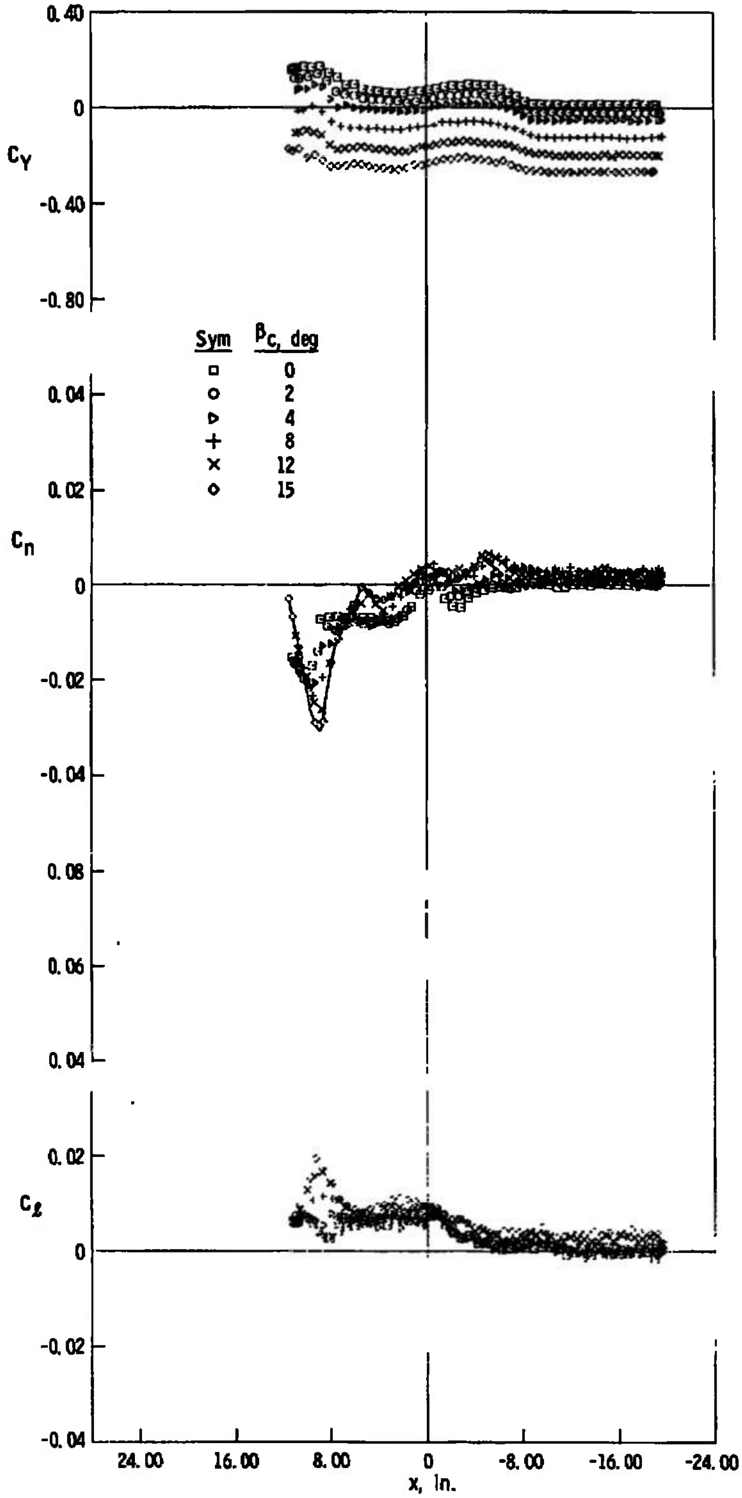

c. z = 3 in., y = –5 in.
Fig. 27 Concluded

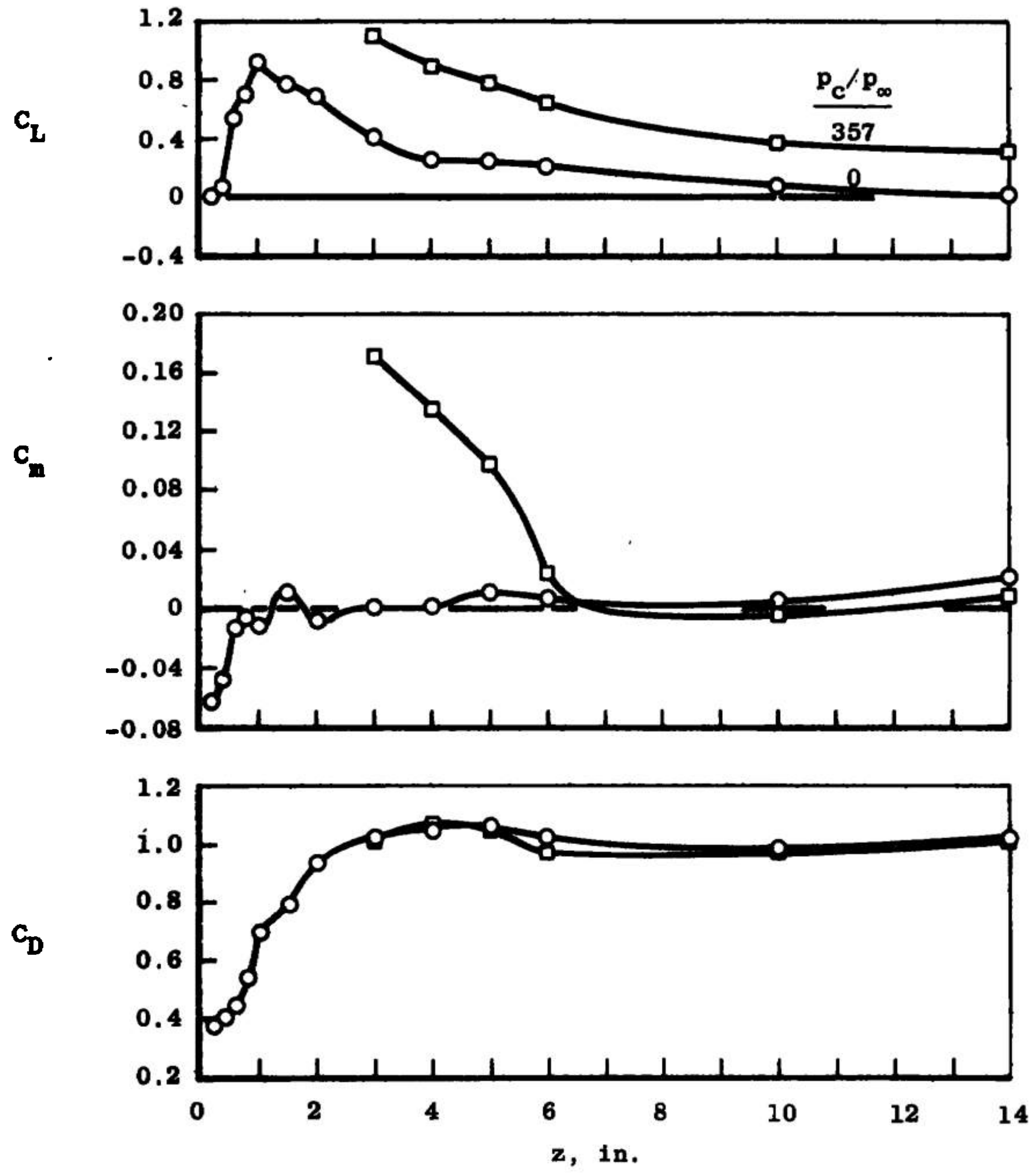

a. $M_\infty = 2$

Fig. 28 Lift, Pitching-Moment, and Drag Characteristics of the Capsule as a Function of z at x = 0, y = 0, $\alpha_c = 0$

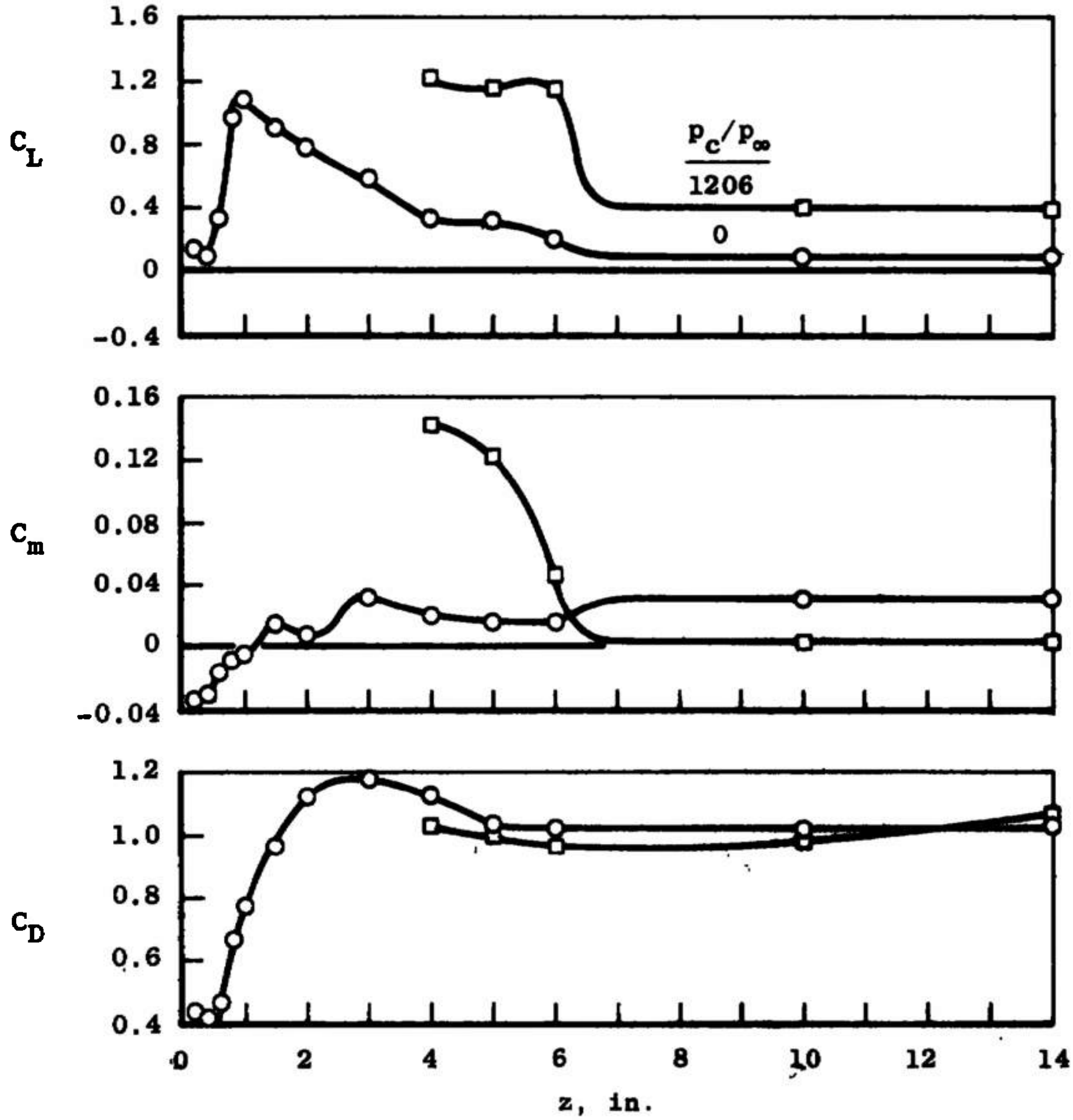

b. M_∞ = 3
Fig. 28 Continued

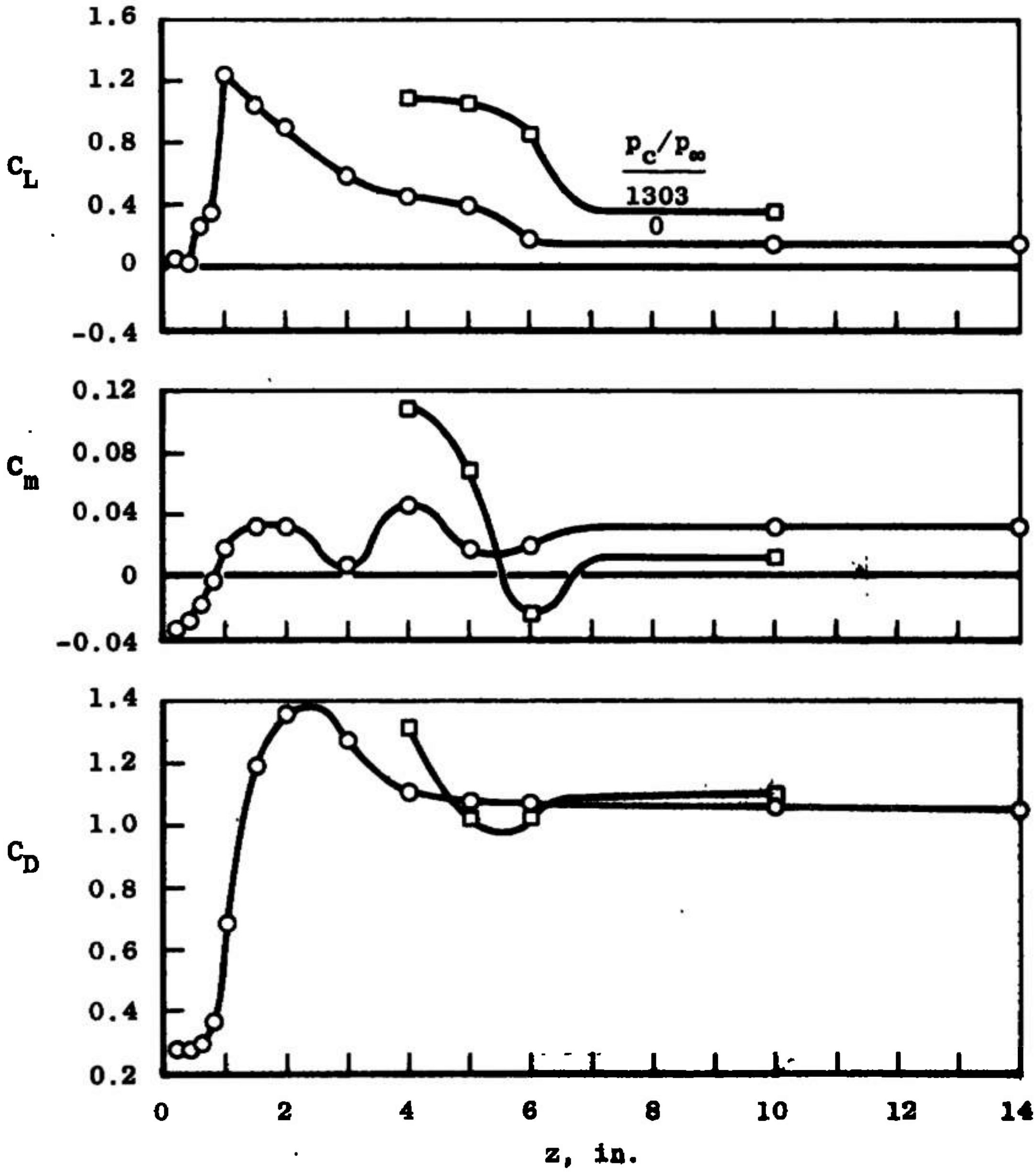

c. $M_\infty = 4$
Fig. 28 Continued

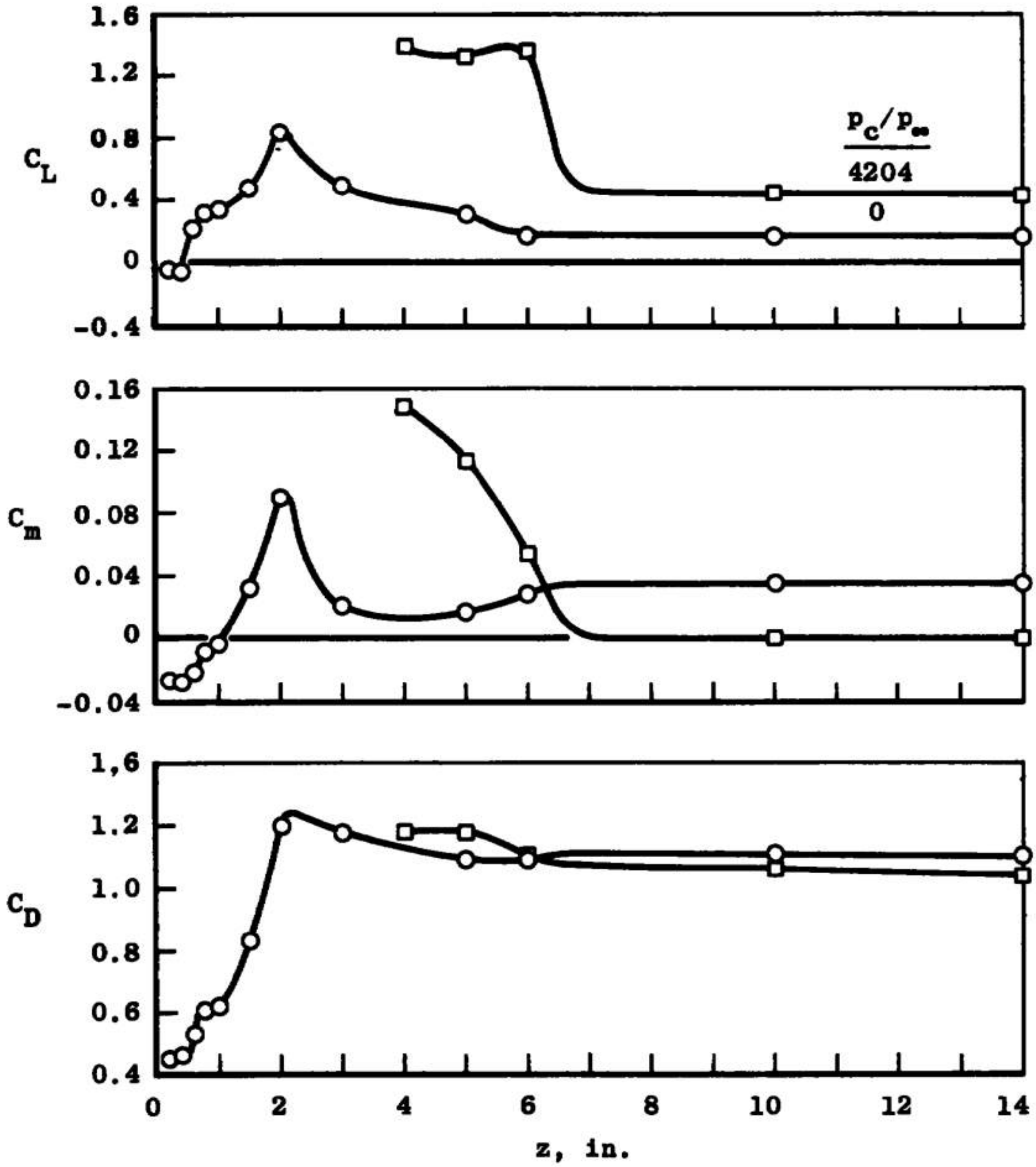

d. $M_\infty = 5$
Fig. 28 Concluded

TABLE I
MODEL PITCH ATTITUDES

α_c, deg	x, in.	y, in.	z, in.*
0	0	0	0.2, 0.4, 0.6, 0.8
-15	$-22 \lesssim x \lesssim 26$		1, 1.5, 2, 3, 4, 5, 6
-12			1, 1.5, 2, 3, 4, 5, 6
-8			1, 1.5, 2, 3, 4, 5, 6, 10
-4			1, 1.5, 2, 3, 4, 5, 6, 10
0			1, 1.5, 2, 3, 4, 5, 6, 10, 14
2			1
3			1.5
4			2, 3, 4, 5, 6, 10, 14
6			3
8			4, 5, 6, 10, 14
10			5
12			6, 10, 14
16			10, 14
20			10, 14
22			10
25			14
-15		5	5
-12			5
- 8			5, 10
- 4			5, 10
0			5, 10, 14
4			5, 10, 14
8			5, 10, 14
10			5
12			10, 14
16			10, 14
20			10, 14
22			10
25	$-22 \lesssim x \lesssim 26$	5	14

*Sym	Remarks
	Fuselage insert off at all Mach numbers. Balance 2 used at Mach numbers 2 and 3, balance 1 at Mach numbers 4 and 5
	Balance 2 used at Mach number 2, balance 1 at Mach numbers 4 and 5, and Mach number 3 for unflagged only.
	Balance 2 used at Mach number 3, balance 1 at Mach numbers 4 and 5
None	Balance 1 used at all Mach numbers

Note: No Data Taken for Jet On at $z \lesssim 3.0$ in.

TABLE II
MODEL SIDESLIP ATTITUDES

β_c, deg	x, in.	y, in.	z, in.
0	$-20 \lesssim x \lesssim 15$	0	3, 4, 6, 8
2			
4			
8			
12			
15		0	
0		5	
2			
4			
8			
12			
15	$-20 \lesssim x \lesssim 15$	5	3, 4, 6, 8

Notes: All Data Obtained on Balance 2 with the Fuselage Insert On

No Data Taken at Mach Number 5 for z = 8 in.

No Data Taken for Jet On at Mach Number 5 for z = 3 in., y = 0

TABLE III
TEST CONDITIONS

Nominal M_∞	Calibrated M_∞	p_o, psia	T_o, °R	p_∞, psia	$Re_\infty \times 10^{-6}$, in.$^{-1}$	Pressure Altitude, ft x 10^{-3}	p_c/p_∞
2	2.00	12.8	580	1.682	0.250	50	0, 357
3	2.99	18.2	580	0.506	0.217	75	0, 1206
4	4.02	71.0	580	0.468	0.485	76	0, 1303
5	5.06	85.0	620	0.157	0.325	100	0, 4204

UNCLASSIFIED
Security Classification

DOCUMENT CONTROL DATA - R & D

(Security classification of title, body of abstract and indexing annotation must be entered when the overall report is classified)

1. ORIGINATING ACTIVITY (Corporate author)	2a. REPORT SECURITY CLASSIFICATION
Arnold Engineering Development Center ARO, Inc., Operating Contractor Arnold Air Force Station, Tennessee 37389	UNCLASSIFIED
	2b. GROUP N/A

3. REPORT TITLE

FORCE TESTS ON A SEPARABLE-POD CREW ESCAPE CAPSULE IN PROXIMITY TO THE PARENT FUSELAGE AT MACH NUMBERS 2 THROUGH 5

4. DESCRIPTIVE NOTES (Type of report and inclusive dates)

July 7 to 31, 1969 - Final Report

This document has been approved for public release its distribution is unlimited. PER TAB 72-19 Dtd 1 Oct, 72.

5. AUTHOR(S) (First name, middle initial, last name)

Jerry H. Jones and L. M. Jenke, ARO, Inc.

6. REPORT DATE	7a. TOTAL NO. OF PAGES	7b. NO. OF REFS
January 1970	126	4

8a. CONTRACT OR GRANT NO.	9a. ORIGINATOR'S REPORT NUMBER(S)
F40600-69-C-0001	AEDC-TR-69-232
b. Program Element 64706F	
c.	9b. OTHER REPORT NO(S) (Any other numbers that may be assigned this report)
d.	N/A

10. DISTRIBUTION STATEMENT

~~This document is subject to special export controls and each transmittal to foreign governments or foreign nationals may be made only with prior approval of Air Force Flight Dynamics Laboratory (FDFR), Wright-Patterson Air Force Base, Ohio 45433.~~

11. SUPPLEMENTARY NOTES	12. SPONSORING MILITARY ACTIVITY
Available in DDC.	Air Force Flight Dynamics Laboratory (FDFR), Wright-Patterson Air Force Base, Ohio 45433

13. ABSTRACT

Static-force tests were conducted on a separable-pod crew escape capsule in close proximity to the forward section of the airplane fuselage. The capsule escape rocket exhaust plume was simulated with high pressure air heated to a total temperature of approximately 100°F. Data were obtained at Mach numbers from 2 through 5 at capsule angles of attack from -15 to 25 deg and angles of sideslip from 0 to 15 deg for various positions of the capsule relative to the fuselage section. All testing was conducted at a fuselage angle of attack and angle of sideslip of zero. Reynolds number, based on the pod model length of 8.978 in., ranged from 1.9×10^6 to 5.2×10^6. Results are presented showing the effects of the fuselage section on the aerodynamic characteristics of the capsule, with and without simulation of the escape rocket exhaust plume. These results indicate that the primary interference effects for the jet-off data are caused by severe flow interactions occurring when the capsule, with its strong bow shock, moves across the fuselage cavity. For the jet-on data the primary interference effects are caused by the jet exhausting into the fuselage cavity, which acts as a flow deflector turning the jet flow back onto the capsule.

~~This document is subject to special export controls and each transmittal to foreign governments or foreign nationals may be made only with prior approval of Air Force Flight Dynamics Laboratory (FDFR), Wright-Patterson, Air Force Base, Ohio 45433.~~

DD FORM 1 NOV 65 1473

UNCLASSIFIED
Security Classification

14. KEY WORDS	LINK A		LINK B		LINK C	
	ROLE	WT	ROLE	WT	ROLE	WT
escape systems						
force						
aircraft						
fuselages						
aerodynamic characteristics						
flight simulation						
supersonic flow						

AFSC
Arnold AFS Tenn